Chemical Reactivity of Methyl-benzenes from Core-photoelectron Spectroscopy and Theory

Velaug Myrseth

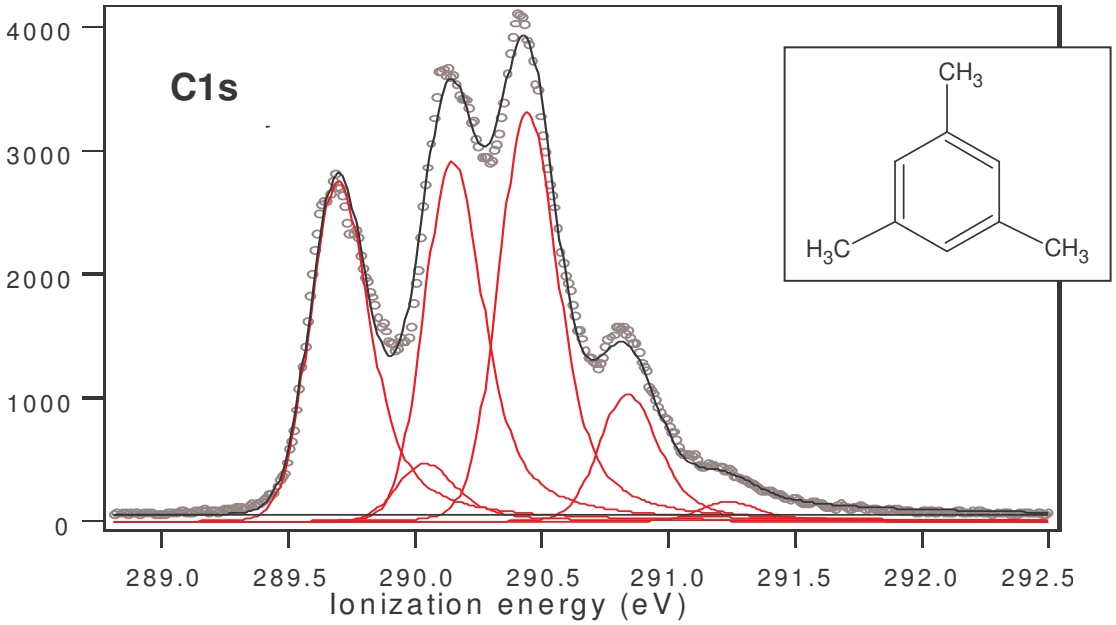

Cand. Scient. Thesis

Department of Chemistry, University of Bergen

May 2000

Acknowledgements

The experimental data of this thesis have been acquired at MAX-lab in Lund, Sweden and at the Advanced Light Source in Berkeley, California. The data analysis and theoretical calculations have been performed at the Chemistry Department, University of Bergen. This work has received a grant of computing time from the Programme for Supercomputing financed by the Research Council of Norway (NFR). Financial support has also been received from the Nordic Academy for Advanced Study (NorFa), from Acta Chemica Scandinavica, and from the L. Meltzer Stipend for students.

First of all, I wish to express my gratitude towards my advisor, Prof. Leif J. Sæthre for his guidance and support. He always had the time to answer questions, and has provided me with invaluable help in finishing this thesis. During the last year and a half, I have been encouraged by his enthusiasm and knowledge many times.

I would also like to thank Prof. Knut J. Børve, University of Bergen, for his advice on the theoretical aspects of this work. Many thanks to Prof. Svante Svensson and his group for their collaboration, and a good time both in Uppsala and in Lund. Thanks also to Prof. T. Darrah Thomas, for his guidance and assistance, and to the whole group in Corvallis for their hospitality. Dr. Margit Bässler at MAX-lab, and Dr. John Bozek and Dr. Edwin Kukk at the Advanced Light Source have provided essential help at the beamlines during our experiments. Many thanks to my fellow students and friends here at the Chemistry Department, especially Asbjørn, for fruitful discussions and technical advice.

Finally, I wish to thank my sister and my family for help and endless support. Their encouragement and good advice have been essential to me throughout this period.

Velaug Myrseth

Bergen, May 2000

Table of contents

Chapter 1

Introduction

Historically, inner-shell photoelectron spectra have been measured in order to determine core-electron ionization energies, which can be related to a variety of chemical properties. Examples of such properties are acid strength, oxidation states, and reactivity [1,2,3]. In this work, the reactivity and orientation of aromatic compounds in electrophilic substitution reactions have been studied by means of high-resolution synchrotron radiation and *ab initio* calculations.

Electrophilic reactions to benzene and benzene derivatives are of fundamental interest in synthetic and mechanistic organic chemistry. The reactions are characterized by two important properties; i.e. the effects of substituents on reactivity and on orientation. With respect to reactivity, electron-withdrawing substituents decrease the reactivity, while electron-donating substituents increase it. When it comes to orientation, substituents can be either ortho-para directing or meta directing. A simple picture has been commonly used to account for these properties [4,5]. The addition of an electrophile to form a positive intermediate, is considered to be the slow and rate-determining step. This step is followed rapidly by the fast detachment of the leaving group. The rate and regioselectivity of the reaction is determined by the energy of the transition state, and hence by the stability of the intermediate carbocation.

This picture emphasizes the ability of the molecule to delocalize the added charge in the transition state. However, a number of studies have shown that for many such systems, the charge distribution of the initial state of the molecule plays a more important role in determining reaction rates [1,2]. In this work, we have used carbon core-ionization energies and theoretical calculations to investigate electrophilic substitution of benzene and some methyl-substituted benzenes: toluene, o-xylene, m-xylene, p-xylene, and mesitylene. The molecules were measured in the gas phase using high-resolution synchrotron radiation, and the spectra were deconvoluted to provide accurate C1s ionization energies.

For these molecules two sets of experimental reactivity data are available. One reaction is replacement of tritium by hydrogen [6], and the relative rates of protodetritiation show extreme position sensitivity of the ring carbons :

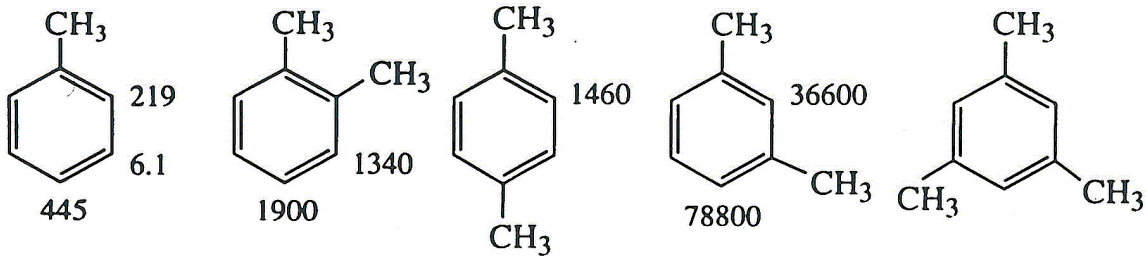

Toluene o-Xylene p-Xylene m-Xylene Mesitylene

These data provide a test set for correlation with C1s energies. In addition, these replacement reactions are not considered to be influenced by sterical hindrance, which will facilitate the comparison. The results will be compared with mesitylene, where we expect a maximum combined effect of the methyl substitution. Experimental reactivity data are also available for the cleavage reaction of substituted phenyltrimetylsilanes [7]. For this reaction reactivity data are available for mesitylene.

From these investigations, we conclude that there is a direct relationship between reactivities and C1s ionization energies for the ring carbons. This has previously been found for ethene, propene, and 2-methylpropene [1]. It has also been concluded in this work that the initial-state distribution plays a significant role in determining the relative activation energies for addition of a proton to the aromatic ring.

Conventional x-ray sources provide radiation with a well-known photon energy. The limitation of these laboratory sources is, however, the resolution. With synchrotron radiation the accuracy with which the photon energy is known is not high, but one can obtain a significantly higher resolution than with x-ray instruments. Today's third-generation synchrotron facilities make it possible to determine the small differences in ionization energies for inequivalent, but similar carbon atoms in the investigated molecules. The high resolution facilitates deconvolution

of complicated multiple spectral peaks for quantitative analysis. As the resolution of inner-shell electron spectroscopy has improved, these spectra have also yielded information on the vibrational excitation that accompanies ionization. For most of the analysis a simple model, the linear coupling intensity model, has been used to describe the vibrational progression [8,9]. It is also possible to examine the vibrational structure more thoroughly by means of extensive theoretical calculations, and this has been done for benzene and d-benzene. Theoretical calculations have also been used to interpret the experimental spectra and to facilitate fitting of the spectra.

As mentioned above the accuracy with which the photon energy of the synchrotron radiation is known is not high. Thus, to find accurate ionization energies, calibration is necessary. CO_2 and CF_4 are the compounds most often used for internal calibration, and accurate C1s ionization energies were determined for these compounds. In addition, a series of small molecules of general chemical interest were calibrated. The results from the calibration work are included in Chapter 5.

1.1 Electrophilic aromatic substitution

Many electrophiles react with aromatic hydrocarbons, and electrophilic aromatic substitution reactions are among the most important reactions for transforming organic compounds. Electrophilic substitution involves first addition of the electrophile and then detachment of the leaving group. This is illustrated for benzene in Figure 1.1. E^+ denotes the electrophile, and the leaving group is H^+. Benzene is a planar unsaturated hexagon whose p_z orbitals form a delocalized electron ring, both above and below the carbon atom plane. Because of its exposed π electrons, benzene is susceptible to electrophilic attack [10]. In the first step of the substitution reaction an intermediate, the arenium ion, is formed and the cyclic system interrupted. In step two the arenium ion (or benzenium ion) looses a proton from the carbon that bears the electrophile and the aromatic sextet of π electrons is regenerated. The energy of activation for the reaction from benzene to the benzenium ion has been shown to be much greater than the energy of activation leading from the benzenuim ion to the final product. Thus, step one

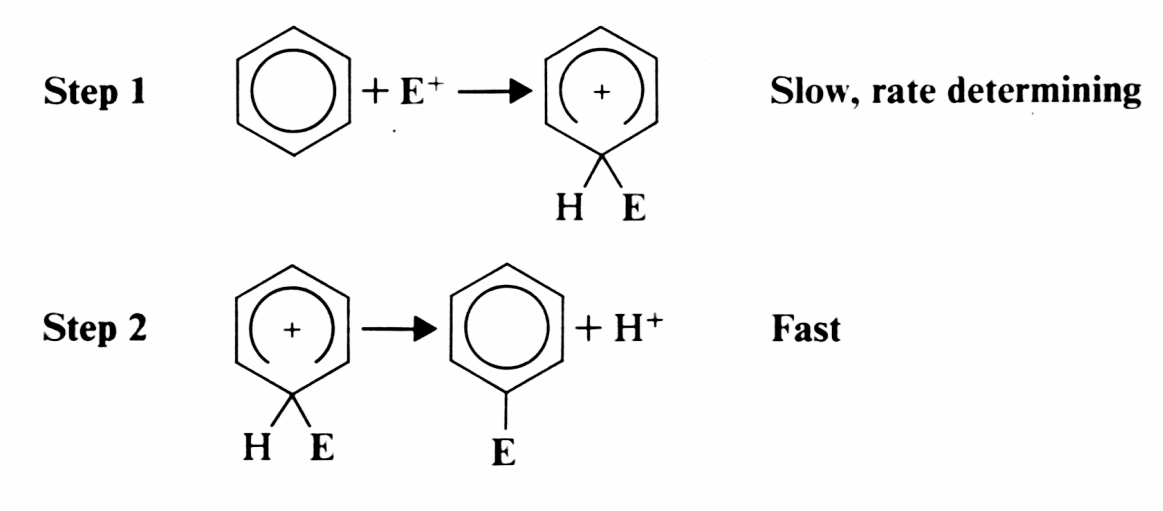

Figure 1.1. Schematic illustration of the reaction mechanism in aromatic electrophilic substitution.

is the slow, rate-determining step in electrophilic aromatic substitution [11]. To determine the quantitative reactivities of various positions in benzene derivatives relative to a benzene position, one can study the reaction of a mixture of benzene and the other compound [6]. These statistically corrected relative reactivities are known as partial rate factors. By taking the logarithm of the rate factor, one obtaines an expression that is proportional to activation energies, and this expression can be plotted against some other property to check for correlation.

Substituent groups on the benzene ring will affect both reactivity and orientation during electrophilic attack. One can divide substituent groups into two classes according to their influence on the reactivity of the ring. Activating groups cause the ring to be more reactive than benzene, while substituents that cause the ring to be less reactive are called deactivating groups. The methyl group is an activating substituent towards electrophilic substitution, meaning that the group increases the relative rate of the reaction. This is because the methyl group releases electrons to the benzene ring, relative to hydrogen, making the aromatic ring even more electron rich. As shown in Figure 1.2 the addition of the electrophile goes first via a transition state, and then the arenium ion is formed. Since the arenium ion is positively charged, one would expect an electron-releasing group to stabilize both the arenium ion and the transition state leading to it.

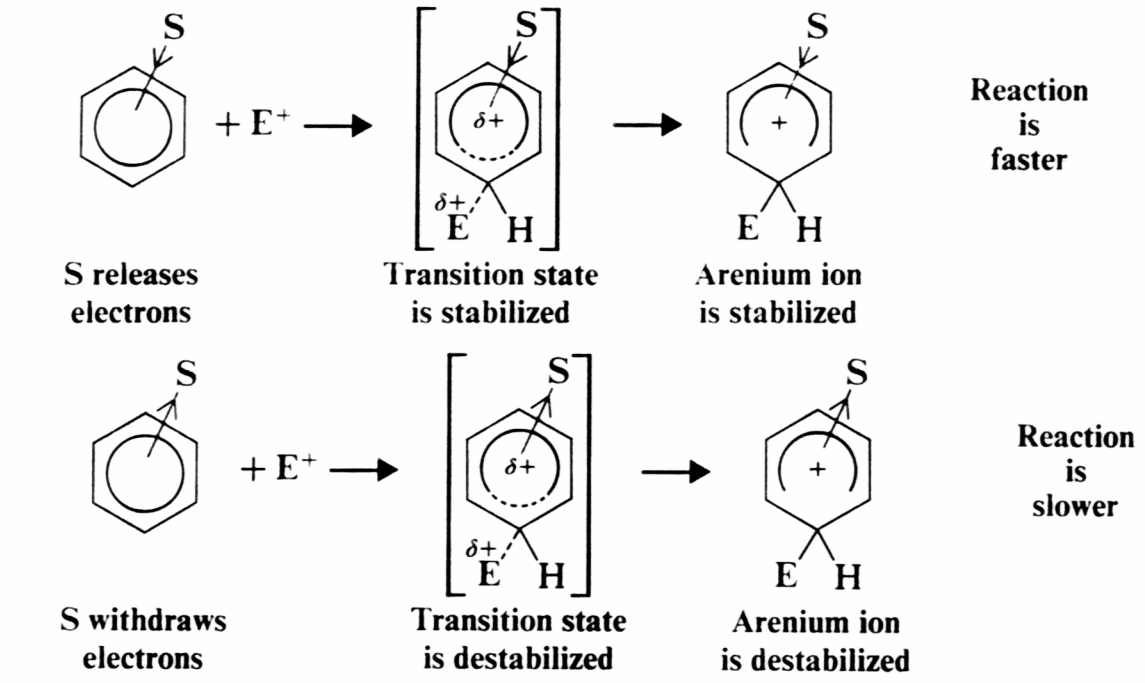

Figure 1.2. Illustration of the effects of electron-releasing and electron-withdrawing substituents on electrophilic addition reactions.

In the traditional view, the increase in reactivity following an electron-releasing substituent is explained by stabilization of the transition state relative to that of the reactants [4,5]. In the same way, an electron-withdrawing group should make the carbocation ion less stable and slow down the reaction rate. Figure 1.3 shows energy profiles for the formation of the arenium ion in the three cases where the substituent is an electron-withdrawing group, hydrogen and an electron-releasing group, respectively. One can see from the figure that the activation energy involving an electron-releasing group is lower than the activation energy involving an electron-withdrawing group. In this model differences in activation energies, and thus, differences in reaction rates are explained by differences in stabilization of the transition state and the

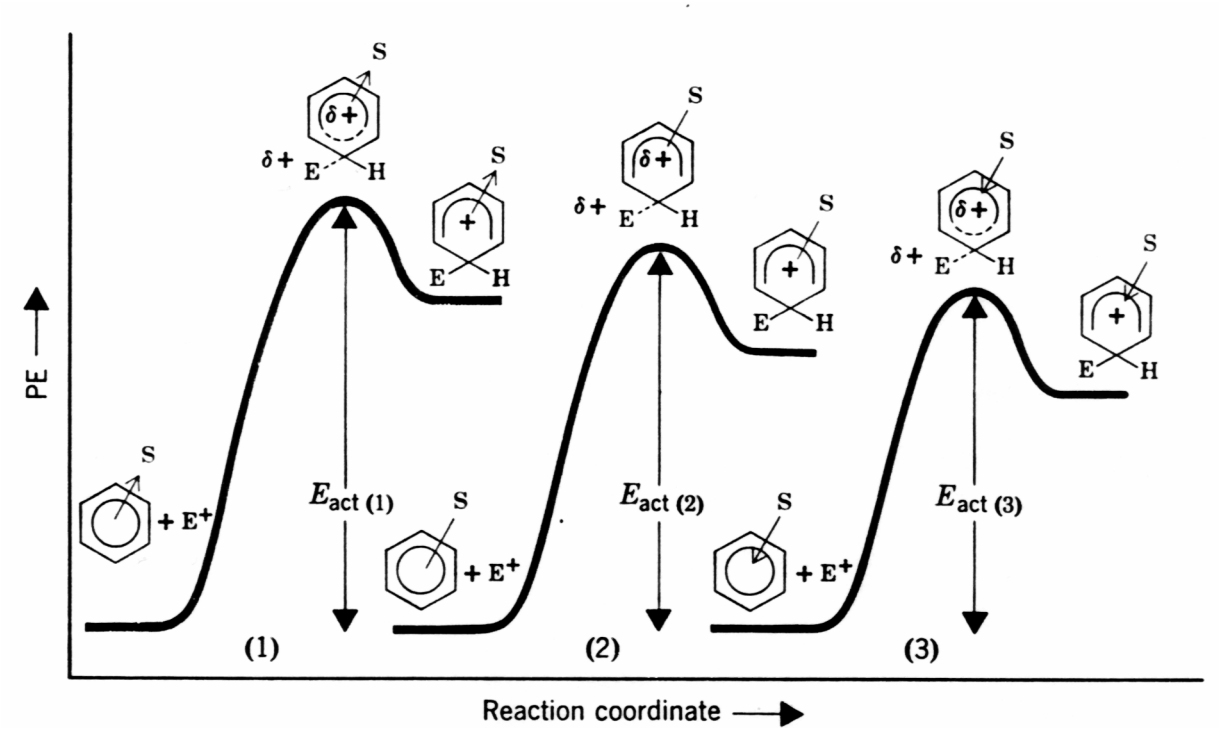

Figure 1.3. Energy profiles for the formation of the arenium ion in three electrophilic aromatic substitution reactions. In (1), S is an electron-withdrawing group. In (2), S=H, and in (3), S is an electron releasing group.

intermediate arenium ion, i.e. by the ability of the arenium ion to delocalize the positive charge. Since one methyl group increases the reactivity of the benzene ring, one would expect multiple methyl substituents to increase the reactivity even more.

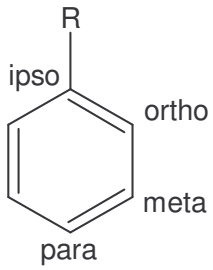

One can also divide substituent groups into two classes according to their influence on the orientation of attack by the incoming electrophile. One class is ortho-para directors, while the second class is meta directing. The different positions on the benzene ring relative to the substituent R is shown in the figure below. Methyl is an ortho-para directing substituent, meaning that

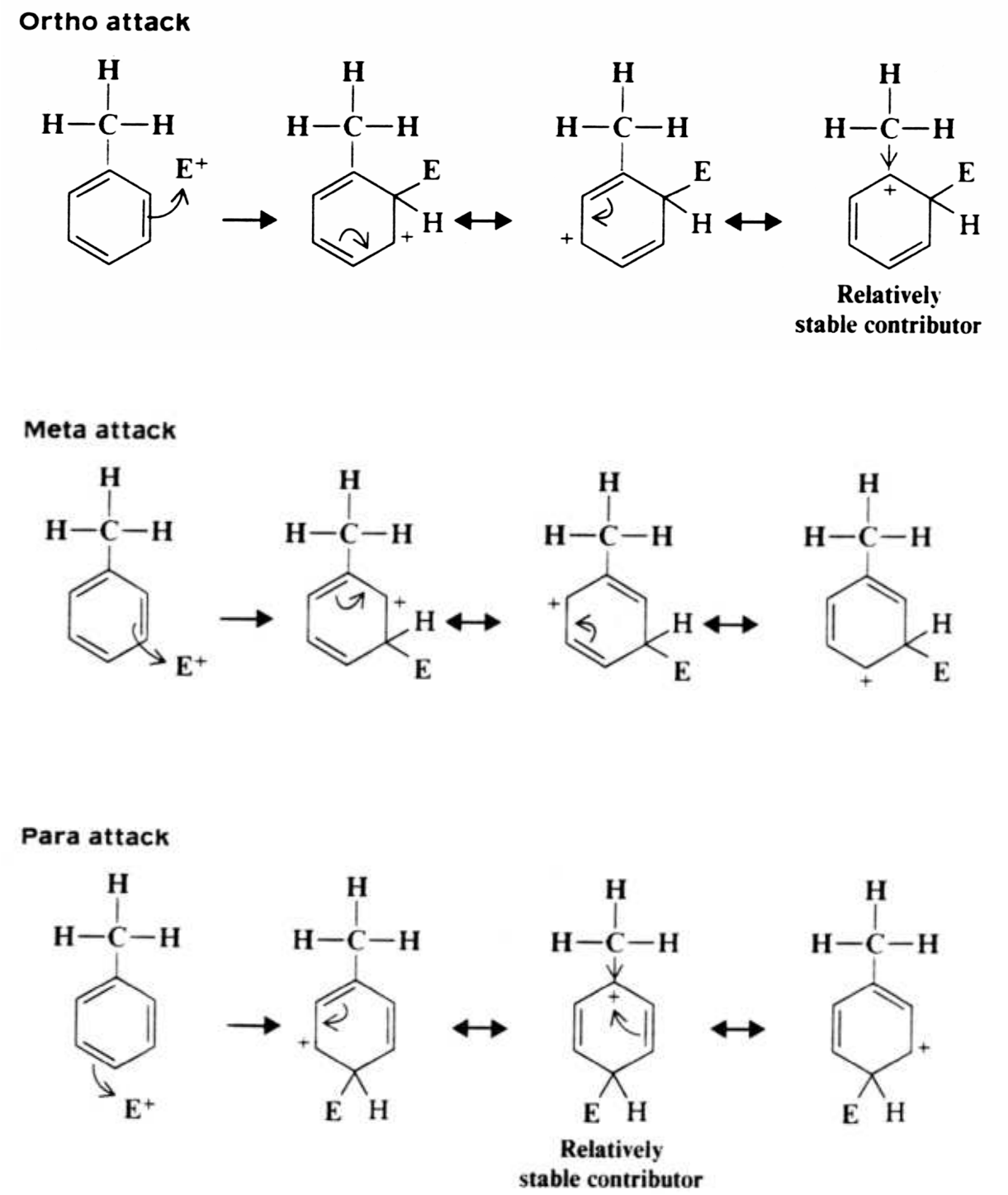

Figure 1.4. Resonance structures for the benzenium cations formed when toluene undergoes electrophilic substitution.

most of the electrophilic substitution takes place at the ortho and para positions of the ring. This can be explained by writing resonance structures for the carbocations formed in the substitution. Figure 1.4 shows the resonance structures for the benzenium ion formed from toluene. From the figure, one can see that in ortho and para attack, one can write resonance structures in which the methyl group is directly attached to a positively charged carbon of the ring. These structures are more stable than the others because in them, the stabilizing influence of the methyl group (by electron release) is most effective. Since the ortho- and para-substituted benzenium ions are more stable, the transition states leading into them occur at lower energy, and ortho and para substitution take place most rapidly.

The substitution reactions studied in this work involve two electrophilic reactions. One is substitution of tritium by hydrogen (protodetritiation) [6]:

$$T\text{-}C_6H_4\text{-}CH_3 + H^+ = H\text{-}C_6H_4\text{-}CH_3 + T^+$$

where the reaction is illustrated for toluene. The other type of reaction involves the cleavage of substituted phenyltrimethyl-silanes (protodetrimethylsilylation) [7]:

$$Me_3Si\text{-}C_6H_4\text{-}CH_3 + H^+ = H\text{-}C_6H_4\text{-}CH_3 + Me_3Si^+$$

The general features of electrophilic substitution described above apply to these specific reactions as well.

In the picture just described, relative activation energies, and thus, relative reaction rates, are rationalized in terms of differences in the ability of the intermediate ion to delocalize the positive charge. This explanation is challenged by another model, where the charge distribution in the neutral molecule is emphasized. The latter model has been applied in this work and will be described in Section 1.3.

1.2 Photoelectron spectroscopy

Electromagnetic radiation has the properties of both a wave and a particle. The radiation is usually described in terms of its energy, E, or its wavelenght, λ. The relation between these units is expressed in equation (1.1):

$$E = h\nu = \frac{hc}{\lambda} \tag{1.1}$$

where h is Planck's constant, ν is the frequency of the wave, c is the speed of light in vacuum and λ is the wavelenght of the light [12]. Photons are particles of light and with the right energy they can interact with matter. If an atom or molecule absorbs a photon, the electronic structure of the atom or molecule will adjust itself to the added quantum of energy. This process can be used to explore the different energy levels of atoms or molecules, and one can obtain useful chemical information about different species. Ultraviolet photoelectron spectroscopy (UPS) is a means of investigating the valence region of an atom or molecule, whereas x-ray photoelectron spectroscopy (XPS) probes the inner shell. Another name for XPS is ESCA, Electron Spectroscopy for Chemical Analysis. For the work conducted in this thesis, the technique of XPS was used.

In XPS, an electron ejected from a core level makes a transition into the continuum at photon energies above the ionization threshold. This is illustrated in Figure 1.5. If the electron suffers no collisions on the way, its kinetic energy E_K on leaving the molecule (or atom) is related to the binding energy E_B of the core level and the photon energy hν by:

$$E_K = h\nu - E_B \tag{1.2}$$

This relation shows that, for a fixed photon energy, the spectrum of photoelectron kinetic energies measured with an electron-energy analyzer reflects the distribution of occupied core states. Several other effects also contribute to the photoelectron spectrum; Auger-electron emission occurs at a fixed energy, independent of the photon energy, when an electron from a

higher lying state fills the core hole; satellite photoelectron peaks appear at lower kinetic energy than the main

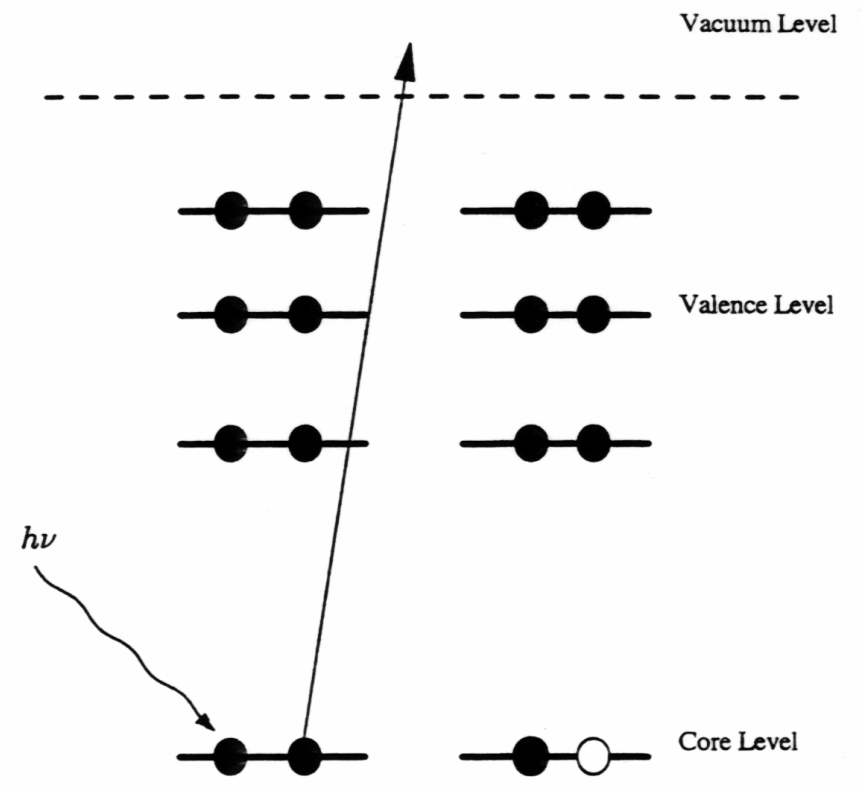

Figure 1.5. Core-level photoionization process where a core electron is ejected into the continuum via a photon of energy hν.

peak when excitation of a second electron to an unoccupied state below the ionization threshold drains away some of the incident photon energy; and the large background at low kinetic energies due to multiply scattered (secondary) electrons. The concept of Auger decay is described in Chapter 3. The other effects will not be discussed in this work.

1.3 Chemical shifts

The chemical information that is contained in a photoelectron spectrum is the ionization energy, which is found from the measured peak position. To a first approximation, the binding energy of the core levels is independent of the environment, so it identifies the atomic species. However, there are small “chemical shifts” in the binding energy that depend on the local chemical bonding. It is these energy shifts that provide chemical-state information. We will show in this work that there is a correlation between shifts in core-ionization energies and reactivity for chemically inequivalent carbon atoms in the same molecule, and also for carbon atoms in different molecules. Benzene is used as reference molecule for the methyl-substituted benzenes. Generally, a larger negative shift indicates a faster reaction, or a lower activation energy.

Proton addition:

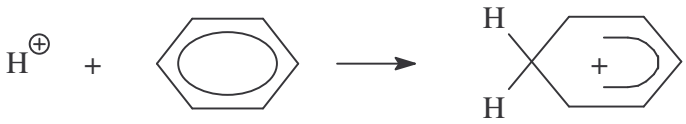

Core ionization:

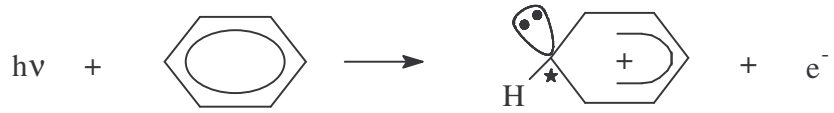

Then the question is, why do ionization energies correlate with activation energies, or the energies needed to form an arenium ion. Addition of a proton to form an arenium ion adds one excess positive charge to the molecule. Similarly, removing a core electron leaves the molecule as a +1 ion, as illustrated in the figure above. The cyclic π system is interrupted in both cases, and the two ions show similar relaxation and polarization properties. There is a considerable body of experimental data and theoretical results that support this view [3,13]. The energies

involved in the two processes are quite different, but are comparable in terms of relative energy shifts.

Historically, the shift in ionization energy between the same atom in different chemical environments has been interpreted in terms of ΔU, the difference in electrostatic energy of holes of unit positive charge localized at different nuclei. However, the ionization energy, I, depends not only on the charge distribution in the initial state of the molecule, traditionally referred to as V, but also on the rearrangement of charge in the resulting ion, R [14]. This gives:

$$\Delta I = \Delta V - \Delta R$$

for the shift in ionization energy [15-19]. V represents the energy required to remove a core electron from a molecule in which the remainder of the electron structure remains unchanged from that of the neutral molecule. In this work, ΔI is found both experimentally and theoretically, while theoretical calculations have been used to compute an accurate estimate of ΔV. Then ΔR can be found from the theoretically calculated values for ΔI and ΔV by: $\Delta R = \Delta V - \Delta I$.

Since there is a direct relationship between electrophilic reactivity and core-ionization energies, ΔI and thus, ΔV and ΔR, can be used to explain differences in reactivites. It is found that ΔV generally contributes more to the shift in ionization energy than ΔR does. That is, initial state effects are more important than relaxation of the final state for the reactivity of a molecule. The final state in core ionization corresponds to the added charge in the transition state for electrophilic reactions. This approach to explaining differences in reactivities is different from that of the traditional textbook, presented above.

Chapter 2

Synchrotron Radiation and Instrumentation

The experiments were performed both at MAX-II in Lund, Sweden and at the Advanced Light Source (ALS) in Berkeley, California. The instruments and beamlines at the two facilities are similar, and the general principles for the experiments will mainly be illustrated with reference to the MAX-II laboratory.

2.1 Synchrotron radiation

Synchrotron radiation is created by generating a hair-thin beam of electrons and accelerating them first in a linear accelerator, and then in a booster ring to nearly the speed of light. The electrons now have relativistic energies. They are stored in a storage ring with ultra high vacuum, UHV, guided by a series of bending magnets, which force them into a curved

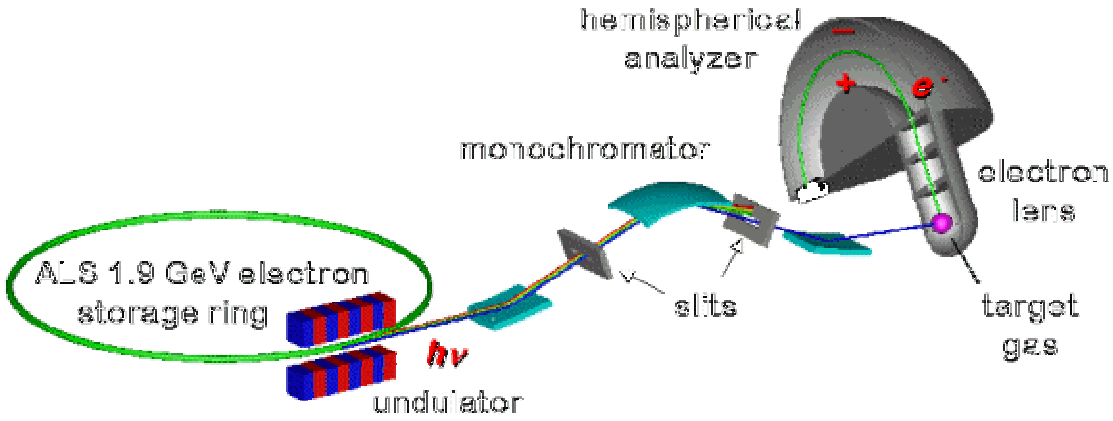

Figure 2.1. Schematic drawing of the experimental layout at a synchrotron facility, illustrated by the storage ring at the Advanced Light Source (ALS), Berkeley, California.

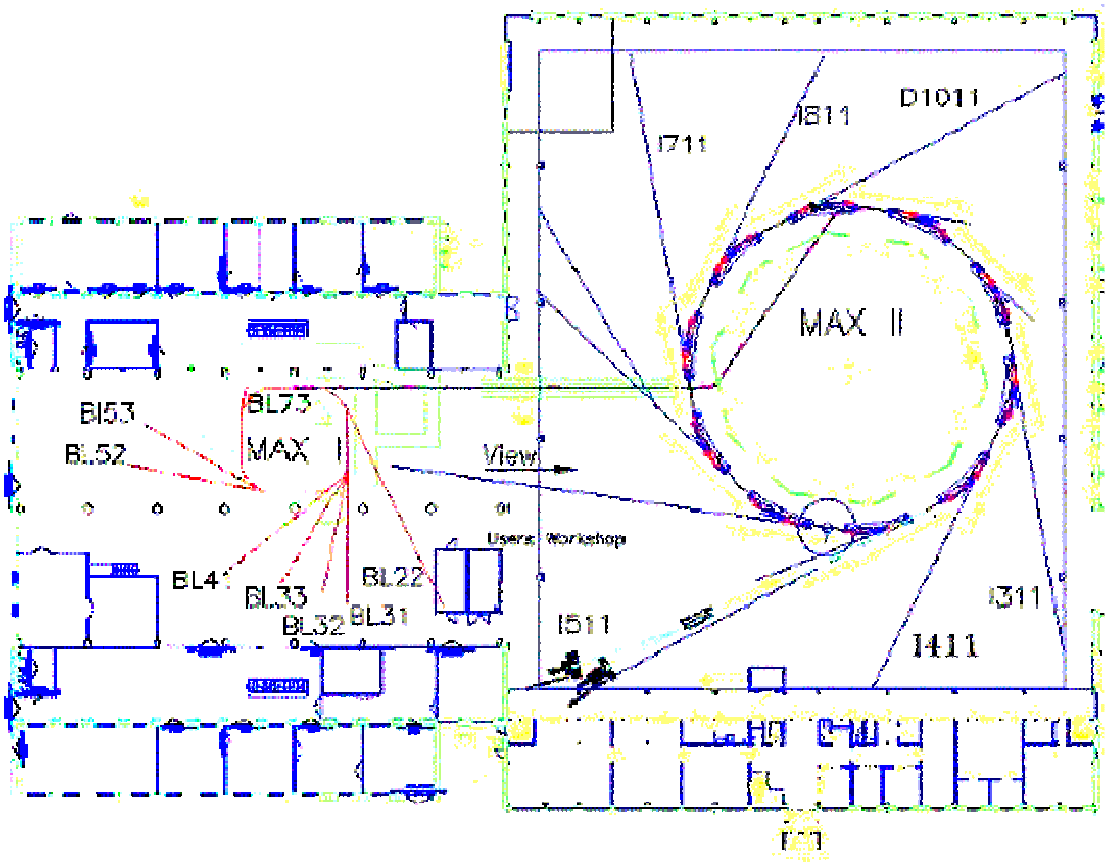

Figure 2.2. View of MAX-lab in Lund, Sweden, showing MAX-I, and the third generation storage ring, MAX-II. Experiments were performed at beamline I411.

trajectory. When their trajectories are bent by the magnetic field they emit electromagnetic radiation in the form of soft X-rays. Radiation with this wavelength, from 100 to 1000 eV, interacts strongly with most materials, and have just the right energy range for examining the atomic and electronic structure of matter. The light is directed down beamlines by focusing optics to experimental endstations. The principle of a synchrotron facility is illustrated in Figure 2.1 for the Advanced Light Source (ALS) storage ring.

Among the most important properties of synchrotron radiation are tuneability, various polarization properties and high brightness [20,21]. Brightness is defined as the flux of photons per unit source area and per unit solid angle of emission [22]. With a high brightness source, x-ray optical systems can use the photons efficiently to get the highest possible flux

onto the sample. Thus, one can afford to loose some intensity while focusing the ray down to very specific photon energies, and high-energy resolution is available in the spectra.

MAX-lab is a Swedish National Research Laboratory for research using synchrotron radiation and high-energy electrons, and for research in accelerator physics [23]. The facility is based on a race-track microtron injector, the 500 MeV electron storage ring MAX-I, and the new 1.5 GeV third generation storage ring MAX-II, as shown in Figure 2.2. Electrons are injected into the storage ring to create a 200 mA beam current, and the lifetime of the beam is more than ten hours. MAX-II has a circumference of 90 m, and consists of ten straight sections. Each straight section is equipped with an insertion device, usually a wiggler or an undulator.

2.2 The Undulator and photon-energy selection

The undulator is the only insertion device that will be discussed here. At any point in the storage ring the synchrotron radiation emerges in a narrow cone tangential to the path of the electron. Undulators are inserted in straight sections and comprise a linear array of dipole magnets with alternating polarity. The array generates a sinusoidal vertical field that drives an electron into an oscillating trajectory in the horizontal plane with the same period as the field. Each dipole is a bend-magnet source radiating along the axis of the undulator. Coherent emission of the radiation is produced from each oscillation, and constructive and destructive interference can take place. The undulator is tuneable, and the harmonics of the undulator can be changed by changing the gap between the poles of the opposing magnetic arrays. This is usually performed remotely by the user. A wide gap shifts the harmonics to higher energies while a small gap shifts them to lower energies [24]. This is illustrated for the first harmonic in Figure 2.3. The intensity is also altered by shifting the interference maxima. One should chose a gap and a harmonic that gives the best intensity of the required energy.

Beamline I411 at MAX-lab used in most of our experiments, receives its radiation from the undulator “Finnen”, which is a permanent magnet hybrid undulator with a 6 cm period. “Finnen” covers the photon energy range 50 eV to about 1500 eV [23]. At the ALS, the experiments were performed at beamline 10.0.1, which receives its radiation from an undulator with a 10 cm period.

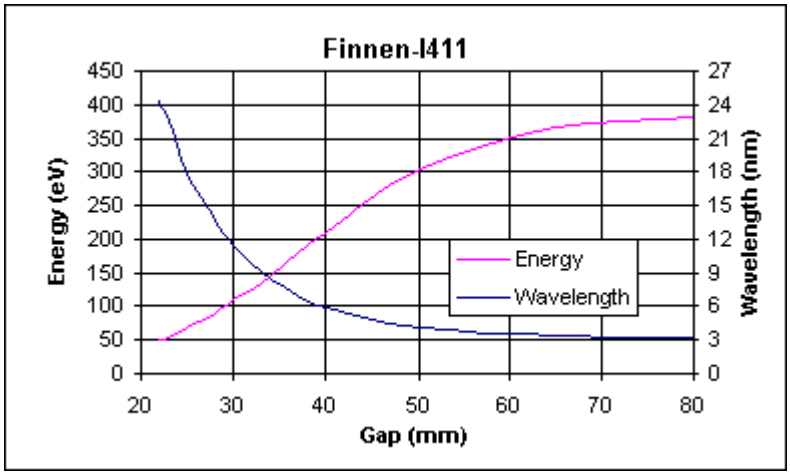

Figure 2.3. First harmonic data for the undulator "Finnen" at beamline I411 at MAX-lab.

All the experiments have been performed with a photon energy of 330 eV. This corresponds to a gap of 30.76 mm, using the third harmonic. To ionize a core electron, a photon energy higher than the binding energy of the electron is needed. Hydrocarbons have C1s ionization energies of approximately 290 eV, while fluorine-substituted hydrocarbons can reach 302 eV or more. In addition, one needs to take into account the effect of post collision interaction, PCI, which results in a broadening of the spectrum (see Chapter 3). To minimize the PCI effect, a photon energy well above threshold is needed. On the other hand, the resolution gets lower with increasing photon energy and a compromise has to be made. A photon energy of 330 eV meets the requirements and is a good compromise.

2.3 Beamline I411

When the synchrotron light leaves the storage ring, it is guided to the experimental endstation via a beamline. The components of beamline I411 are an array of focusing optics, the monochromator and a differential pumping section, as illustrated in Figure 2.4. All of the optical components must be kept under ultra-high vacuum to avoid contamination of reflecting surfaces and thereby reducing the intensity of the radiation. The monochromator is a modified SX-700 with 1220 l/mm grating and a plane-elliptical focusing mirror. The required

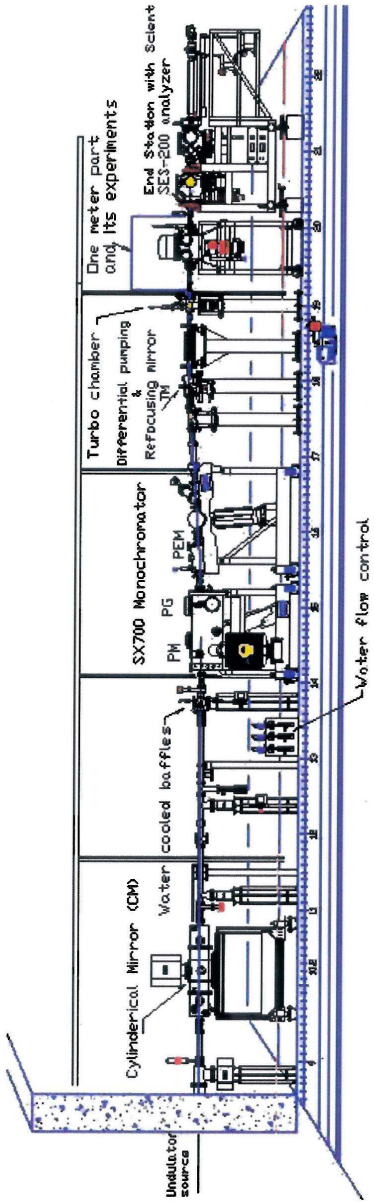

Figure 2.4. The soft x-ray gas phase beamline I411 at the MAX-II storage ring in Lund, Sweden.

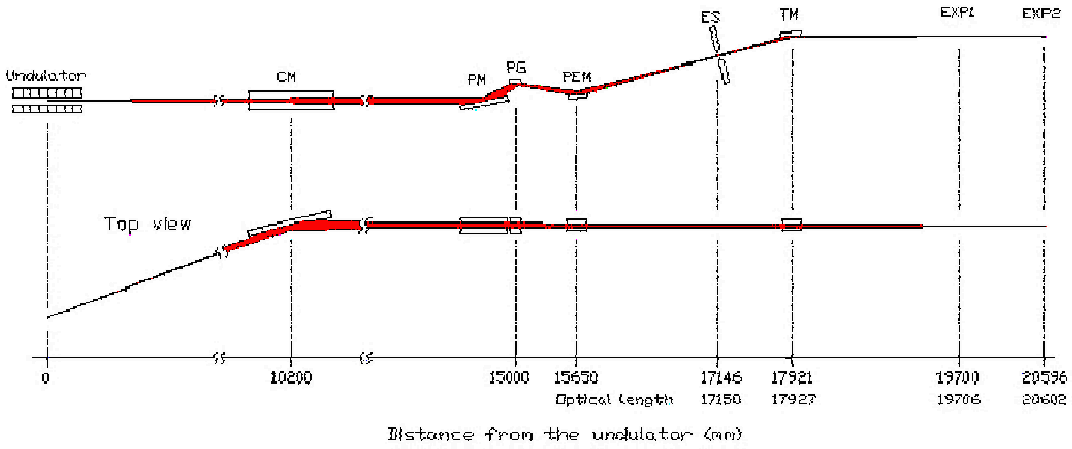

Figure 2.5. Optical layout of beamline I411 at MAX-lab.

photon energy is selected by rotating the plane grating [25]. In Figure 2.5 the optical layout of beamline I411 is shown.

The energy resolution of the monochromator, $\Delta E/E$, is 10^3-10^4. Here ΔE is the full width at half maximum, Fwhm, of the monochromatized photon beam at a selected photon energy [24]. In photoelectron spectroscopy, one wants to have as high resolution as possible. Closing the monochromator slits in order to gain resolution will decrease the intensity. A high photon flux is important for gas phase measurements due to the low density of the target sample, so a compromise has to be made. Most of our experiments were performed with a slit size of 5μm, except for the calibration spectra where a slit size of 10 μm was used to save time. For calibration, only vertical energies were used (see eq. (2.2) below), and it is then acceptable to reduce the resolution.

Even though the resolution of the monochromatized photon beam is good, the accuracy with which the actual photon energy is known is not high. A more detailed discussion of how this affects our work will be included in Section 5.1.

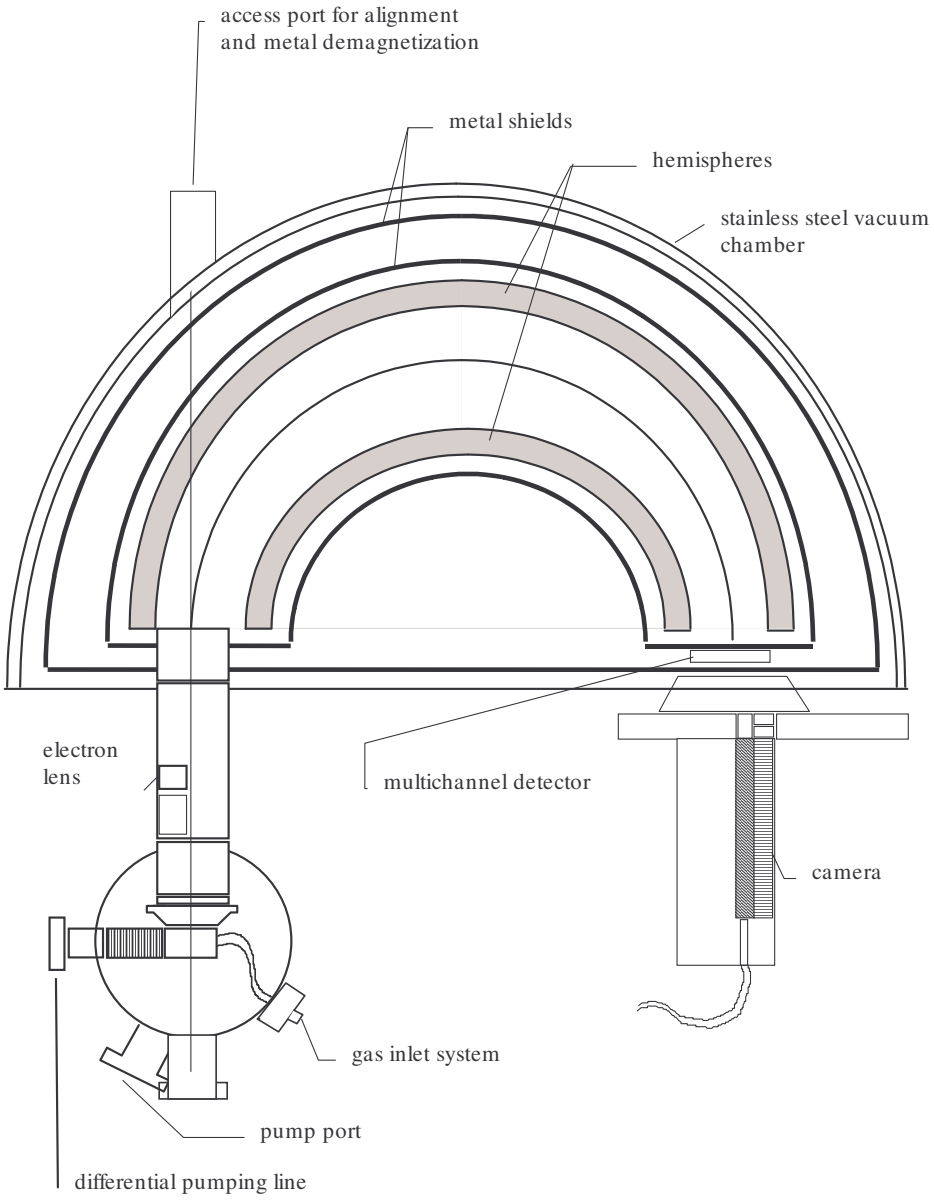

Figure 2.6. A schematic drawing of the Scienta analyzer.

2.4 Endstation

The end-station of beamline I411 has the versatility of being able to handle both solid, liquid and gaseous samples. The system consists of separate analyzer and preparation chambers accessible via a long-travel manipulator [26]. The analyzer chamber is equipped with a hemispherical electron energy analyzer (SCIENTA) which can be rotated around the

incoming beam for polarization dependent measurements [27]. A schematic drawing of the Scienta is shown in Figure 2.6.

The photoelectrons are produced in the gas cell, when the incoming light ionizes the molecules. Then the electrons enter an electron lens, where they are focused and accelerated/ retarded to a constant pass energy by varying the potential of the lens. The pass energy is the energy of an electron that will travel in a circular path at the mean radius of the analyzer. All of our experiments were performed with a pass energy of 20 meV. Since the analyzer is operating at a fixed pass energy during the acquisition of a spectrum, the chosen energy interval has to be scanned by accelerating or retarding the photoelectrons. The purpose of the analyzer is to disperse the electron trajectories with different energies by means of two half-spherical electrodes oppositely charged. Finally the electrons arrive at the multichannel detector. The detector is based on microchannel plates in a chevron configuration as an electron multiplier. The multiplied electron signal is detected as flashes on a phosphor screen by a CCD camera, and these flashes are counted by computer software which also controls the voltage scanning such that the electron lines are swept over a chosen width of the detector.

2.5 Experimental parameters

In acquiring a spectrum, there are many adjustable parameters to be set. Some of them, the undulator gap, monochromator slit and pass energy, have already been discussed. Other important parameters are step size and number of sweeps. The step size determines the distance between each point measured by the detector in the chosen energy range. Increasing the step size leads to lower resolution, while a decrease in step size requires more time for acquisition of each spectrum. Normally a step size of 0.01 eV has been used in our experiments, which is a good compromise. For the calibration spectra a wider energy range is scanned to cover the ionization energies of both the calibrant and of the compound of interest. Thus, to save time, a step size of 0.02 eV was used for calibration measurements.

When acquiring a spectrum, each new sweep is added to the previous one, and one can decide how many sweeps to sum. To avoid drift in the spectrum, we found that not more than five sweeps at a time was appropriate. Then, by the end of the acquisition, the spectra for each compound can be added to a total spectrum, after checking for possible drift.

2.6 Experimental details

All compounds used in the experiments were acquired commercially and used without further purification. The samples were transferred to a dry and clean test tube and connected to the gas inlet system. Before the experiment started, the samples were frozen down twice, with the use of liquid nitrogen, and the gas inlet system was pumped out. This was done to remove any impurities or remaining air in the sample.

The pressure in the gas cell was kept between $5 \cdot 10^{-7}$ - $1 \cdot 10^{-5}$. The pressure needs to be adjusted for each compound and each instrumental setting, to optimize the resolution and the intensity. For instance, it was found that in some experiments, increasing the pressure lead to a decrease in intensity. Normally, a higher number of gas molecules in the gas cell would lead to a higher number of electrons expelled. After the pressure is stable, one can open up for radiation in the gas cell and start acquiring spectra.

2.7 Data analysis

The experimental spectra were deconvoluted using the least squares curve-fitting program Igor Pro [28]. For core-ionization energies close to threshold, the line shape is distorted by the interaction of the low-energy photoelectron and the Auger electron. This effect of postcollision interaction, PCI, broadens a photoelectron spectrum and shifts the peak positions to a higher binding energy. PCI is described in more detail in Chapter 3. To account for this effect, the program made use of curve-fitting macros implemented by Edwin Kukk [29]. The macros allowed for analytical PCI-shapes, using the PCI-function of van der Straten, Morgenstern and Niehaus [30]. The agreement between the experimental and calculated spectrum is given by χ^2, the goodness of fit parameter. Ideally, it should be close to unity for a good fit. A short manual for the curve-fitting macro is included in Appendix A.

The parameters to be optimized in a fit are the following:

1. **En= Energy** The energy of the peak maximum.
2. **Int= Intensity** The intensity of the peak.
3. **Fwhm(L) and Fwhm(G)** Full width at half maximum of the lorentzian and gaussian components of the peak.

4. **Asym= Asymmetry** Asymmetry parameter of the PCI-shape.

The background can be defined as constant, and it can also be optimized during a fit. In performing the least squares fits, one should be careful not to end up in a local minimum. This can be avoided by increasing or decreasing the variations in the fitting parameters during optimization.

One can also specify the analytical shape of the peak. Two shapes are available- "p" is a "PCI-shape", an asymmetrically distorted Voigt profile, convoluted by a Gaussian. The second, "v", defines a pseudo Voigt shape, which is a linear combination of a Lorentzian and a Gaussian. It is less precise than the first one and does not include asymmetry. In this work, only the PCI-shape has been used.

The asymmetry parameters of the PCI-function are calculated for each peak according to relation (2.1):

$$Asym = \sqrt{13{,}6}\left(\frac{1}{\sqrt{k_e}} - \frac{1}{\sqrt{A_e}}\right) \tag{2.1}$$

where Asym is the asymmetry parameter, k_e equals the kinetic energy of the peak, and A_e is the Auger kinetic energy of the atom in eV [30]. Eq. (2.1) is not valid for photon energies very close to the ionization threshold, but is well justified for our experiments. As mentioned above, the asymmetry parameters can also be optimized in the fit.

Another feature available in the curve-fitting macro is linking of parameters. Smart linking of parameters is necessary for a successful fit. With all parameters free an excellent match to the experimental data is usually achieved, but the results do not necessarily make any sense physically. One should use all available knowledge about the spectrum to be analyzed in order to reduce the number of free parameters to a minimum. The experimental spectra and fits are presented and described in Chapter 5.

Vertical ionization energies can be found by taking the average over the vibrational profile, using the relation:

$$I(vert) = E_{avg} = \frac{\sum_n E_n I_n}{\sum_n I_n} \tag{2.2}$$

where E_n is the ionization energy of the individual peaks and I_n the intensities.

2.8 Energy calibration

This section describes the procedure used in calibrating the experimental data acquired at the ALS. The energy scale correction of the Scienta analyzer was provided by measurements of the xenon $N_{45}OO$ Auger lines. Comparing our measurements with those given by Siegbahn *et al.* [31], we found that a correction of -1.25 eV was necessary.

The asymmetry parameters of the PCI-function were calculated for each peak according to relation (2.1). The Auger energies are 250 eV for carbon and 200 eV for argon [32]. For the kinetic energies k_e we used the peak energies of the spectra before calibration of the energy scale. Testing for CO_2 we found that this only leads to a negligible error in asymmetry parameters, and does not influence the final result significantly.

Before determining an adiabatic ionization energy, one needs to correct for the shift in peak position due to PCI:

$$\Delta I(PCI) = \frac{Asym}{2} x\Gamma_L \tag{2.3}$$

where ΔI (PCI) is the shift in ionization energy, Asym is the asymmetry parameter from relation (2.1) and Γ_L is the lifetime of the respective atoms. The lifetime of Ar is 120 meV, while the lifetime of carbon atoms only attatched to hydrogen and the lifetime of carbon attached to one or more fluorine atoms is set to 95 meV and 75 meV, respectively [33]. The PCI-corrections were typically in the range 0.006-0.010 eV and did not influence the resulting adiabatic energies significantly.

Over a wide scanning range, the analyzer uses different high-voltage supplies to establish the retarding voltage. We need to check the actual voltages to do a proper calibration. There are three voltages within the Scienta instrument that takes part in measuring the kinetic energies of the electrons; A1, A2 and A8. According to voltage measurements done after the experiments, A1 and A8 were, to a good approximation, constant throughout the runs. The principle difference from run to run was in A2. The necessary voltage correction was found, by Edwin Kukk, to be:

$$Volt.corr. = 0.00014\left(I_c - I_{Ar}\right) \tag{2.4}$$

where I_C and I_{Ar} are the ionization energies of the adiabatic carbon and argon peaks respectively. The corrections are typically about 0.006 eV. The adiabatic ionization energies are then found from the equation:

$$I_{C(adiabatic)} = I_{Ar(litterature)} + (I_c - I_{Ar})_{measured} - (\Delta I_C\,(PCI) - \Delta I_{Ar}\,(PCI)) - \text{Volt. corr.} \tag{2.5}$$

when $I_{Ar(litterature)} = 248.629$ eV [34].

Chapter 3

Lineshape functions

3.1 Post-Collision Interaction

Inner-shell photoionization at energies close to threshold can result in certain types of correlation effects known as post-collision interactions (PCI). After ionization from a core orbital, the molecule (or atom) is left in an unstable state and must expend the excess energy. This can be done in two ways:

1. Fluorescence decay. An electron from a higher energy molecular (or atomic) orbital drops down into the core hole and the excess energy is emitted in the form of an x-ray.
2. Auger decay. The excess energy is carried away by a second electron, called the Auger electron, that is ejected into the continuum of the ion. For the decay of core holes of the lighter elements, the Auger process dominates.

The two decay processes are illustrated in Figure 3.1. For photon energies close to threshold the Auger electron has a much higher kinetic energy than the photoelectron and will overtake the photoelectron at some point. Thus, the slow moving photoelectron can shield the faster moving Auger electron such that there is an energy exchange between them. PCI is seen in core-photoelectron spectra as an asymmetry, a tail towards lower kinetic energy, and a broadening of the peaks. The peak maximum will also be shifted in energy. As mentioned in Section 2.7, the PCI-function of van der Straten, Morgenstern, and Niehaus [30] has been used in this work to define the analytical PCI-shapes.

3.2 Vibrational structure

Removing a core electron will, in general, change the equilibrium geometry of a molecule, i.e. alter the bond lengths and bond angles. Alterations in geometric structure tend

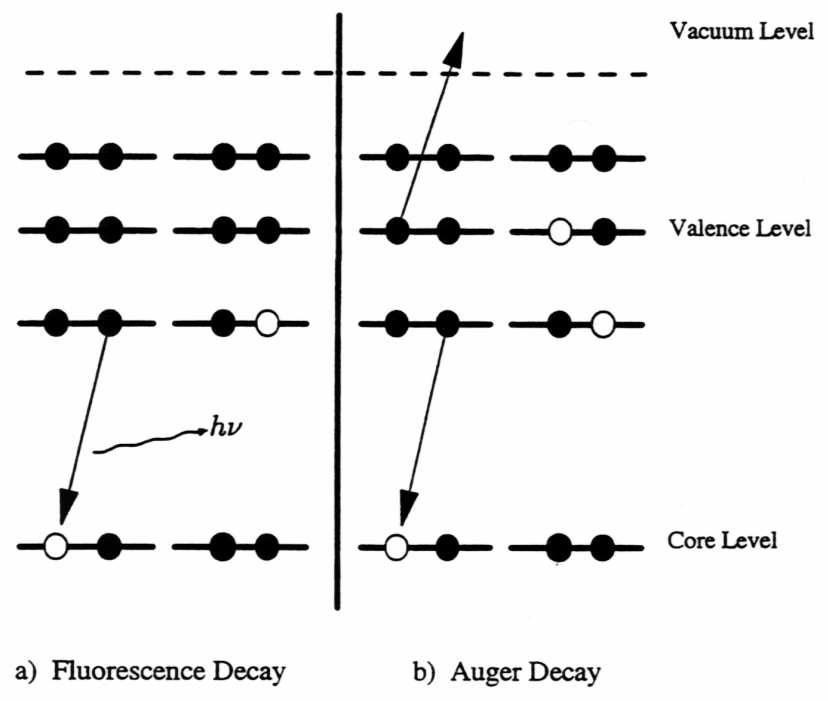

Figure 3.1. Schematic representation of two possible electronic decay mechanisms. a) X-ray emission during relaxation of a higher energy electron. b) Auger decay, where an electron is ejected when the core hole is filled.

to promote excitation of vibrational quanta in the final state. These excitations are observed as a progression of peaks at higher ionization energies. They accompany the peak corresponding to the fundamental electronic transition. The spacings between the successive peaks correspond to the characteristic vibrational frequencies of the excited state.

The analysis of vibronic transitions is based on the Franck-Condon principle which states that, because the mass of an electron is so different from that of the nuclei, an electronic transition occurs within a stationary nuclear framework. As a result, the bond length of the molecule remains unchanged during the transition. This is called a vertical transition. Once the electrons have adopted their final distribution, the nuclear locations readjust. The intensity of each vibrational peak is the square of the overlap of the ground-state and the final-state vibrational wavefunction. The successive overlaps will stimulate a vibrational progression for each electronic final state. This principle is illustrated in Figure 3.2. The figure contains a schematic drawing of three different final states. The intensity in the corresponding photoelectron spectrum is shown to the right. The two lowest states correspond to ionization

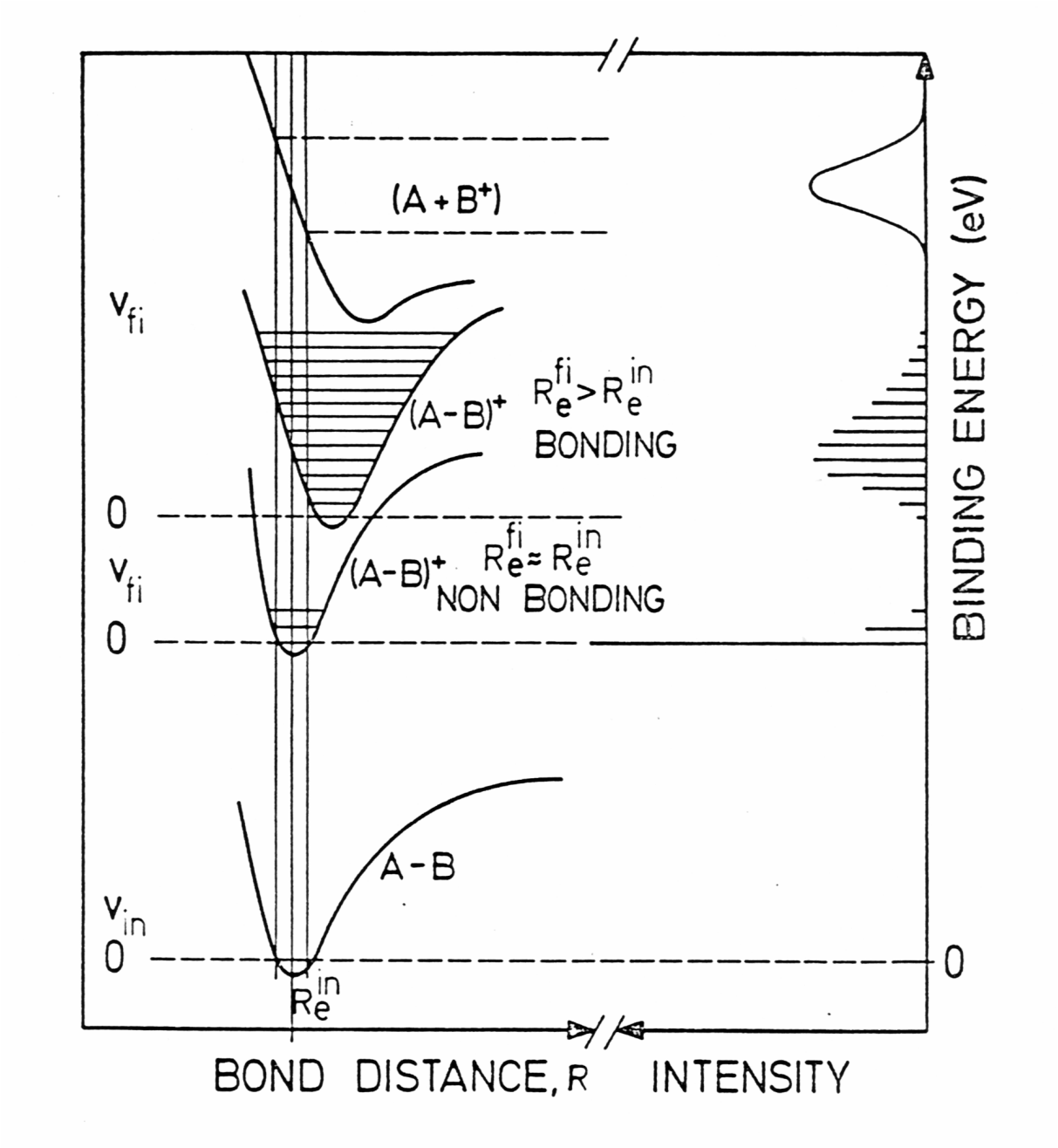

Figure 3.2. The Franck-Condon principle adapted to photoionization. Three different final states are shown for a diatomic molecule, A-B. The two lowest states correspond to ionization from a non-bonding and a bonding orbital, respectively. The uppermost curve is repulsive within the Franck-Condon area.

from a non-bonding and a bonding orbital, respectively. The uppermost curve is repulsive within the Franck-Condon area, and the photoelectron band contains no structure. If there is an increase in bond length upon ionization, a broader vibrational progression is observed. Usually, the electronic transition is very fast compared to the period of the vibrational motion and, therefore, is considered to be vertical.

The transition from $\nu=0$ in the initial state to $\nu=0$ in the final state is called an adiabatic transition. This is the first and usually the most intense peak of the vibrational progression observed in a photoelectron spectrum.

Even with the high resolution available at today's third generation synchrotrons, resolving vibrational progressions of molecules can be very difficult. Except for a few simple molecules one is dependent on extensive theoretical calculations for assignment of vibrational modes. This has been done for benzene and deuterated benzene, and the vibrational analysis is described in Section 5.2. For the methyl-substituted benzenes, the vibrational structure is a lot more complicated since the molecules contain several chemically different carbon atoms, each with its own set of excited modes. A complete theoretical vibrational analysis for the benzene derivatives is possible but was not performed in this work.

3.3 The Linear Coupling Model

The linear coupling model [8,9,35,36] permits fitting of complex vibrational envelopes in molecular spectra using a very small number of free parameters. The model assumes that the initial and final states are described by identical harmonic potential surfaces differing only in their equilibrium positions. This leads to simple expressions for both the vibrational energies and intensities (Franck-Condon factors). The vibrational energies are given by

$$E(n_1,...,n_q) = \sum_{r=1}^{q} n_r \cdot \hbar\omega_r \tag{3.1}$$

where ω_r is the vibrational frequency and n_r is the vibrational quantum number of the r*th* mode. The intensities are given by a product of Poisson distributions taken over all the totally symmetric normal modes:

$$I(o-n_1,...,0-n_q) = I(0-0,...,0-0)\cdot\prod_{r=1}^{q}\frac{S_r^{n_r}}{n_r!} \tag{3.2}$$

where I(0-n) denotes the Franck-Condon factor for the transition from ν=0 in the electronic ground state to ν'=n in the electronic final state. The so-called S factor can be thought of as an average vibrational quantum number. For any totally symmetric mode, r, we can write the intensity as:

$$I(0-n_r) = \frac{S_r^{n_r}}{n_r!}\cdot e^{-S_r} \tag{3.3}$$

where the S-factor can be determined from the photoelectron spectrum as the ratio of intensities I(0-1) / I(0-0). S_r is related to the change in normal coordinates, δ, through:

$$S_r = \frac{\delta^2\mu\omega_r}{2\hbar} \tag{3.4}$$

where μ is the reduced mass for the normal coordinate and ω is the vibrational frequency of the normal mode. For the symmetric stretching mode of A1 symmetry in methane (CH_4), involving equal changes in the bond lengths of all hydrogen atoms, δ is related to the change in bond length through:

$$\delta = \frac{1}{\sqrt{m}}\sum_{i=1}^{m}\Delta r_i = \sqrt{m}\Delta r \tag{3.5}$$

where m is the number of bonds and Δr_i is the change in each bond associated with the vibrational mode. Thus, the S factor can bee seen, via eq. (3.4) and (3.5), to be proportional to the number of C-H bonds. This implies that an S factor determined from a careful curve

fitting of methane can be scaled to predict the intensity for the same vibrational mode observed in other hydrocarbons. Expression (3.2) can be solved for one normal mode, giving:

$$\frac{I(0-n_r)}{I(0-0)} = \frac{S^{n_r}}{n_r!} \tag{3.6}$$

This method will be referred to as the linear coupling intensity model, and it has been used in Refs. 8,9,37, and 38. It is shown in other work that the model can be extrapolated for use with more complicated molecules containing both CH, CH_2 and CH_3 chemical groups [9,38].

Chapter 4
Theory

In order to interpret spectra of large molecules with complex vibrational structure, one is dependent on theoretical calculations. In this work the calculations are also used to predict shifts in ionization energies for molecules relative to benzene and to predict internal shifts between chemically different carbon atoms in each molecule. Furthermore, the initial and final state contributions to the core-ionization energies have been separated with the help of theoretical calculations. The results from the calculations are presented in Chapter 5 and in Appendix D and F.

4.1 Electronic structure calculations

Ab initio methods compute approximate solutions to the Schrödinger equation using a series of rigorous mathematical approximations [39]. No experimental data concerning the atoms or molecule are used to deduce values for the integrals, as opposed to *semi-empirical* methods [40,41]. The computations are based solely on the laws of quantum mechanics and on the values of a small number of physical constants, like the speed of light and Planck's constant.

In this work both Density Functional Theory (DFT) and the Restricted Hartree Fock method (RHF) were used, both of which are *ab initio* methods. From the RHF calculations molecular orbital energies, ε_{HF}, are obtained.

In Hartree-Fock theory the energy of the molecule has the form [42]:

$$E_{HF} = V + \langle hP \rangle + \tfrac{1}{2}\langle PJ(P) \rangle - \tfrac{1}{2}\langle PK(P) \rangle$$

where: V is the nuclear repulsion energy,
P is the spin-dependent density matrix,
<hP> is the one-electron (kinetic plus potential) energy,

½<PJ(P)> is the classical coulomb repulsion of the electrons, and
-1/2<PK(P)> is the exchange energy resulting from the indistinguishability of electrons.

In density functional theory the exact exchange (HF) for a single determinant is replaced by a more general expression, the exchange-correlation functional, which can include terms accounting for both exchange energy and the electron correlation which is omitted from Hartree-Fock theory:

$$E_{KS} = V + \langle hP \rangle + \tfrac{1}{2}\langle PJ(P) \rangle + E_X[P] + E_C[P]$$

where $E_X[P]$ is the exchange functional, and $E_C[P]$ is the correlational functional. Hartree-Fock theory is really a special case of density functional theory, with $E_X[P]$ given by the exchange integral $-1/2\langle PK(P) \rangle$ and $E_C=0$. The functionals normally used in density functional theory are integrals of some function of the density, ρ, and the density gradient, $\nabla\rho$:

$$E_X[P] = \int f_X(\rho_\alpha(r), \rho_\beta(r), \nabla\rho_\alpha(r), \nabla\rho_\beta(r))dr$$

and correspondingly for $E_C[P]$, where $\rho_\alpha(r)$ and $\rho_\beta(r)$ is the density of electrons with spin α and spin β, respectively, at position **r**. The DFT methods differ in which function f_X is used for E_X and which (if any) f_C is used for E_C.

4.1.1 The Becke3LYP method

In this work a hybrid method has been used in which the exchange functional is a linear combination of the Hartree-Fock exchange and a functional integral of the form above. It is called Becke's Three Parameter hybrid method using the LYP Correlation Functional (Becke3LYP) [43a] and the combined exchange and correlation functional has the form:

$$A*E_X^{Slater} + (1-A)*E_X^{HF} + B*\Delta E_X^{Becke} + E_C^{VWN} + C*\Delta E_C^{non\text{-}local}$$

where E_X^{Slater}, E_X^{HF}, and E_X^{Becke} are the exchange functionals of Slater [44,45,46], Hartree-Fock and Becke [47] respectively, E_C^{VWN} is the correlational functional of Vosko, Wilk and Nusair [48], and $E_C^{non\text{-}local}$ is taken from Lee, Yang, and Parr [49,50]. The constants A, B, and C are those determined by Becke by fitting to the G1 molecule set [43a-c]. The use of experimentally deduced parameters categorizes Becke3LYP as a *semi-empirical* method.

4.2 Hole-state calculations

For the core-ionized species calculations involving an inner-shell hole are not straight forward with standard packages for electronic-structure calculations. Using the variation theorem one wants to acquire as low energies as possible for the calculated orbitals [40]. In a core-ionized state this would mean relaxing a valence electron to fill the core hole, and the hole would disappear. Instead of making a calculation for a species with a core hole, the equivalent-cores approximation and the effective core potential model have been used to model a localized core hole.

4.2.1 The equivalent-cores approximation

In the equivalent-cores approximation the core-ionized carbon atom is replaced by a valence-ionized nitrogen atom, and the calculation is done for the +1 ion. This is isovalent to the core-ionized molecule and has a core charge that is the same as for the core-ionized molecule. For instance, core ionization of benzene may be written:

$$C_6H_6 + h\nu \rightarrow C^*C_5H_6^+ + e^- \qquad (4.1)$$

where C* denotes the core-ionized atom. The binding energy of the electron, E_B, is given as the difference between the energies of the final and initial state:

$$E_B = E_{C^*C5H6+} - E_{C6H6}$$

In the equivalent-cores approximation the ionization process is modelled by the following pseudo reaction:

$$C_6H_6 + h\nu \rightarrow NC_5H_6^+ + e^-$$

Taken literally, carbon is replaced by nitrogen, which amounts to a nuclear reaction where one neutron in the carbon nucleus splits into a proton and an electron. The electron subsequently fills the core hole. Hence, the pseudo reaction is not useful for estimating E_B,

because of the large and unknown energy involved in changing C* into N^+. However, the equivalent-cores approximation is useful for obtaining differences in core-electron binding energies. For example, the binding energy E_B' of a core electron in toluene may be written:

$$E_B' = E_{C^*C5H5CH3+} - E_{C6H5CH3}$$

from the corresponding core ionization:

$$C_6H_5CH_3 + h\nu \rightarrow C^*C_5H_5CH_3^+ + e^- \qquad (4.2)$$

Reversing (4.1) and adding it to (4.2) gives:

$$C^*C_5H_6^+ + C_6H_5CH_3 \rightarrow C_6H_6 + C^*C_5H_5CH_3^+ \qquad (4.3)$$

with $\Delta E_{rxn} = E_{C^*C5H7CH3+} + E_{C6H6} - E_{C6H5CH3} - E_{C^*C5H6+} = E_B' - E_B = \Delta E_B$.

Thus, an expression for the shift in binding energy between benzene and toluene is obtained from the reaction energy of (4.3). Similar to benzene, the ionization process in toluene may be modelled by:

$$C_6H_5CH_3 + h\nu \rightarrow NC_5H_5CH_3^+ + e^-$$

Reaction (4.3) may then be replaced by a similar reaction where all core-ionized species are replaced by their equivalent-core analogous:

$$NC_5H_6^+ + C_6H_5CH_3 \rightarrow C_6H_6 + NC_5H_5CH_3^+ \qquad (4.4)$$

The energy of the nuclear reaction $C^* \rightarrow N^+$ cancels in the expression for ΔE_{rxn} of (4.4), and $\Delta E_{rxn(4.4)}$ becomes equal to $\Delta E_{rxn(4.3)}$. Concluding, ΔE_B for toluene relative to benzene can be approximated by ΔE_{rxn} for the pseudo reaction (4.4).

The equivalent-cores approximation contains inherent errors, since it cannot accurately describe the interaction of the valence electrons with the core [51,52]. Thus, calculations based on this approach must rely on a cancellation of this intrinsic error by errors arising from other approximations. One problem is that the vibrational frequencies are calculated using a harmonic oscillator model. This normally results in vibrational frequencies that are higher than the observed experimental frequencies, which is also the case in this work. However, it has not been examined how well the frequency calculations within the equivalent-cores approximation can reproduce the harmonic frequencies, and the exact source of the discrepancy between calculated and experimental frequencies is not known. Another shortcoming of the model is that it does not always predict changes in bond lengths and bond angles correctly. This is an important issue as the calculated vibrational spectrum is extremely sensitive to the changes in bond lengths and angles. A different way of simulating a core hole is described in the next section.

4.2.2 Effective core potential

As an improvement over the equivalent-cores approximation one can model the effect of the core hole using an effective core potential, ECP. In this method all core-valence interactions are approximated with *l*-dependent projection operators, and a totally symmetric screening type potential. *l* is the angular momentum quantum number. The new operators, which are parametrized such that the ECP operator should reproduce atomic all-electron results, are added to the Hamiltonian and the one-electron ECP equations are obtained variationally in the same way as the usual Hartree-Fock equations. In our case ECP was used to describe the core orbitals containing a core hole in a simple way.

Similar problems as with the equivalent-cores approximation arise in this method. Vibrational frequencies higher than the observed experimental frequencies are obtained. Scaling each frequency individually by empirical constants is a common way of handling the problem and has also been done in this work. Secondly, the predicted changes in bond lengths and bond angles are not accurate compared to experimental observations. It is possible to adjust the bond lengths according to experimental data, but this has not been done in this work. Still, the changes in bond lengths and bond angles obtained from the ECP model are more correct than those obtained from the equivalent cores approximation.

The two methods just described for modelling a core hole will be compared in Section 5.4.

4.3 Effects of initial-state potential on core-ionization energies

It is often desirable to separate the initial-state contribution, ΔV, from that caused by relaxation of the final state, ΔR, in order to obtain chemical insight from shifts in core-ionization energies. These quantities are related through: $\Delta I = \Delta V - \Delta R$, where ΔI is ionization energy, ΔV is initial state potential energy and ΔR is relaxation energy of the final state.

ΔV can be estimated from Hartree-Fock orbital energies or from electrostatic potentials at nuclear positions. However, both these approaches suffer from shortcomings and a reformulation for V has been developed by Børve and Thomas [14]. Koopmans' theorem states that within Hartree-Fock theory the orbital energy ε_{HF} of a core orbital φ_c is the negative of the ionization potential for the removal of an electron from that orbital [40]:

$$I_c \approx -\varepsilon_{HF}$$

The theorem rests on the assumption that on ionization the remaining electrons do not adjust their positions to the new potential in the ion. In [14] Koopmans' theorem as applied to core-ionization is extended to the class of valence-correlated wave functions and used to formulate an accurate estimator of the energy needed to remove a core electron without rearrangement of spectator electrons. When used to compute initial-state effects in shifts of ionization energies, an accurate and simple approximation to this theorem is given by:

$$\Delta V^{EKT} \approx -\Delta\varepsilon_{HF} + (\Delta U^{VCI} - \Delta U^{HF}) \qquad (4.5)$$

where $-\Delta\varepsilon_{HF}$ is the shift in orbital energies computed using Koopmans' theorem, and ΔU^{VCI} and ΔU^{HF} are differences in electrostatic energies of holes of unit positive charge computed at the atom to be ionized, obtained at the valence-correlated and Hartree-Fock levels respectively. In other words the shift in core orbital energy is corrected for the effect of electron correlation by adding the difference between potential-model estimates computed from correlated and Hartree-Fock-based electrostatic potential, respectively. This simple approximation is found to give results in very good agreement with the extended Koopmans' theorem and has been used in this work to estimate ΔV. Then ΔR can be found from ΔI and ΔV by: $\Delta R = \Delta V - \Delta I$.

4.4 Normal-mode calculations

In this work normal mode calculations have been restricted to benzene and deutero-benzene, and the results are presented in Section 5.2. For polyatomic molecules calculation of Franck-Condon factors is complicated because the normal modes of the ground state are not the same as those of the core-ionized molecule. However, under the conditions of our experiment, it is assumed that the vibrational structure can be predicted by using a simple Franck-Condon model [8,54], described below. In this case molecular geometries, normal modes, and vibrational frequencies of both the initial and core-ionized molecules are required.

Table 4.1. Correlation table for the species of the D_{6h} group and its subgroups [53].

D_{6h}	A_{1g}	A_{2g}	B_{1g}	B_{2g}	E_{1g}	E_{2g}	A_{1u}	A_{2u}	B_{1u}	B_{2u}	E_{1u}	E_{2u}
C_{2v}	A_1	B_1	A_2	B_2	$A_2 + B_2$	$A_1 + B_1$	A_2	B_2	A_1	B_1	$A_1 + B_1$	$A_2 + B_2$

Gaussian calculations [55] give all the basic information needed, and from these the change in geometry along each normal coordinate can be calculated. Then Franck-Condon factors are calculated in the harmonic oscillator approximation. The calculated vibrational energies are generally found to be larger than the experimental values by around 10% [8], due to anharmonicity not included in the model. In this work the computed frequencies are scaled individually by empirical constants. Since the fundamental frequencies are known from IR measurements [56] for the ground state, these can be used, together with the calculated ground-state frequencies, to form scaling factors to apply to the calculated vibrational frequencies of the core-ionized molecules. To identify the individual normal modes and their frequencies in the ground state and final state, a program made available to us by Knut Børve was applied [57], where Gaussian output files for both states are used as input. The program allows for individual scaling of the frequencies, performes Franck-Condon analysis for the totally symmetric modes, and provides computation of change in normal coordinate, Δq, and intensities for the modes of interest. The scaling factors were found to range from 0.953 to 1.008 for benzene, and from 0.955 to 1.007 for deuterated benzene. It happens that modes close in vibrational frequency switch places during the frequency analysis, and to identify corresponding modes, Table 4.1 was used [53].

For the probability of excitation to a combination mode, one takes the product of the corresponding single Franck-Condon factors; for the energy of the combination mode the sum of the energies of each of the contributing modes are used. This is formulated in equations (3.1) and (3.2). From these results the intensity and energy of all significant combinations are generated.

4.5 Computational details

All calculations were performed using the Gaussian 94 program package [55] and the double-zeta basis set *d*95(*p*, *d*) of Dunning and Huzinaga [58,59]. This basis set has been used earlier with success in similar calculations [9,38,54]. Gaussian 94 was also used to compute normal modes and harmonic frequencies which were used as input to the Franck-Condon analysis.

In both DFT and RHF calculations geometries were optimized for the ground state. Benzene has D_{6h} symmetry. The dimethyl-substituted benzenes have C_{2v} symmetry, while toluene has C_s and mesitylene C_{3h} symmetry.

For molecules with several chemically different carbon atoms the final state binding energy for every non-equivalent position has to be calculated. If the molecule is fixed in the initial state geometry, no geometry optimization is done for the final state, and only vertical energy shifts are predicted. In order to obtain adiabatic ionization energies, the final state geometries were optimized. In most cases, this had to be done in a lower order point group than the neutral molecule, usually C_s or C_1. Only in cases where the ionized carbon is located on the two-fold axis is the symmetry conserved.

All calculations within the equivalent-cores approximation and within the ECP model were performed at the DFT level of accuracy and with basis sets as described above. In the equivalent cores model, only vertical energies were computed. For the ECP calculations the compact core potential by Stevens *et al.* [60] was used, scaled to account for only a single 1s electron as discussed by Karlsen and Børve [61]. Both adiabatic and vertical energies were calculated within the ECP approach.

During the vibrational analysis for benzene in Chapter 5 it was noticed that the chosen ECP in combination with the *d*95(*p*, *d*) basis set did not predict bond lengths as well as anticipated. As mentioned above a correct prediction of geometry changes is extremely important in calculation of Franck-Condon factors. A series of test calculations was therefore performed for core-ionized methane at the correct C-H bond length. Both carbon and nitrogen basis sets were used. A minimum energy was found with a scaling factor of 0.945 using the N-basis set. For the C-basis set a scaling factor much less than this was found for the minimum energy. It was therefore decided to use the N-basis set for the core-ionized carbon atom in the vibrational analysis of benzene.

Chapter 5

Results and discussion

5.1 Calibration

Section 5.1 presents both results of calibration work done on a series of small molecules and calibration results for the methyl-substituted benzenes.

5.1.1 Calibration of several small molecules

This section presents and discusses the results of calibration work done on several small molecules. All the experiments were performed at the Advanced Light Source (ALS). Our primary concern is to establish accurate C1s ionization energies for CO_2 and CF_4. These are compounds most often used for internal calibration. In addition we have calibrated a series of small molecules of general chemical interest. These include carbon monoxide CO, the fluoromethanes CH_3F and CHF_3, and the hydrocarbons methane CH_4, ethane C_2H_6, ethene C_2H_4, and ethyne C_2H_2.

In most experimental work calibration is important. Imperfections and instabilities in measuring devices cause instrument errors. It is therefore important to establish suitable calibration procedures to enable direct comparison of data obtained from different instruments and laboratories. Absolute values are also necessary to ensure exact analysis of the experimental data.

The chemical information contained in a photoelectron spectrum is the ionization energy, which is found as the difference between the photon energy and the kinetic energy of the expelled electrons. In traditional x-ray photoelectron spectroscopy, the x-ray (photon) energy is accurately known, and techniques have been developed for accurate measurement of the electron kinetic energies [62,63,64]. The accuracy that can be obtained is better than 0.05 eV, and measurements made at different laboratories usually agree well within this uncertainty. The limitation of the laboratory sources is, however, the resolution, and for a

molecule the measurement represents an average over the vibrational profile, or, in other terms, the vertical ionization energies.

With synchrotron radiation, on the other hand, the accuracy with which the photon energy is known is not high. For a given setting of the monochromator, the apparent photon energy may change from one day to the next by a large fraction of an electron volt. Also if one is working away from the region in which the monochromator has been calibrated, the photon energy may be absolutely in error by an electron volt or more. Thus, for accurate measurements of ionization energies, it is necessary to include an internal standard for which the ionization energy is well known.

A good standard calibrant should have it's peak close to the compound of interest, but not overlapping. In addition, it should be available at a low cost. Both CO_2 and CF_4 meet these requirements for the measurement of C1s energies. However, in a previous study, where CF_4 was used as calibrant, a consistent discrepancy was noticed between the measured ionization energies and the ones obtained from traditional x-ray photoelectron spectroscopy [65]. This might be due to a small but unknown vibrational excitation in CF_4. A vibrational progression is clearly visible in the spectrum of CO_2 [66]. In this work it was therefore decided to use argon as the primary standard. Since Ar is monoatomic, there is no vibrational excitation and the vertical and adiabatic energies are identical. The ionization energy of Ar $2p_{3/2}$, 248.629 eV, lies 40-50 eV away from the C1s ionization energies, and is well known from the litterature [34]. In this study Ar was mixed with the compound of interest, including CO_2 and CF_4. For the methyl-substituted benzenes measured at MAX II, CO_2 was used as internal standard with ionization energies as obtained from the ALS measurements. The procedures for analysis of the data and correction of the energy scale are described in sections 2.7 and 2.8.

5.1.1.1 Results

We will only make short comments to each of the individual fits, since the main emphasis of this chapter is the calibration results. Generally, available knowledge about the molecular symmetry, vibrational energies and theoretical calculations is used to reduce the number of free parameters in each fit to a minimum. The spectra of the investigated molecules are shown in Figures 5.1-5.10. The points show the experimental spectrum and the lines through the points show the results of least-squares fit to the data. The contribution from vibrational excitation is also included in the spectra. Table 5.1 presents the energy corrections

Table 5.1. Experimental data and calculated energy corrections for calibration of the molecules in consideration. Adiabatic ionization energies (eV) for C1s.

Molecule	I_C (meas.)	$Asym_C$	ΔI_C (PCI)	I_{Ar} (meas.)	$Asym_{Ar}$	ΔI_{Ar} (PCI)	Volt. corr.	I_C (adiab)
Methane	292.116	0.3660	0.0174	250.054	0.1517	0.0091	0.0059	290.689
Ethane	291.674	0.3625	0.0172	249.756	0.1509	0.0091	0.0059	290.545
Ethene	292.141	0.3624	0.0172	250.073	0.1517	0.0091	0.0059	290.695
Ethyne	[a]292.653	0.3701	0.0176	250.103	0.1518	0.0091	0.0060	291.176
CO	297.202	0.4107	0.0195	249.758	0.1510	0.0091	0.0066	296.069
CO_2	299.325	0.4153	0.0197	250.286	0.1523	0.0091	0.0069	297.664
CF_4	303.022	0.4770	0.0179	249.752	0.1509	0.0091	0.0075	301.898
CH_3F	295.143	0.3914	0.0147	250.295	0.1523	0.0091	0.0063	293.478
CHF_3	300.809	0.4495	0.0169	250.293	0.1523	0.0091	0.0071	299.144

[a] Gerade peak.

and the resulting adiabatic energies, and Table 5.2 presents the intensities and the appropriate linking for the peaks of the different fits. The full width at half maximum, Fwhm, and asymmetry parameters from the fits are given in Appendix B.

Figure 5.1 shows the methane spectrum, which was fitted with no linking since this is a relatively simple spectrum with only the symmetric C-H stretching mode excited [8,66]. As a result of the high resolution, the peaks are well separated. We obtain an almost constant energy separation between the four peaks, ca. 400 meV, which is consistent with theoretical calculations [66,67]. The S-factor of 0.428 is in good agreement with recent results [66], and we obtain a low χ^2 (0.63) for the fit.

In Figure 5.2 the ethane spectrum and the fit are shown. The energies and the intensities are linked, so that the pairs of peaks, 010/000 and 110/100, have equal spacing and equal intensity ratios. The assignment is based on theoretical calculations [8]. ν_2 (010) is a C-C-H bending mode for the hydrogens attached to the spectator carbon. The next peak is the C-H stretching mode, ν_1 (100), of the core-ionized carbon. Finally, peak number four (110) is

Table 5.2. C1s ionization energies, I_C, and intensities of the vibrational progression. I_C (vert) are the vertical ionization energies. All energies in eV.

Molecule	Peak	I_C	Linking[b]	Intensity	Linking[b]	I_C (vert)
Methane	1	290.689	-	2313	-	290.844
	2	291.089	-	990	-	
	3	291.488	-	161	-	
	4	291.892	-	13	-	
Ethane	1	290.545	-	1647	-	290.711
	2	290.727	-	301	-	
	3	290.945	-	652	-	
	4	291.127	3+2-1	119	(1)*3*2/1	
	5	291.348	-	85	-	
	6	291.531	5+2-1	16	(1)*5*2/1	
Ethene	1	290.695	-	2314	-	290.823
	2	290.884	-	733	-	
	3	291.095	-	539	-	
	4	291.284	3+2-1	171	(1)*3*2/1	
	5	291.509	-	27	-	
	6	291.698	5+2-1	8	(1)*5*2/1	
Ethyne	1	[a]291.176	-	2675	-	291.264
	2	291.074	(-0.102)+1	2055	(0.768)*1	
	3	291.332	(0.156)+1	910	(0.340)*1	
	4	291.440	(0.264)+1	1078	(0.403)*1	
	5	291.511	(0.335)+1	264	(0.0985)*1	
	6	291.703	(0.527)+1	305	(0.114)*1	
	7	291.589	(0.414)+1	250	(0.0935)*1	
	8	291.769	(0.593)+1	114	(0.0425)*1	
	9	291.847	(0.671)+1	54	(0.0201)*1	
CO	1	296.069	-	1980	-	296.229
	2	296.374	-	1193	-	
	3	296.676	-	282	-	
	4	296.962	-	25	-	
CO_2	1	297.664	-	3138	-	297.699
	2	297.830	(0.1656)+1	746	-	
	3	297.995	(0.1656)+2	42	-	
	4	298.161	(0.1656)+3	1	-	
CF_4	1	301.898	-	2207	-	301.898
CH_3F	1	293.478	-	1079	-	293.557
	2	293.868	-	240	-	
	3	294.280	-	16	-	
CHF_3	1	299.144	-	1252	-	299.155
	2	299.298	-	95	-	

[a] Gerade peak. [b]The number in parenthesis shows the factor added/subtracted or multiplied. The other numbers show the linking of the peaks.

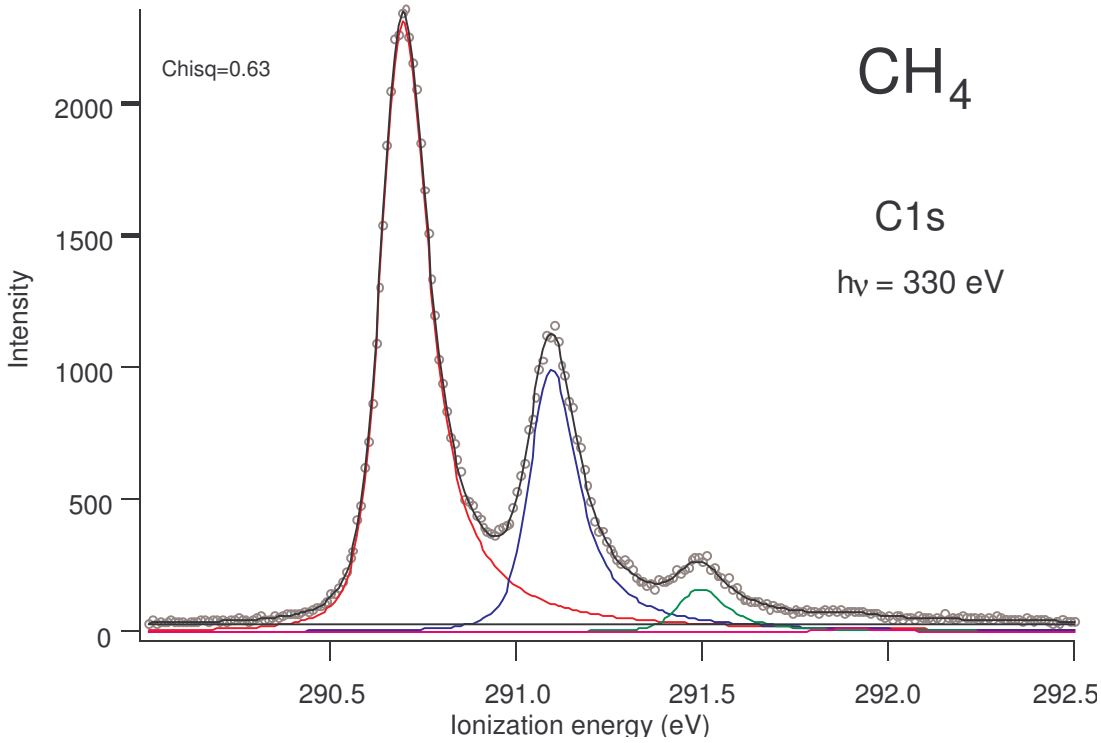

Figure 5.1. C1s photoelectron spectrum of methane.

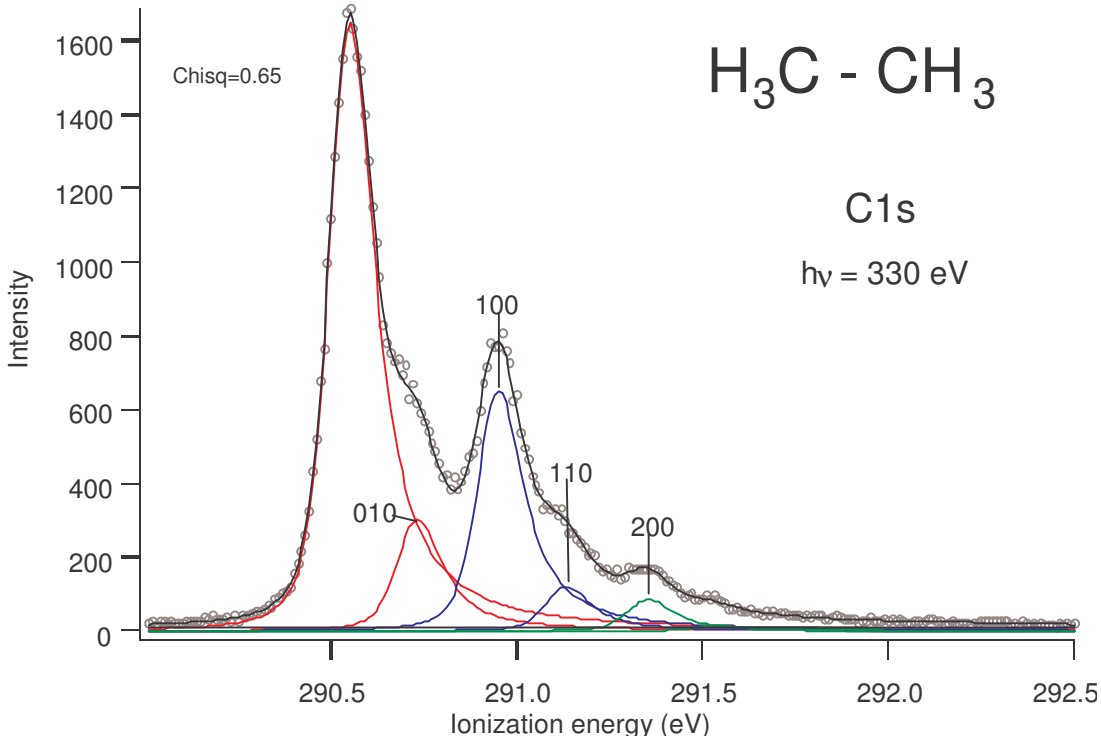

Figure 5.2. C1s photoelectron spectrum of ethane.

a combination mode of the two first ones. The resulting fit is in good agreement with the experimental spectrum.

The spectrum and fit of the ethene molecule is presented in Figure 5.3. Also in this fit we used theoretical calculations [8] to determine the peaks to be linked. Only the most intense modes are included. ν_4 (0001) involves H-C-H bending primarily on the spectator carbon. ν_1 (1000) is a local C-H stretching mode for the hydrogens attatched to the core-ionized carbon, while peak number four (1001) is a combination mode of the two. The fit is in good agreement with the experimental curve.

Figure 5.4 shows the experimental and calculated curves of the ethyne spectrum. The energies and intensities are all linked and scaled according to Franck Condon factors calculated by Thomas *et al.* [8]. The adiabatic peak is splitted into one σ_u and one σ_g orbital, of about 100 meV energy difference [68]. The u-g split high-energy shoulder arises from a C-C stretching mode. Theoretical calculations show that other modes are only weakly or not excited [8]. The resulting fit has a higher χ^2 (3.89) than the preceding fits, indicating limitations of the employed theoretical model.

The spectrum of CO is shown in Figure 5.5, and since the peaks are well separated, linking is not necessary in this fit. The vibrational mode excited here is the C-O stretching. A good fit to the experimental data is obtained.

Figure 5.6 shows the spectrum of CO_2. The linking parameters of the energy separation of the peaks, 165.6 meV, is taken from a previous fit of high resolution data [69], and the resulting fit is in good agreement with the experimental spectrum. In this fit the asymmetry parameters, according to relation (2.1), are corrected for the new, calibrated kinetic energies of the different peaks. However, this correction had only negligible influence on the final energies, as only a shift of +1 meV was found. The vibrational energies and intensity ratios found in this fit were later used to fit the calibration spectra of the benzene derivatives.

CF_4 is fitted with only one peak, as shown in Figure 5.7. A fit with two peaks, separated by 100 meV, was also tried, since a small vibrational peak is predicted by theory [70]. The difference in adiabatic energies of the two fits were only 3 meV. For simplicity, the former fit was chosen, even though fitting with two peaks gives a slightly better χ^2.

Figure 5.8 shows the spectrum and fit of CHF_3. To keep the gaussian Fwhm from getting too small, we had to set the lorentzian width fixed at 79 meV [33]. The small

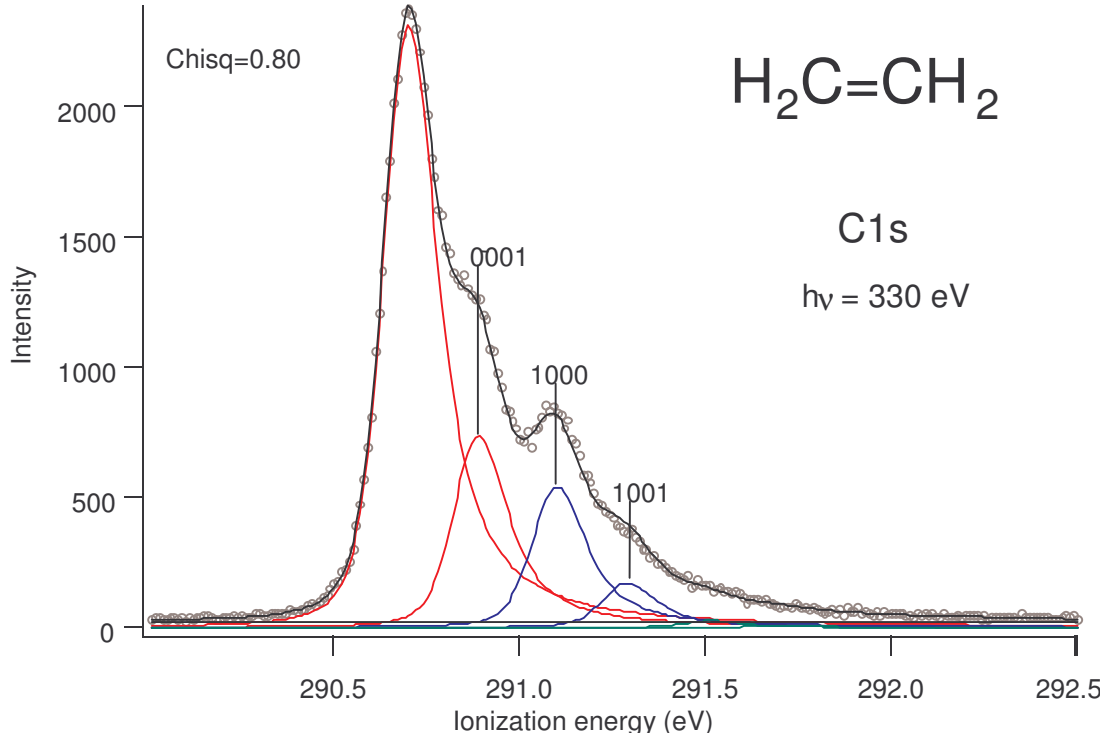

Figure 5.3. C1s photoelectron spectrum of ethene.

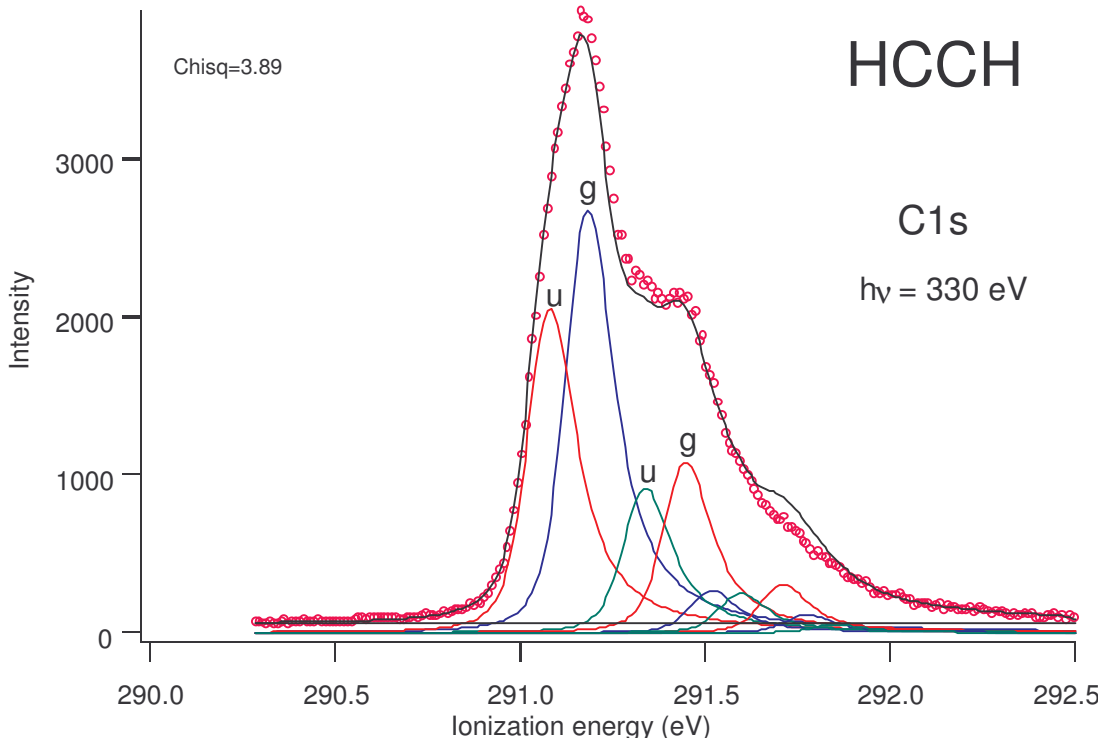

Figure 5.4. C1s photoelectron spectrum of ethyne.

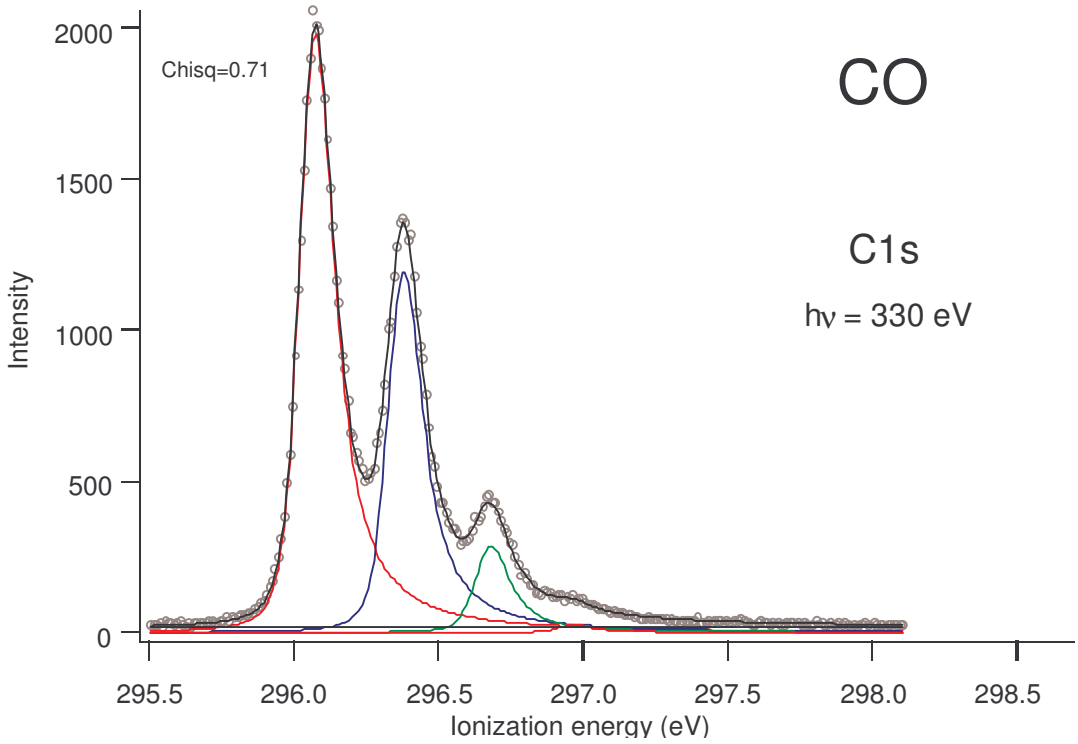

Figure 5.5. C1s photoelectron spectrum of CO.

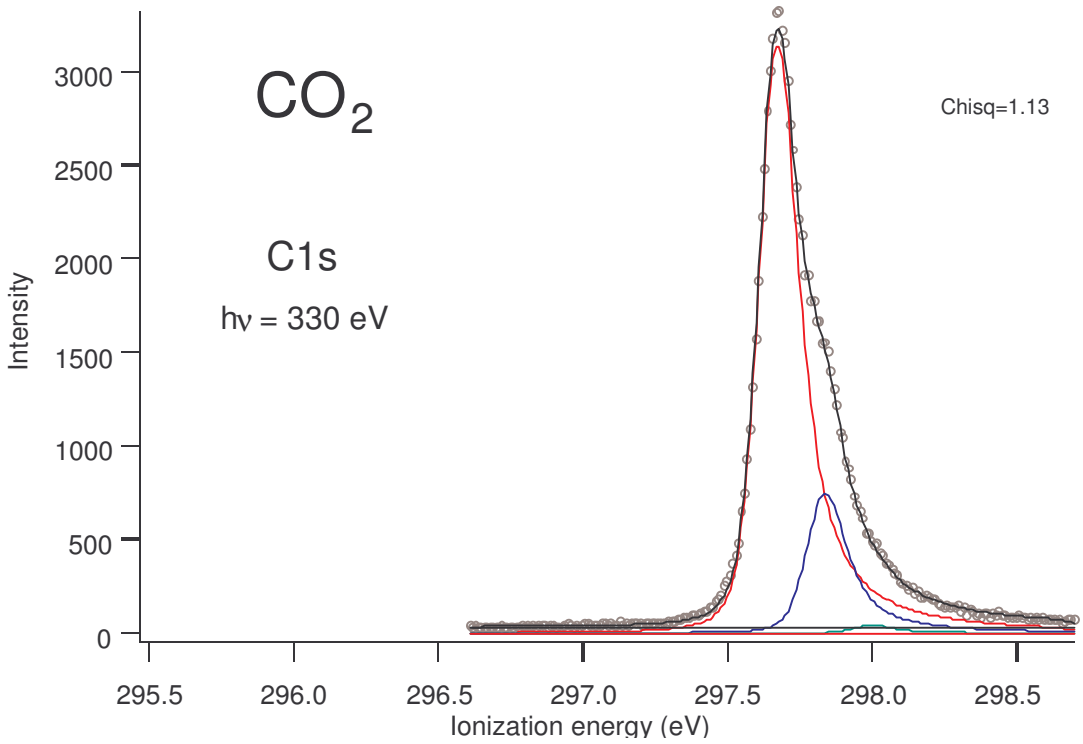

Figure 5.6. C1s photoelectron spectrum of CO_2.

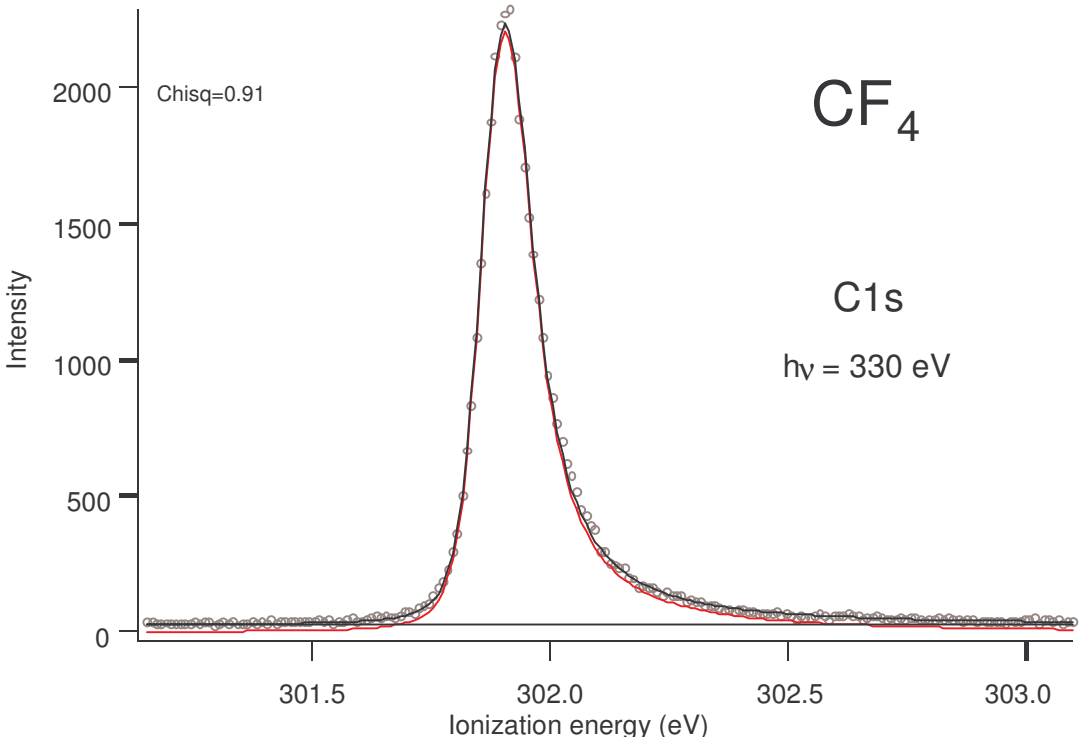

Figure 5.7. C1s photoelectron spectrum of CF_4.

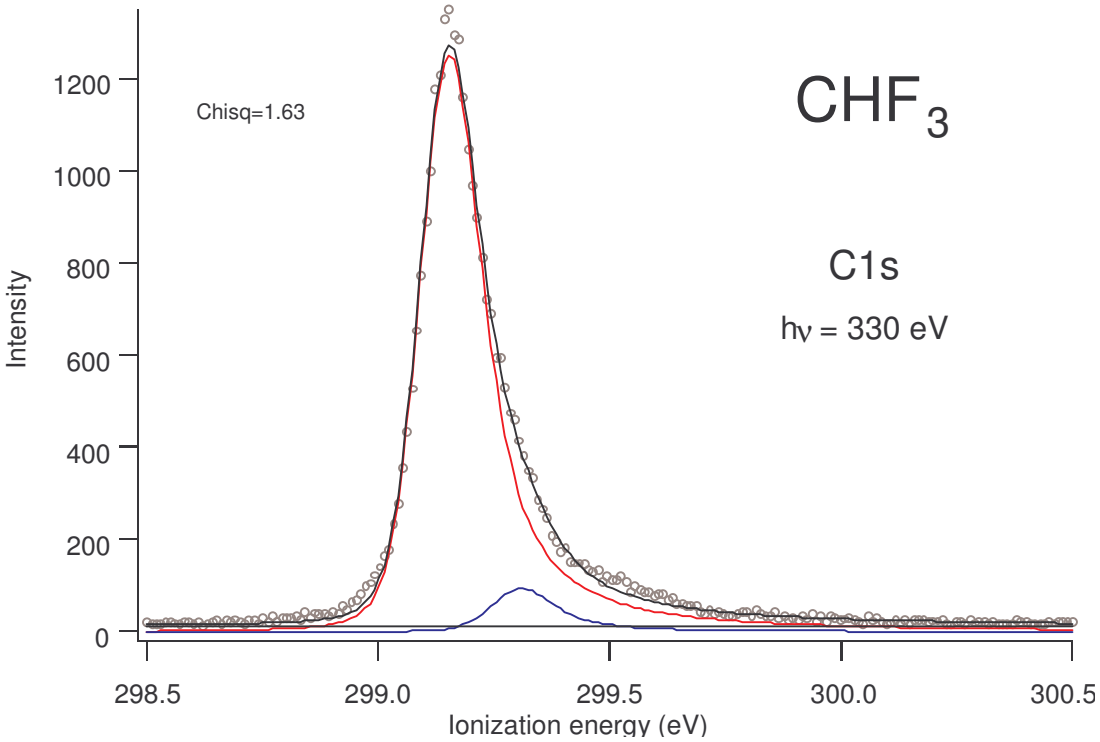

Figure 5.8. C1s photoelectron spectrum of CHF_3.

vibrational peak is separated from the main peak by 154 meV. This corresponds to the C-F stretching mode [56]. The C-H stretch is not included in the fit.

The spectrum and fit of CH_3F is presented in Figure 5.9. No linking was used in this fit, since theoretical calculations were lacking. The vibrational progression represents a C-H stretching mode.

Figure 5.10 shows an example of one of the argon spectra and the fit. Ar $2p_{3/2}$ is well separated from the $2p_{1/2}$ peak and has no vibrational structure. The argon spectra were all fitted with a low χ^2.

5.1.1.2 Discussion

All the above experiments were done within a short period of time and with the same instrumentation and settings. We therefore have reasons to believe that the measurements are internally consistent. Table 5.3 presents the calibrated adiabatic and vertical energies found in this work and in some other previous work. We estimate the uncertainty of our experiments to be ±0.01 eV. Within this uncertainty there is reasonable agreement between our results and previous measurements. A significant deviation is, however, found for CF_4 where the adiabatic (and vertical) energy found by Thomas and Shaw, 301.96 eV [63], deviate by +0.062 eV from our value. Calibration measurements on CH_4, C_2H_4, C_2H_2, CO and CO_2 were done at ALS in 1998 [65]. These were calibrated relative to CF_4 at 301.96 eV, and the average deviation from the values of this work is +0.098 eV. The energies are also too high compared to adiabatic measurements done by others. This indicates that the adiabatic ionization energy of 301.898 eV for CF_4, found in this work, is more reliable.

The vertical energies obtained in this work are generally in good agreement with previous measurements, the largest deviation, except CF_4, being 0.014 eV for methane. However, the adiabatic energies show a larger deviation. This is most likely because adiabatic ionization energies are more influenced by the quality of the resolution than vertical energies. For methane, the adiabatic energy of 290.76 eV found by Tronc *et al*. [71] differs by +0.07 eV from this work. On the other hand, there is a good correspondence between this work and the results of Asplund *et al*. [67], with a difference of only 0.018 eV. For CO_2, the agreement with Tronc *et al*. [71] and Nordgren *et al*. [72] is very good.

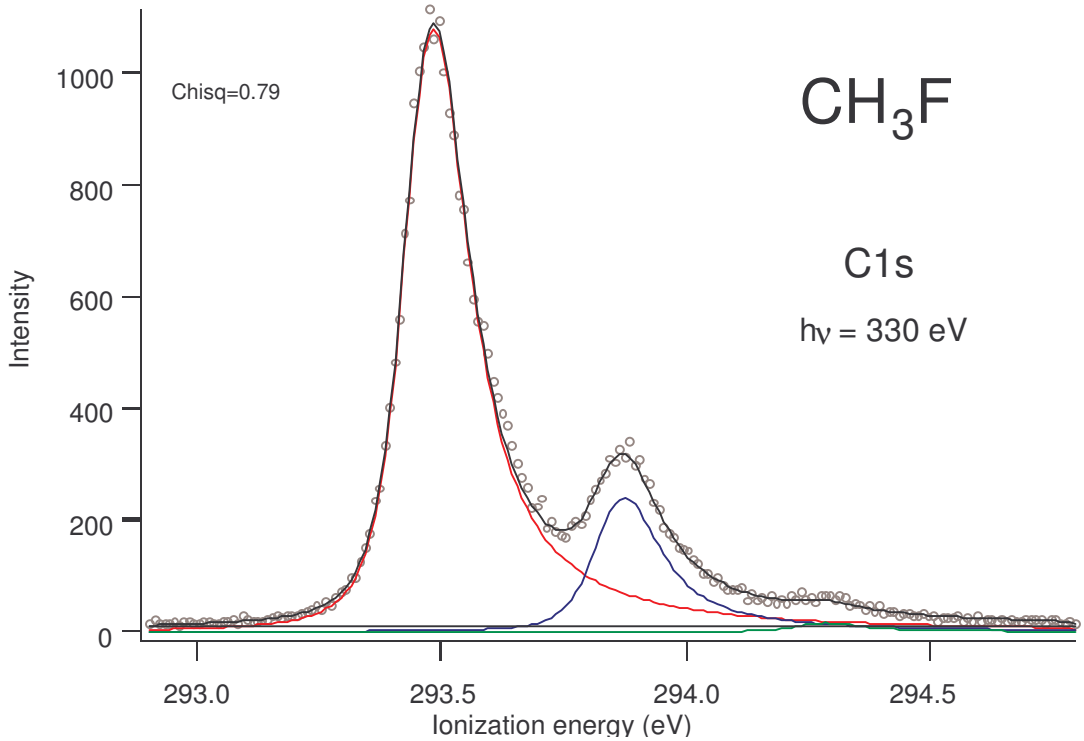

Figure 5.9. C1s photoelectron spectrum of CH_3F.

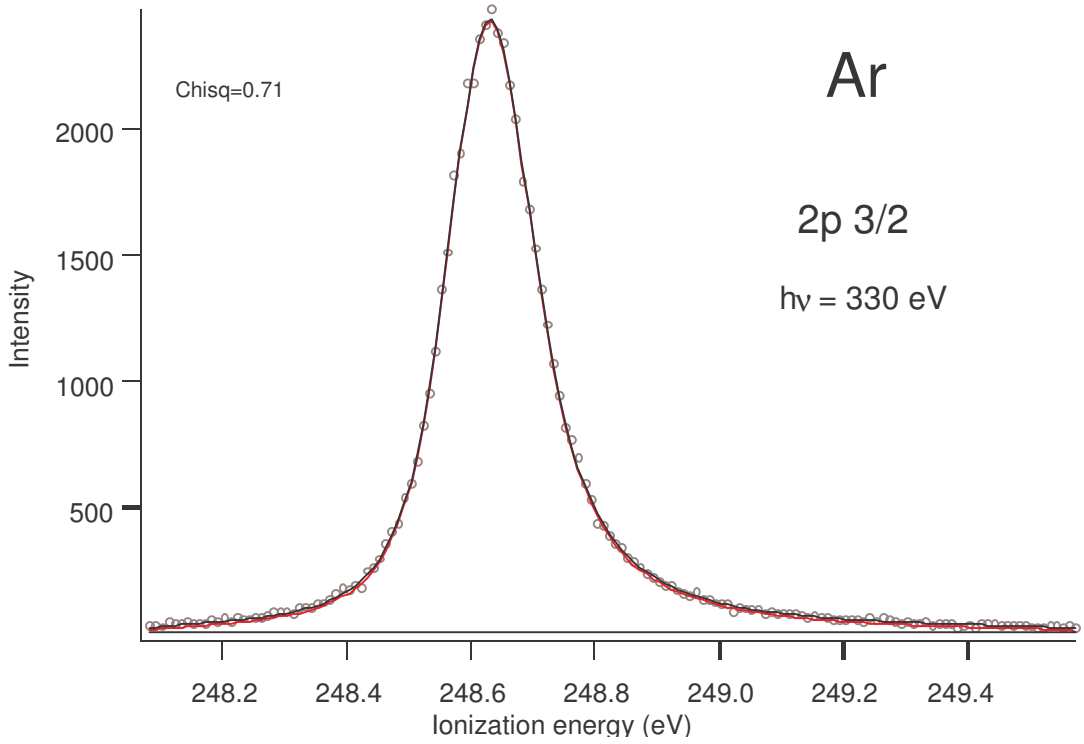

Figure 5.10. Photoelectron spectrum of Ar $2p_{3/2}$ with methane.

Table 5.3. Adiabatic and vertical C1s energies for the calibrated molecules and comparison with earlier measurements. All energies in eV.

	I_C (adiab)		I_C (vert)	
Molecule	**This work**	**Other work**	**This work**	**Other work**
Methane	290.689	290.76[a]	290.844	290.83[e]
		290.707[b]		
Ethane	290.545		290.711	290.71[e]
				290.70[f]
Ethene	290.695	290.74[a]	290.823	290.82[f]
Ethyne[x]	291.176	291.20[a]	291.264	291.14[g]
CO	296.069	296.05[a]	296.229	296.24[h]
CO_2	297.664	297.66[a]	297.699	297.69[i]
		297.651[c]		297.71[d]
CF_4	301.898	301.96[d]	301.898	301.96[d]
				301.96[j]
CH_3F	293.478		293.557	
CHF_3	299.144		299.155	

[x]Gerade peak.
[a]Tronc *et al.* [71], [b]Asplund *et al.* [67], [c]Nordgren *et al.* [72], [d]Thomas *et al.* [63], [e]Pireaux *et al.* [73], [f]Sæthre *et al.* [74], [g]Cavell [75], [h]Smith, Thomas [76], [i]Johansson *et al.* [64], [j]Griffiths *et al.* [77].

5.1.2 Calibration of methyl-substituted benzenes

All the calibration spectra of the methyl-substituted benzenes were acquired at MAX-II, with the instrumental settings as described in Chapter 2. The data were analyzed using Igor Pro [28]. As internal calibrant CO_2 was used, which has an ionization energy of 297.699 eV found in the preceding section. This is close to the compounds of interest, but not overlapping. The CO_2 spectra was fitted using the vibrational energies and intensity ratios found in section 5.1.1, and a low χ^2 was obtained for all the CO_2 spectra.

To fit the calibration spectra of the methyl-substituted benzenes, the high-resolution spectra and fits were used as input, since the latter have smaller step size than the actual calibration spectra and also a lower uncertainty due to a higher number of counts. These fits are described in detail in Section 5.3. All intensity ratios, energy separations, asymmetries, and Fwhm of the calibration spectra were set to be fixed and identical to the resulting parameters of the least squares fits of the high-resolution spectra. Only absolute energies and intensities were allowed to vary in the calibration spectra. All fits were in reasonable agreement with the experimental spectra.

5.2 Vibrational analysis of benzene

The benzene spectrum has been the subject of numerous studies [78,79,80,81,82,83], but one has not yet been able to resolve the spectrum to a great extend and understand the vibrational progression thoroughly. However, with the high resolution now available at third generation synchrotrons, new features of the vibrational structure are revealed, and a splitting of the main peak is observed for the first time. The benzene spectrum is shown in Figure 5.11. Theoretical calculations provide crucial information when analyzing experimental spectra of large molecules, and in this section theory will be used to investigate the characteristic features in the spectra of both benzene and deuterated benzene.

Upon forming a localized core hole, benzene and d-benzene undergo a change of point group, from the high order D_{6h} group to C_{2v}. Only vibrational modes that are totally symmetric in the final state, i.e. belong to A_1, are appreciably excited in the ionization process [61]. The theoretical method used in the vibrational analysis is described in Section 4.4. The spectra of benzene and d-benzene were acquired at MAX-II.

5.2.1 Benzene

Table 5.4 contains the results of the vibrational analysis for the benzene molecule, including frequencies, intensities and the characteristics of each mode excited in the final state. Upon excitation, the composition of a mode may change, but its characteristics are conserved to a large extent. The individual modes are identified from experimental IR spectra

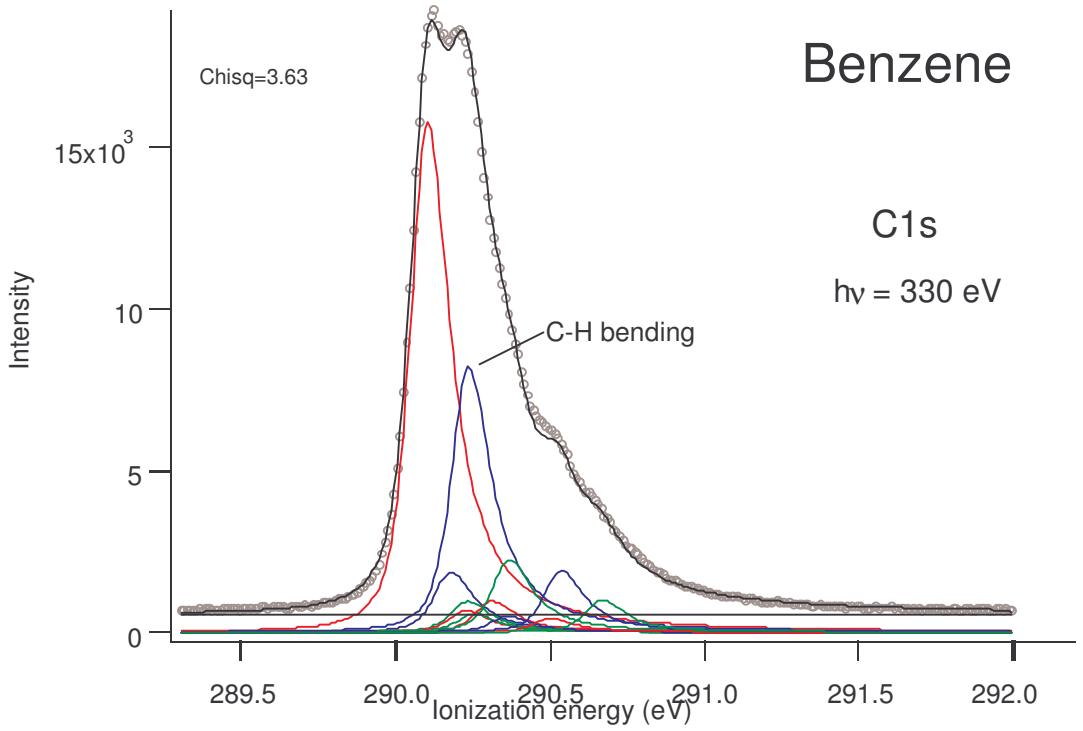

Figure 5.11. C1s photoelectron spectrum of benzene.

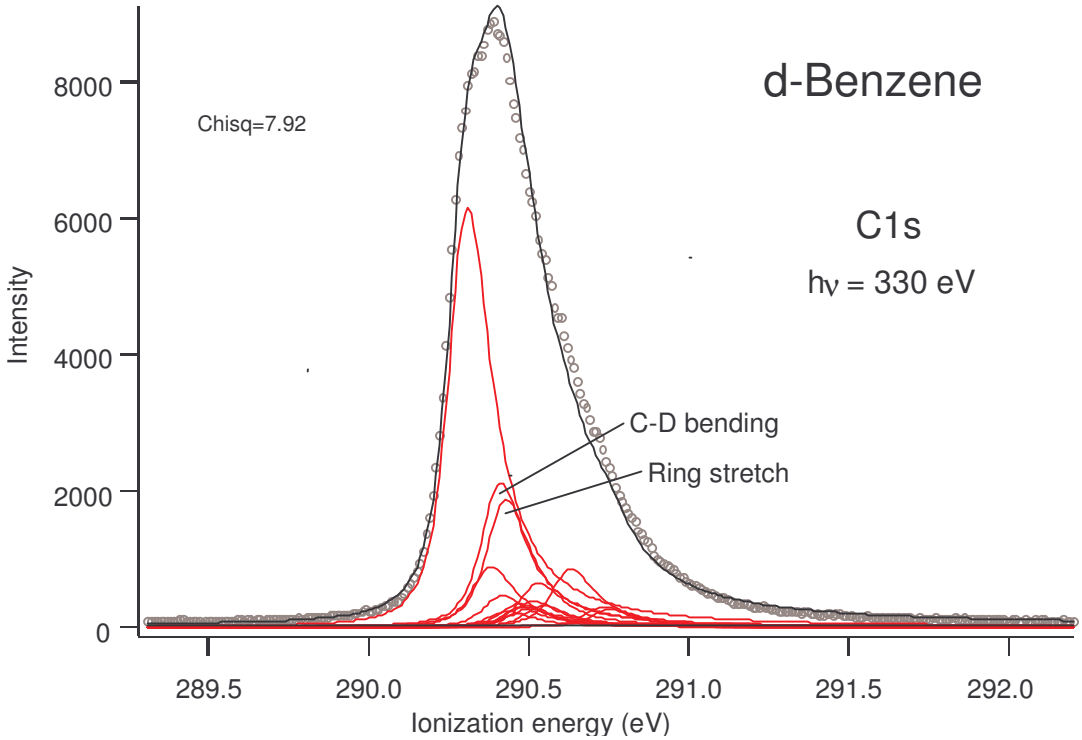

Figure 5.12. C1s photoelectron spectrum of d-benzene.

of the ground-state molecules, and the notations (ν_1, ν_2,...) are also adopted from the same source [56].

The final calculations of the benzene molecule using [57] include 11 vibrational states, which account for 88.7 % of the total calculated intensity. The number of states not included in this analysis is large, but each of the remaining vibrational states contribute very little to the total intensity. The frequencies and intensities obtained were used to fit the experimental data. Figure 5.11 shows the spectrum and the resulting fit for benzene. For simplicity the notations from IR are used to label the different peaks in the fit. The fitting parameters are given in Appendix C.

The vibrational analysis showed that at least 11 normal modes have A_1 symmetry, but only 6 (listed in Table 5.4) are sufficiently excited to be of interest here. In addition, 3 combination modes are excited. From the spectra it is clear that one mode is dominating; this is the C-H bending with a frequency of 132 meV. As seen in Figure 5.11 the strong excitation of the C-H bending mode is mainly responsible for the splitting of the main peak. The ν=2 and ν=3 states are also included for this mode. A ring deformation of 76 meV and a C-H stretching mode of 433 meV also contribute significantly to the total intensity. We obtain a reasonably low χ^2 (3.63) for the fit, but one can see from the spectrum that some intensity towards the high energy tail of the peak is lacking. This is probably due to modes with low intensities, not included in this study.

The Gaussian Fwhm and the asymmetry were fixed in the least squares fit to the experimental spectrum, as these are known from instrumental settings. However, the Lorentzian Fwhm was optimized, and a value of 126.5 meV was obtained, as seen in Appendix C. Compared to previous measured lifetimes of hydrocarbons [38,54], this is too high, as they are normally around 100 meV. However, the model does not take into account the problem of splitting of the degenerate core orbitals of benzene. RHF-calculations suggest that the four C1s levels are split by 15, 32, and 15 meV with an intensity distribution of 1:2:2:1 (see Appendix D). Rennie *et al.* also suggest a splitting of the degenerate core orbitals [78], with an energy separation of 15: 30:15 meV. The fitting model of Rennie *et al.* cannot determine whether the vibrational modes undergo a core splitting, but such a splitting could explain the somewhat broad peaks of our fit.

Table 5.4. Calculated frequencies and excited modes in ionized benzene. B3LYP calculations was used for the ground state, and in combination with ECP calculations for the final state. All energies in meV.

Mode no.[a]	Irrep init. state	Frequency initial state[a]	Irrep final state	Frequency final state[b]	Intensity final state	Type of mode[a]
				0	1	Adiabat
ν_{18}	E_{2g}	75	A1	76	0.1171	Ring deformation
ν_2	A_{1g}	123	A1	127	0.0426	Ring stretch
ν_6	B_{1u}	125	A1	128	0.0606	Ring deformation
ν_{14}	E_{1u}	129	A1	132	0.5189	C-H bend
ν_{17}	E_{2g}	146	A1	150	0.0363	C-H bend
$\nu_{18} + \nu_{14}$		204		209	0.0608	
$\nu_6 + \nu_{14}$		254		261	0.0313	
$2\nu_{14}$		257		265	0.1422	
$3\nu_{14}$		386		397	0.0273	
ν_1	A_{1g}	380	A1	433	0.1207	C-H stretch
$\nu_{14} + \nu_1$		508		566	0.0626	

[a] From IR spectra [56].

[b] Scaled according to experimental values from IR.

5.2.2 Deutero-benzene

Table 5.5 contains the results of the vibrational analysis for deutero-benzene, including frequencies, intensities and the characteristics of each mode excited in the final state. The calculations include 14 vibrational states, which account for 80.9 % of the total calculated intensity. As for the benzene molecule, the intensity ratios and energy separation found was used to fit the experimental spectrum shown in Figure 5.12. Also here, notations from IR spectra were used to label the different normal modes. Resulting fitting parameters are presented in Appendix C.

Table 5.5. Calculated frequencies and excited modes in ionized d-benzene. B3LYP calculations was used for the ground state in combination with ECP calculations for the final state. All energies in meV.

Mode no.[a]	Irrep init. state	Frequency initial state[a]	Irrep	Frequency final state[b]	Intensity	Type of mode[a]
				0	1	Adiabat
ν_{18}	E_{2g}	72	A1	73	0.1431	Ring deformation
ν_{14}	E_{1u}	101	A1	103	0.3440	C-D bend
ν_{17}	E_{2g}	108	A1	110	0.0751	C-D bend
ν_2	A_{1g}	117	A1	120	0.3051	Ring stretch
ν_6	B_{1u}	120	A1	125	0.0374	Ring deformation
ν_9	B_{2u}	159	A1	163	0.0560	Ring stretch
$\nu_{18} + \nu_{14}$		172		176	0.0491	
$\nu_{18} + \nu_2$		188		193	0.0436	
$2\nu_{14}$		202		206	0.0628	
$\nu_{14} + \nu_2$		218		223	0.1051	
$2\nu_2$		234		240	0.0504	
ν_1	A_{1g}	284	A1	323	0.1391	C-D stretch
$\nu_{14} + \nu_1$		385		427	0.0479	
$\nu_2 + \nu_1$		401		443	0.0423	

[a] From IR spectra [56].

[b] Scaled according to experimental values from IR spectra.

In the vibrational analysis, at least 11 normal modes were found to have A_1 symmetry, but only 7 contribute significantly to the overall intensity. In addition, 5 combination modes are included. From Figure 5.12 it is clear that two modes are dominating; a C-D bending mode of 103 meV and a ring stretching mode of 120 meV. For both modes the ν=2 excitation is included as well. Intensity is lacking in the spectra on the high-energy tail of the peak, even more for deutero-benzene than normal benzene. It has been shown before that there will be

greater population of the higher vibrational states for deuterated molecules than for the molecules with hydrogen [8,84]. This can be explained by the isotope effect. The vibrational frequencies are smaller for deuterated than for protonated molecules, due to a larger reduced mass. Consequently, S_r (defined in Eq. 3.4) must be larger for the deuterated species if the average vibrational energy is to remain the same. Since only 80.9% of the total intensity is included in the deutero benzene fit, as compared to 88.7% for benzene, it is reasonable to expect the missing intensity to come from the higher vibrational states.

In the d-benzene spectrum, no splitting of the peak is directly observed. This observation indicates that the splitting of the benzene peak has to do with a mode containing motion of hydrogens, which is consistent with our identification of the dominating mode in the benzene case as a C-C-H bending mode.

5.3 The methyl-substituted benzenes

The methyl-substituted benzenes are molecules with a relatively large number of atoms, and therefore experience excitations of many vibrational modes upon core ionization. Also the fact that they contain several chemically different carbon atoms, makes their photoelectron spectrum complicated. It is in principle possible to resolve this vibrational structure with extensive theoretical calculations, as shown for benzene in the previous section. Such calculations are suggested as a future project, but were not performed in this work since it is expected to be quite time consuming. Instead, a semi-empirical model was used. The method assumes that the C1s spectrum of benzene can be used as a model for the ring carbons of the methyl substituted benzenes. In addition, a single peak was chosen to model the vibrational structure involving C-H modes. In this way the benzene spectrum was fitted with only two peaks as shown in Fig. 5.13. From the discussion in the previous section, this simple fitting model obviously represents an oversimplification of the actual vibrational structure of benzene. However, our immediate concern here is to extract ionization energies to be compared with reactivity data, and it is assumed that these are not too much affected by the fitting model. The ipso-carbons were given slightly higher intensity since these carbons are not attached to hydrogens. Theoretical calculations [55] were used to assign the sequence of

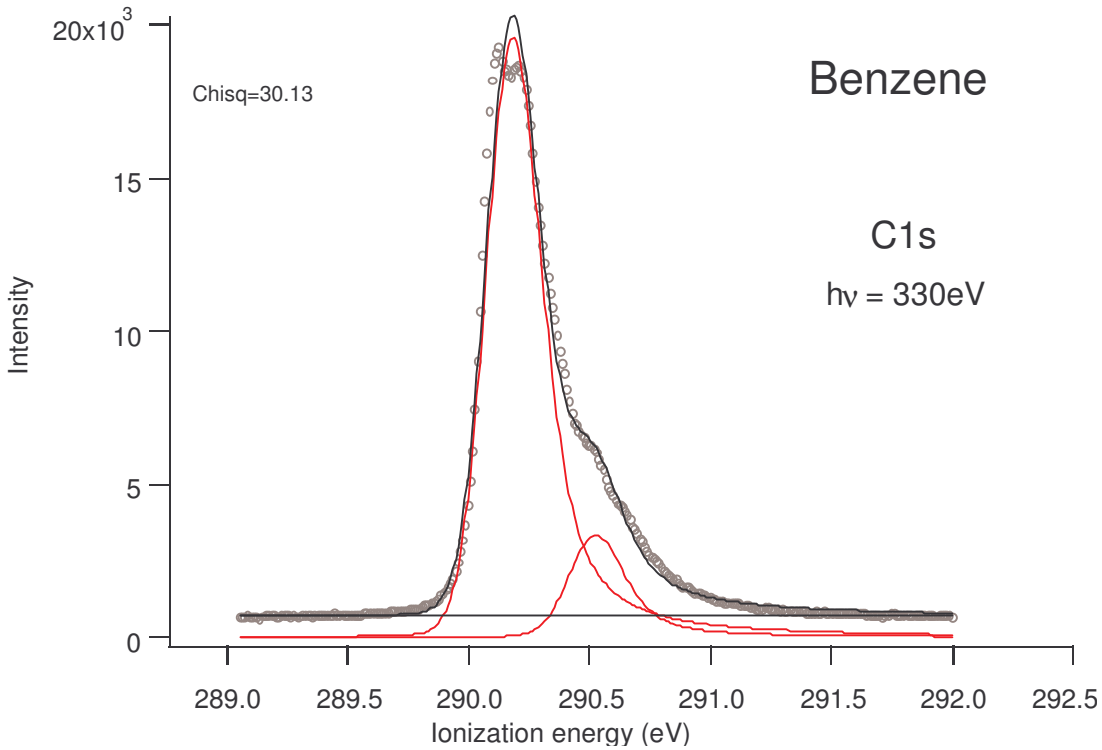

Figure 5.13. C1s photoelectron spectrum of benzene.

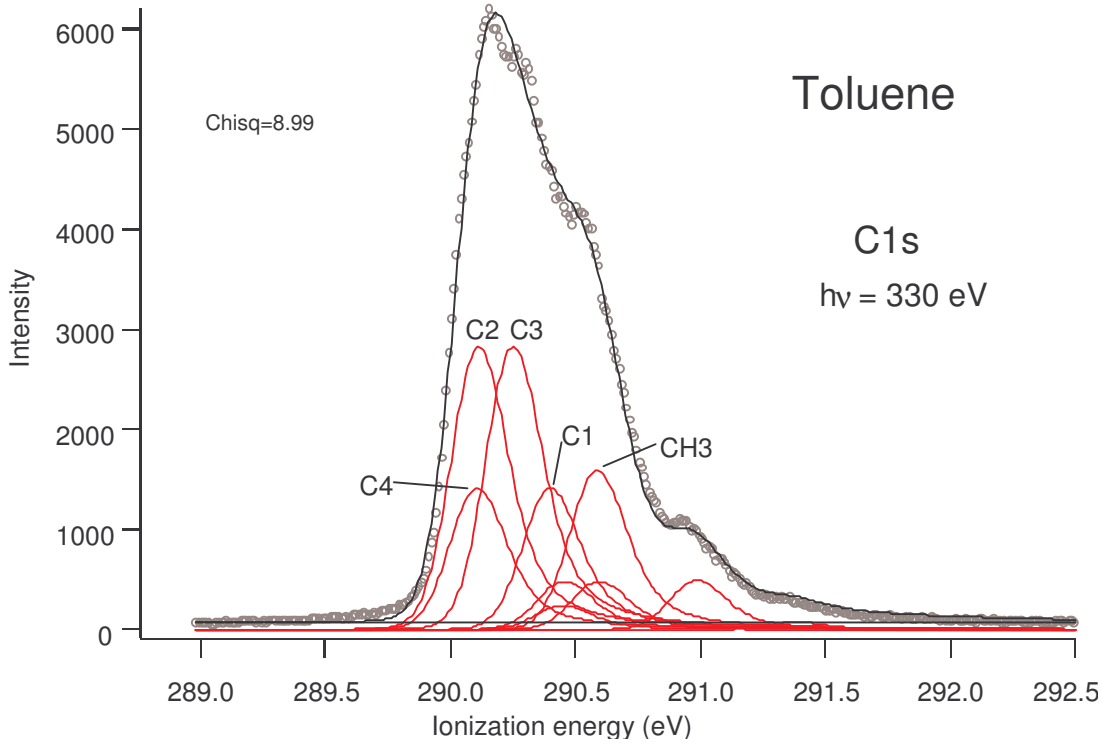

Figure 5.14. C1s photoelectron spectrum of toluene.

Table 5.6. Parameters used to fit consecutive peaks in the experimental spectra of the methyl-substituted benzenes.

Molecule	Energy separation (eV)	Intensity ratio	Asym	Fwhm (eV)
Benzene	0	1	0.62	0.277
	0.343	0.1704		
Methane	0	1	-	-
	0.397	0.3103		
	0.794	0.0481		

the peaks of the different ring carbons in the spectra. Tabulated theoretical shifts are found in Section 5.4.

A similar method was used to describe the methyl groups, in which a spectrum of methane, acquired under similar experimental conditions, was fitted with a least squares fit (see Figure 5.1). The resulting intensity ratios and energy separations were then used to describe the methyl groups, according to the linear coupling intensity model (see Chapter 3). Except for toluene, the Fwhm and asymmetry of the methyl groups were optimized during the fits, since the methyl group is normally well separated from the ring carbons in the spectrum. Table 5.6 shows the resulting fit parameters for benzene and methane, used to fit the peaks of the different carbons in the methyl-substituted benzenes. All the spectra of the benzene derivatives were acquired at MAX-II.

5.3.1 Toluene.

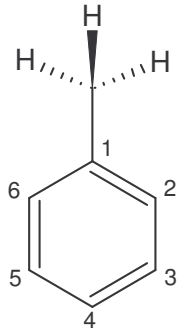

Figure 5.14 presents the spectrum and fit of toluene. In Appendix E, the fitting parameters, with resulting energies and intensities, are tabulated. The fit is not able to distinguish between the ortho-and para-positions of the molecule, as the two peaks, C2 and C4

respectively, end up with essentially the same ionization energy. Theoretical calculations, Table 5.8, suggest that C2 should be slightly more negatively shifted than C4. This disagreement between experiment and theory may be due to a too simple fitting model. The meta-position is the least activated position on the ring and has the highest ionization energy of the reactive ring carbons. Then follows the ipso-carbon, at even higher ionization energy, and finally the methyl group. One can see from the fit that the main part of the peak is quite poorly described by our model, while the high energy tail is more accurately described. The Fwhm parameters have no direct physical meaning, as they were only meant to be optimized with the intention of covering the area of the peaks as completely as possible.

5.3.2 o-Xylene

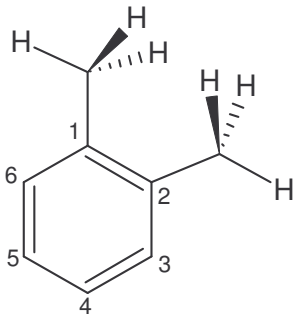

The o-xylene spectrum and fit is presented in Figure 5.15, and the fitting parameters are found in Appendix E. Also for o-xylene, the fit is not able to distinguish between positions C3 and C4. C3 is ortho and meta to the methyl groups, while C4 is meta and para to the methyl groups. Theoretical calculations, Table 5.8, show that C3 is shiftet towards lower binding energies by 0.03 eV (eq. core). Again, the reason for this discrepancy is possibly the crude model used to fit the spectrum. Towards higher ionization energy follows the ipso carbon, C1, and finally the methyl group. From the spectrum one can see that our model is not able to reproduce the experimental spectrum completely. Still, a fairly low χ^2 (4.14) is obtained, and the deviations from the experimental spectrum are acceptable within our model.

5.3.3 m-Xylene

Figure 5.16 shows the spectrum and fit of m-xylene. In Appendix E the fitting parameters are tabulated. One can see from the spectrum that the differences between the peaks and the valleys in the fit are generally too small relative to the experimental spectrum. This may be due to the large Fwhm used for each peak. The positions C2 and C4 are ortho to

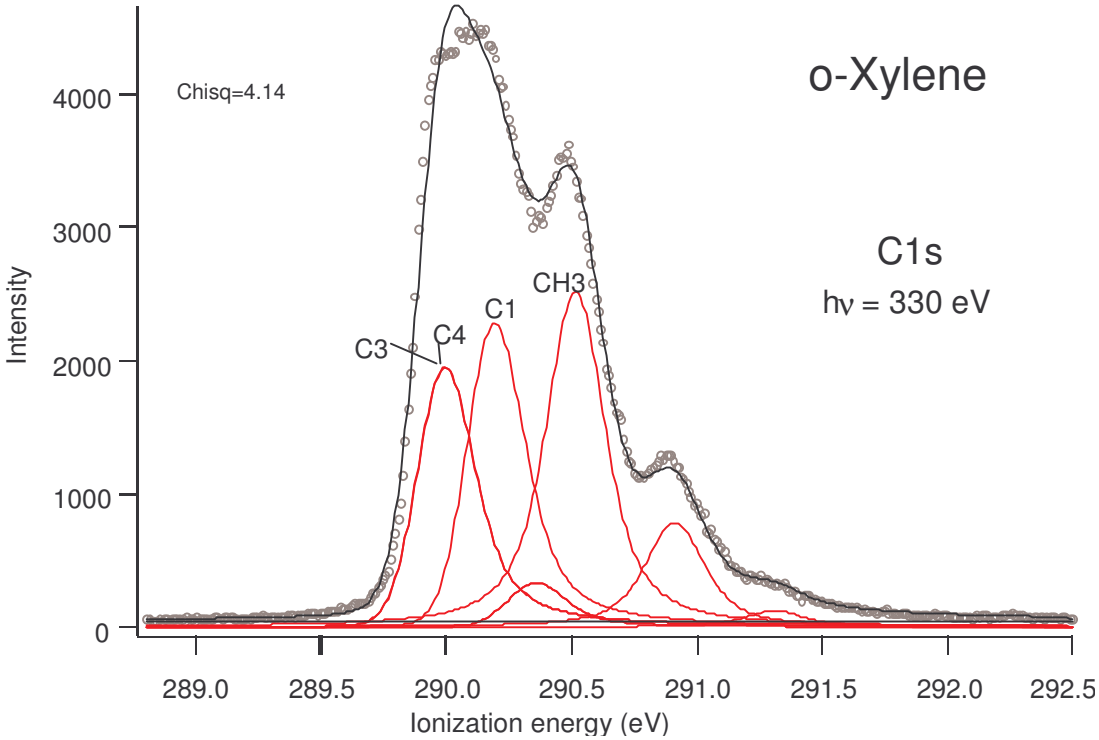

Figure 5.15. C1s photoelectron spectrum of o-Xylene.

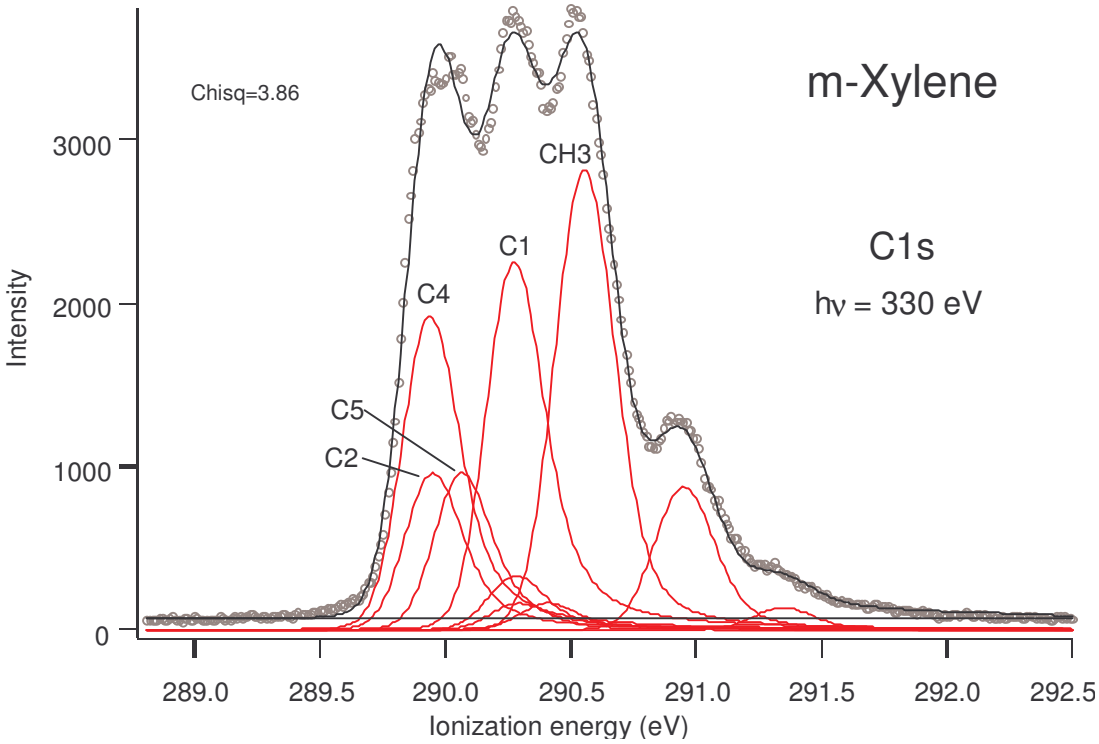

Figure 5.16. C1s photoelectron spectrum of m-Xylene.

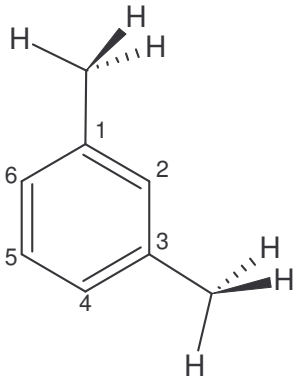

both methyl groups and ortho and para to the methyl groups, respectively. From theoretical calculations, C2 and C4 are separated by 0.05 eV, C2 having the lowest ionization energy. In the fit they are separated only by 0.01 eV. Again, this discrepancy is probably caused by the inaccuracy of our fitting model. Position C5, which is less shifted than C2 and C4, is meta to both methyl groups. Last in the spectra come the ipso-carbon and the methyl group. The experimental spectrum is rather poorly deconvoluted by our model, although the main features of the spectrum are described by the fit.

5.3.4 p-Xylene

The spectrum and fit of p-xylene is presented in Figure 5.17, and the fitting parameters are found in Appendix E. p-Xylene belong to the high order point group, C_{2h}, and contains only two chemically different ring carbons which can be represented by position C1 and C2. Position C2 is ortho and meta to the two methyl groups, and one should expect an activation of carbon 2 relative to carbon 1. In our fit, C1 and C2 are well separated by 0.19 eV, which is in good agreement with a theoretically predicted shift of 0.20 eV (Table 5.8). Still, the low-energy side of the spectrum is not well described by our model.

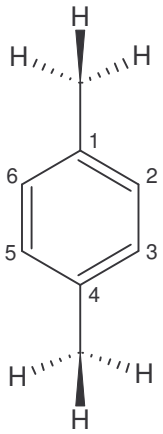

5.3.5 Mesitylene

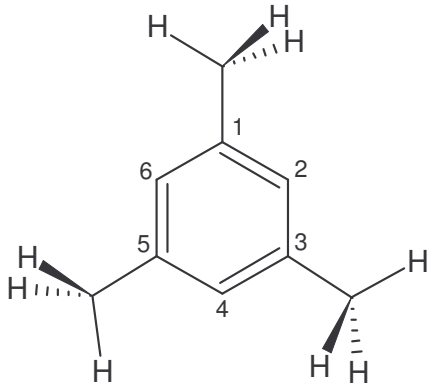

Mesitylene is a molecule of an even higher order point group, C_{3h}, than p-xylene, and the spectrum and fit is shown in Figure 5.18. The fitting parameters are tabulated in Appendix E. It is seen that the reactive ring carbon C2 in mesitylene has the largest shift relative to benzene of all the considered molecules. The peaks are well separated and the model produces an acceptable

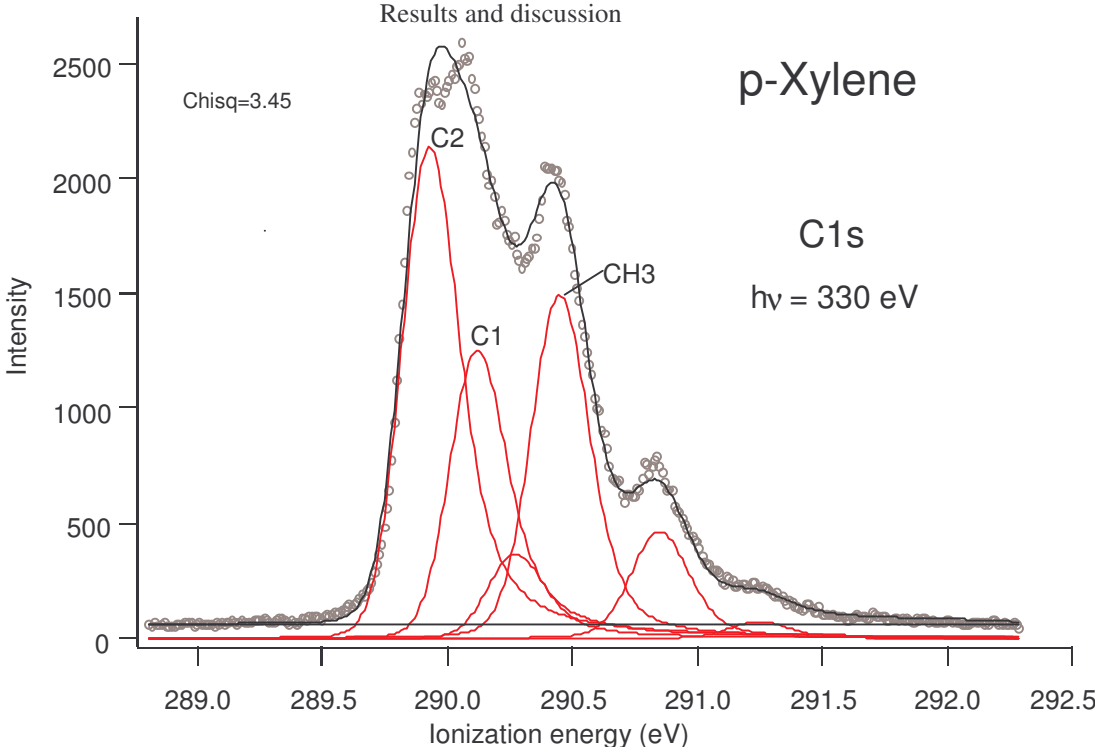

Figure 5.17. C1s photoelectron spectrum of p-Xylene.

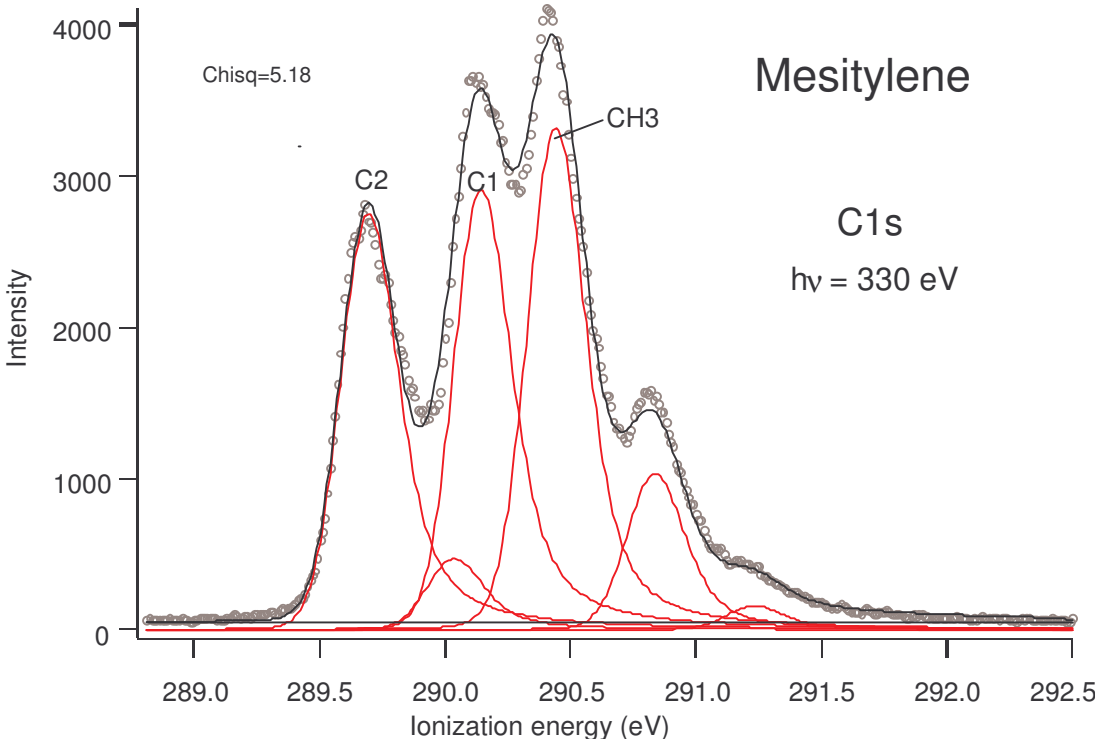

Figure 5.18. C1s photoelectron spectrum of Mesitylene.

Table 5.7. Vertical C1s ionization energies of the benzene derivatives. The numbering of the carbon atoms is shown in the text. C1 is attached to a methyl group. All energies in eV.

Molecule	C1	C2	C3	C4	C5	C6	CH_3
Toluene	290.375	290.138	290.276	290.132	290.276	290.138	290.679
o-Xylene	290.135	290.135	289.990	289.989	289.989	289.990	290.613
m-Xylene	290.179	289.904	290.179	289.893	290.021	289.893	290.582
p-Xylene	290.122	289.981	289.981	290.122	289.981	289.981	290.583
Mesitylene	290.097	289.696	290.097	289.696	290.097	289.696	290.517

fit to the experimental spectrum. As predicted by theoretical calculations (Table 5.8), C2 comes first, followed by the ipso-carbon, and then the methyl group.

The conclusion is that our fitting model represents a reasonable approach in describing the experimental spectra of the methyl-substituted benzenes, and that useful chemical information may be drawn from the obtained ionization energies. Table 5.7 shows the vertical ionization energies for the different carbons. For a more accurate description of the spectra, extensive theoretical calculations regarding the vibrational structure of the molecules are needed.

5.4 Reactivity of methyl-substituted benzenes

5.4.1 Shifts in ionization energy

For the ionized state of the molecules both equivalent-cores and ECP calculations were performed. Within the ECP approach, both vertical and adiabatic energies were calculated. The results are shown in Table 5.8. As can be seen from the table, there are not much difference between the vertical and the adiabatic energies found. Experimentally, only vertical energies can be obtained within our model, and in the rest of the discussion only

Table 5.8. Vertical ionization energy shifts, ΔI (vertical), relative to benzene for the benzene derivatives, obtained from the equivalent core approximation calculations. Vertical, ΔI (vertical), and adiabatic, ΔI (adiabatic), ionization energy shifts relative to benzene, obtained from ECP calculations. The numbering of the carbon atoms is shown in the text. All energies in eV.

Molecule	Position	ΔI_{exp} (vertical)	$\Delta I_{Eq.\ core}$ (vertical)	ΔI_{ECP} (vertical)	ΔI_{ECP} (adiabatic)
Toluene	C1	-0.01	-0.01	-0.07	-0.06
	C2, C6	-0.25	-0.28	-0.32	-0.34
	C3, C5	-0.11	-0.17	-0.17	-0.18
	C4	-0.25	-0.24	-0.24	-0.26
	CH_3	0.29	0.48	0.16	0.06
o-Xylene	C1, C2	-0.25	-0.23	-0.33	-0.30
	C3, C6	-0.40	-0.42	-0.46	-0.43
	C4, C5	-0.40	-0.39	-0.39	-0.38
	CH_3	0.23	0.39	0.08	0.09
m-Xylene	C1, C3	-0.21	-0.15	-0.23	-0.19
	C2	-0.48	-0.55	-0.62	-0.64
	C4, C6	-0.49	-0.50	-0.53	-0.52
	C5	-0.36	-0.33	-0.33	-0.34
	CH_3	0.20	0.39	0.08	0.07
p-Xylene	C1, C4	-0.26	-0.24	-0.31	-0.30
	C2, C3, C5, C6	-0.40	-0.43	-0.47	-0.49
	CH_3	0.20	0.37	0.07	-0.03
Mesitylene	C1, C3, C5	-0.29	-0.29	-0.37	-0.32
	C2, C4, C6	-0.69	-0.74	-0.81	-0.79
	CH_3	0.13	0.30	0.00	0.03

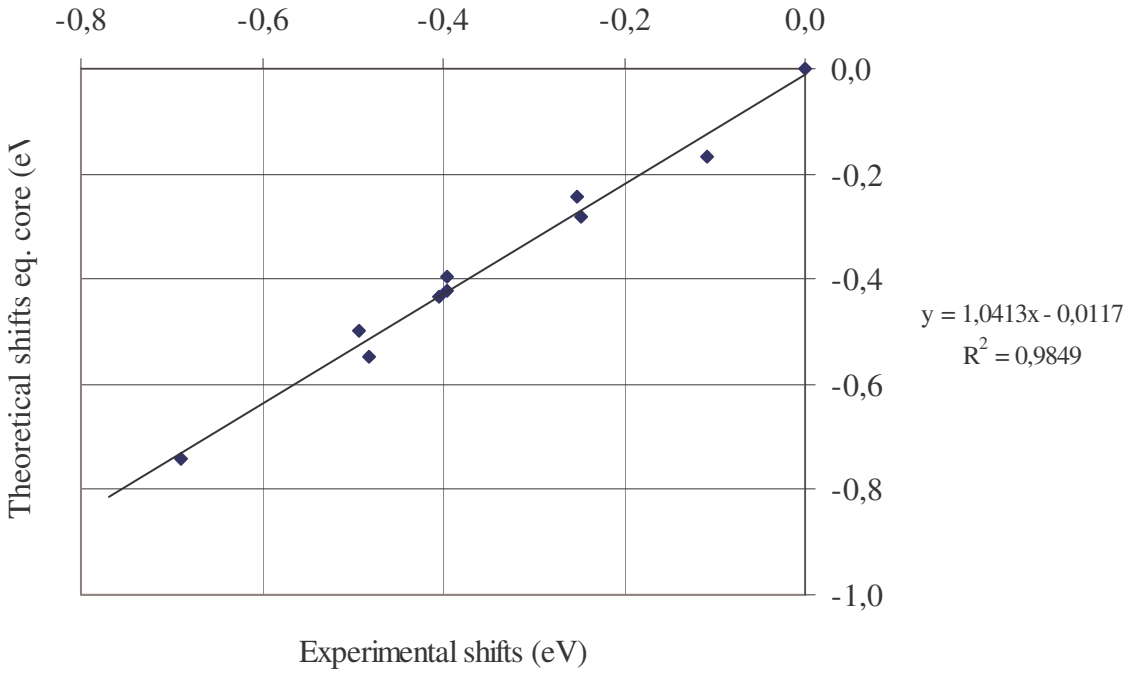

Figure 5.19. Correlation of theoretical (eq. cores) with experimental ionization energy shifts.

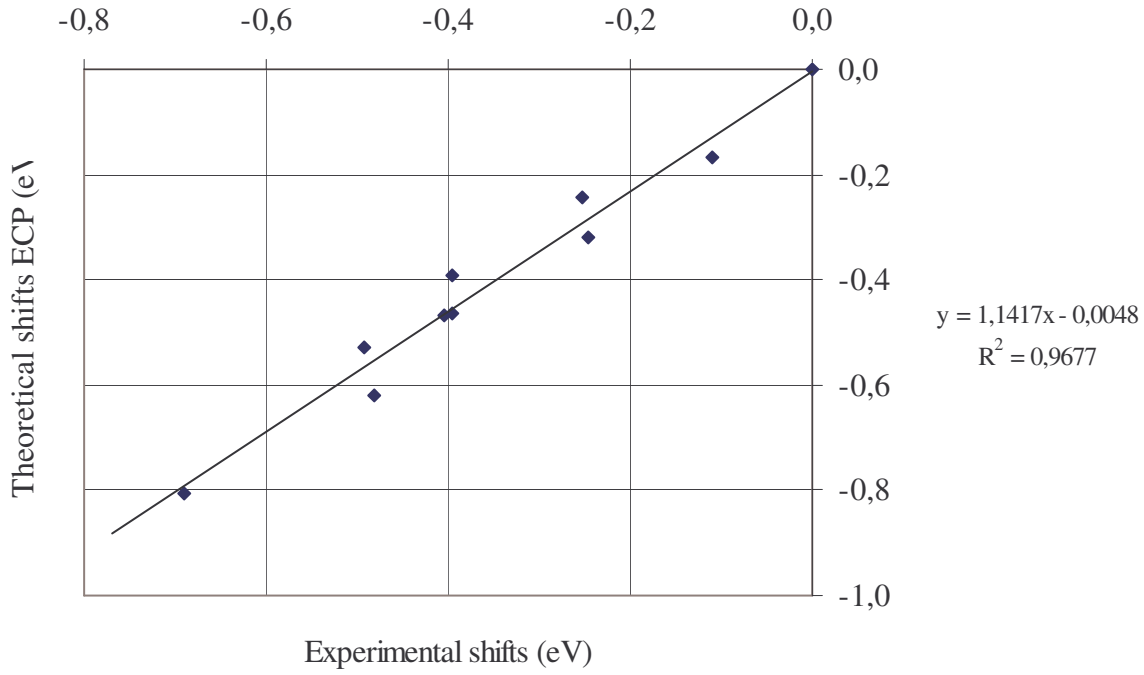

Figure 5.20. Correlation of theoretical (ECP) with experimental ionization energy shifts.

vertical energies will be considered. It is noteworthy that the shift of the methyl group is poorly described by both the equivalent-cores and by the ECP approach. It is overestimated by the former and underestimated by the latter. However, since the ring carbons and benzene both are sp^2 hybridized, the shifts for these atoms are well reproduced by both models. The correlation between experimental and theoretical shifts is found from the plots in Figures 5.19 and 5.20, for the equivalent-cores and the ECP calculations, respectively. In the figures only values for the reactive ring carbons are included since these will be used below for comparison with reactivity data. From the correlation coefficients one can see that the equivalent-cores approximation gives the best agreement with the experimental shifts. The slopes of the curves show that equivalent-cores approximation overestimates the shifts by about 4%, compared to 14% for the ECP approach. This is a somewhat surprising result, since the ECP is expected to describe the effects of a core hole more accurately than the equivalent-cores scheme. It suggests that the parametrization of the ECP needs to be improved, or that the combination of an all-electron calculation for the ground state with a frozen ECP calculation for the final state must be reconsidered and further investigated.

5.4.2 Reactivity

Experimentally determined values for the reactivity of the methylated benzenes are available in the litterature, see Table 5.9. In this section two such reactions will be compared with ionization energies. Electrophilic substitution of tritium by hydrogen (protodetritiation) in trifluoroacetic acid is one reaction in which it is possible to observe the relative rates of reaction for the different positions in the aromatic rings [6]. The reaction mechanisms and partial rate factors were described in more detail in Chapter 1. According to Arrhenius the logarithm of the rate constant k is proportional to the activation energy. Figure 5.21 plots the logarithm of k_I, the rate constant for the protodetritiation, *versus* the experimental shifts. As predicted there is a good correlation between chemical reactivity and shift in C1s ionization energies. A linear regression line with a correlation coefficient of 0.953 is obtained. From the plot one can see that toluene is the least reactive molecule with the smallest shifts, followed by o-xylene and p-xylene at almost identical shifts, and m-xylene as the most shifted and the most reactive. Experimental reaction data for C5 in m-xylene is missing. It was noted in Section 5.3 that mesitylene has the largest shift of all the benzene derivatives, and from

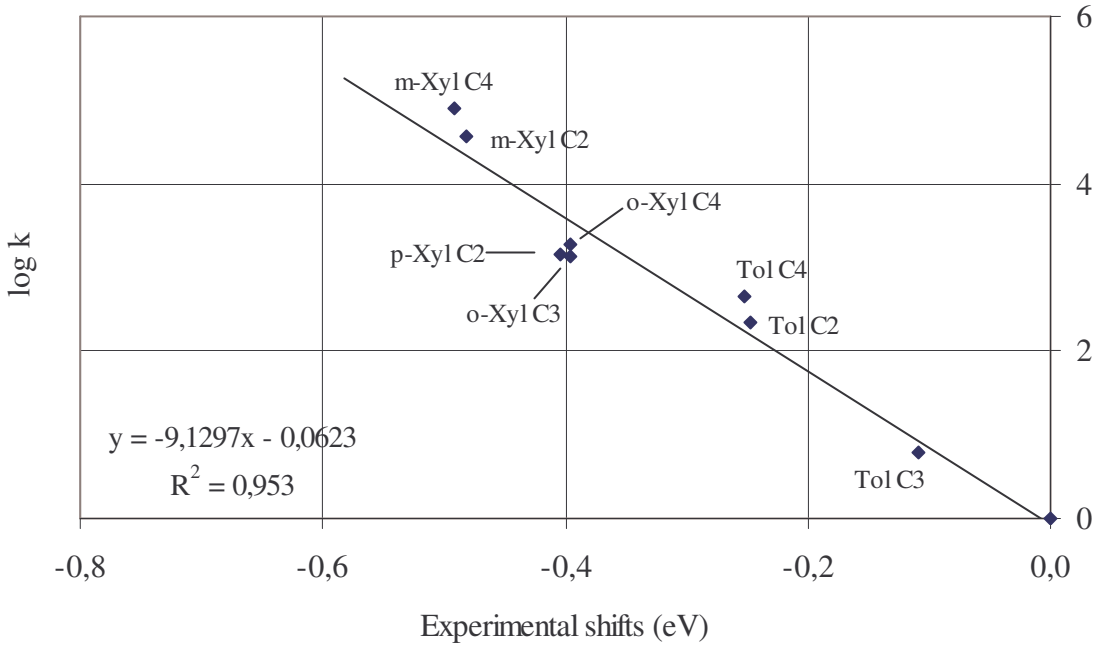

Figure 5.21. Correlation of reactivity, k_I, with experimental shifts.

Table 5.9. Reactivity data for the methyl-substituted benzenes. k_I is obtained from [6]. k_{II} and $k_{II,calc}$ is obtained from [7]. $k_{II,calc}$ is the predicted reactivity in a compound calculated on the assumption that the efffects of the methyl groups, as revealed in toluene, are additive.

Molecule	Position	k_I	k_{II}	$k_{II,calc}$
Benzene	All	1	1	1
Toluene	C2	219	18.3	18.3
	C3, C5	6.1	2.38	2.38
	C4, C6	445	22.8	22.8
o- Xylene	C3, C6	1340	71.9	43.6
	C4, C5	1900	56.1	54.3
m- Xylene	C2	36600	3530	335
	C4, C6	78800	422	417
	C5	No data	6	5.7
p- Xylene	C2, C3, C5, C6	1460	42.9	43.6
Mesitylene	C2, C4, C6	No data	53000	7640

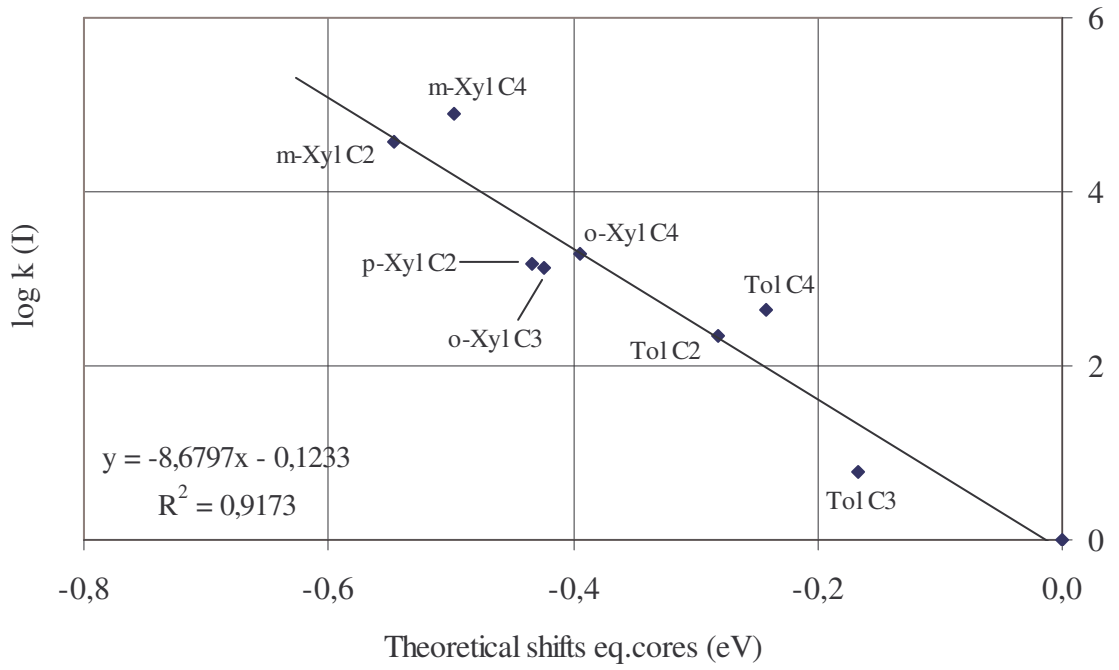

Figure 5.22. Correlation of reactivity, k_I, with theoretical shifts (eq. cores).

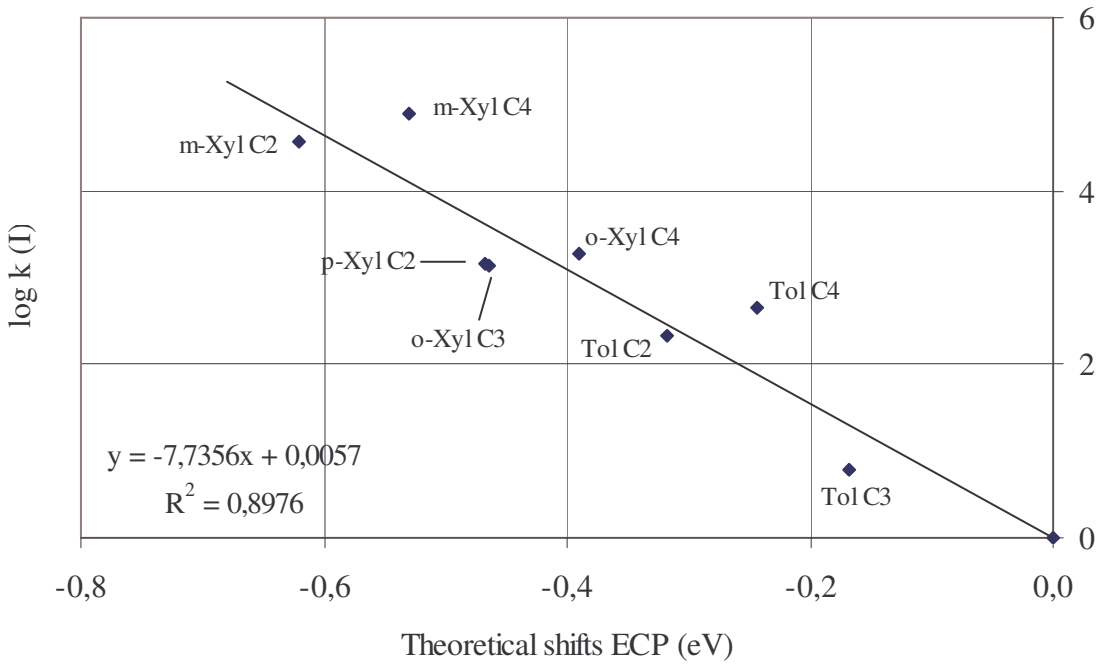

Figure 5.23. Correlation of reactivity, k_I, with theoretical shifts (ECP).

Figure 5.21 one can predict that mesitylene is also the most reactive. In fact, the obtained correlation may be used to predict the rate constant for protodetritiation of mesitylene. From the correlation coefficients, mesitylene is predicted to be $1.7 \cdot 10^6$ times more reactive than benzene.

It is also of interest to compare the reactivity data with theory. Figures 5.22 and 5.23 display the correlation of reactivity with theoretically calculated shifts, and also here a good correlation is obtained. Again we see that the equivalent-cores approximation correlates better with experimental data and this approximation will in the rest of the discussion be the only theoretical data considered. In general, however, experimental shifts correlate better with reactivities than those predicted by theory.

Another reaction that can be used to measure relative reaction rates is cleavage of the tolyl-and xylyl-trimethylsilanes and of phenyl-and mesityl-trimethylsilane by aqueous-methanolic perchloric acid [7,85]. The reactivity of each compound relative to that of phenyltrimethylsilane, k_{II}, is derived by a stepwise procedure, covering several acid concentrations, and tabulated in Table 5.9. The correlation with experimental shifts is shown in Figure 5.24, and it is clear that the correlation here is not as good as the correlation in Figure 5.21. According to these measurements, mesitylene is clearly the most reactive, as predicted above. There are three points in Figure 5.24 that deviate significantly from the linear regression line, namely mesitylene and C2 and C5 in m-xylene. Mesitylene and m-xylene C2 are more reactive than expected because of release of steric strain on going from the ground state to the transition state in the cleavage reaction [86,87]. This is also true for o-xylene C3, but the effect for o-xylene is not great enough to be visible. m-Xylene C5 has lower reactivity than expected, but this cannot be explained within this model.

In Table 5.9 is also included $k_{II,calc}$, which is the predicted reactivity of a xylyl or mesityl compound based on the assumption that the effects of the methyl groups, as revealed in the tolyl compounds, are additive. log k_{calc} is plottet *versus* experimental shifts in Figure 5.25, and it is clear that mesitylene and m-xylene C2 here show reactivities in better agreement with those predicted from ionization energies. o-Xylene C3 and C4 have switched places with regards to reactivity, as a result of steric strain effects not included in this model. A higher correlation coefficient, 0.876, is obtained.

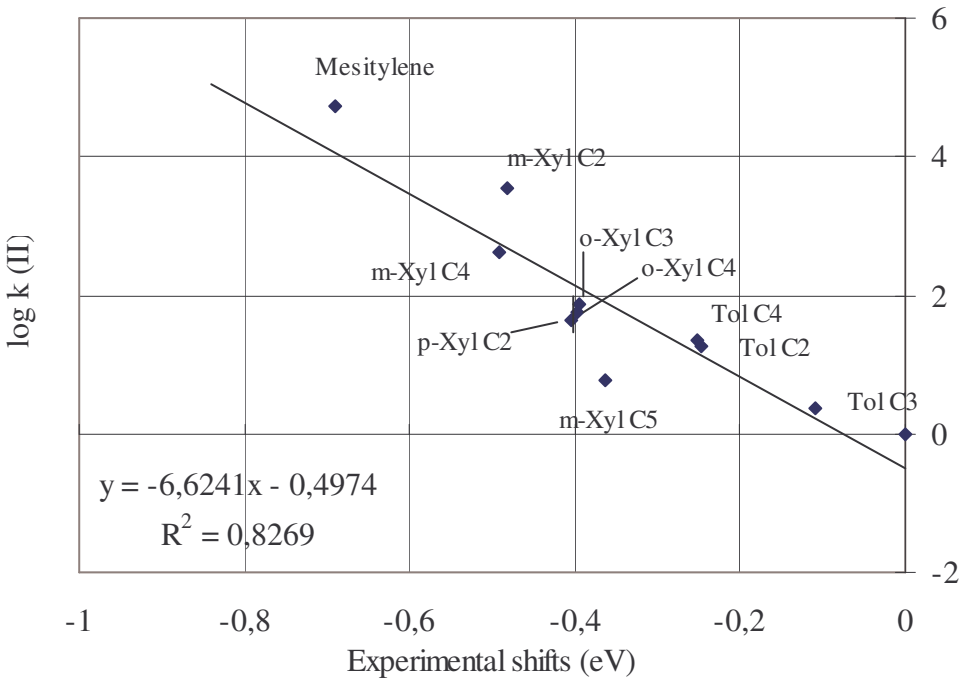

Figure 5.24. Correlation of reactivity, k_{II}, with experimental shifts.

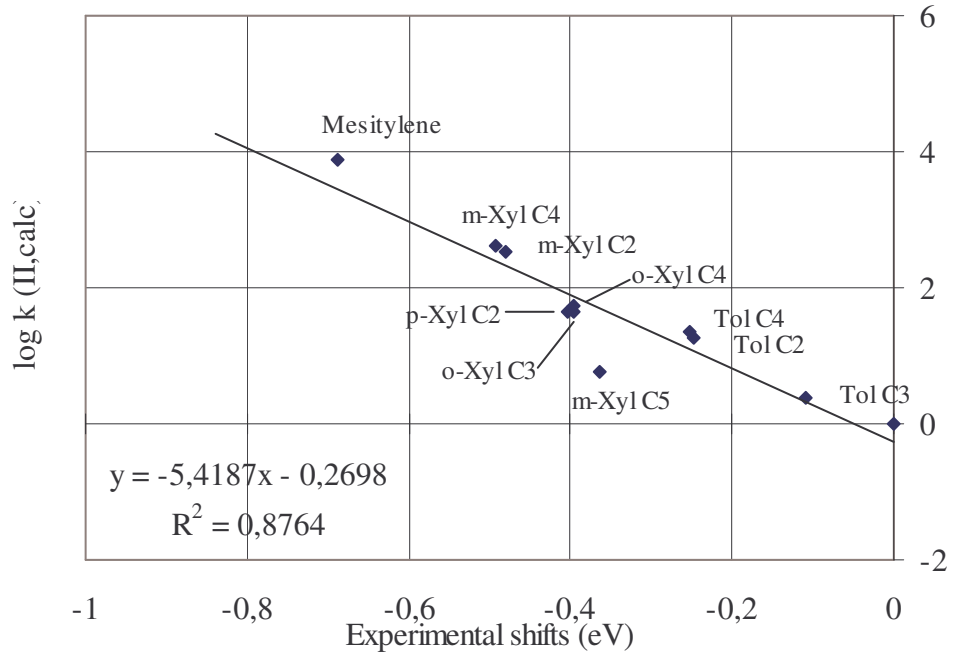

Figure 5.25. Correlation of predicted reactivity, $k_{II,calc}$, with experimental shifts.

Table 5.10. Calculated shifts in ionization energy, ground state potentials, and final state relaxation energy of the reactive ring carbons in the benzene derivatives. All energies in eV.

Molecule	Position	ΔI_{exp}	$\Delta I_{Eq.core}$	$\Delta\varepsilon_{HF}$	ΔU^{VCI}	ΔU^{HF}	ΔV	ΔR
Toluene	C2, C6	-0.25	-0.28	0.207	-0.202	-0.207	-0.20	0.08
	C3, C5	-0.11	-0.17	0.061	-0.103	-0.078	-0.09	0.08
	C4	-0.25	-0.24	0.164	-0.145	-0.169	-0.14	0.10
o- Xylene	C3, C6	-0.40	-0.42	0.272	-0.300	-0.278	-0.29	0.13
	C4, C5	-0.40	-0.39	0.219	-0.242	-0.238	-0.22	0.17
m- Xylene	C2	-0.48	-0.55	0.421	-0.397	-0.412	-0.41	0.14
	C4, C6	-0.49	-0.50	0.357	-0.336	-0.365	-0.33	0.17
	C5	-0.36	-0.33	0.138	-0.206	-0.161	-0.18	0.15
p- Xylene	C2, C3, C5, C6	-0.40	-0.43	0.263	-0.293	-0.276	-0.28	0.15
Mesitylene	C2, C4, C6	-0.69	-0.74	0.558	-0.522	-0.564	-0.52	0.23

5.4.3 Initial- and final-state effects on ionization energies

Now that a relationship between shifts in core ionization energies and reactivities are established, it is interesting to investigate what effects determine the ionization energies of the different molecules. Historically, the shift in ionization energy between the same atom in different chemical environments was interpreted in terms of ΔU, the difference in electrostatic energy of holes of unit positive charge localized at different nuclei. However, the ionization energy depends not only on the charge distribution in the initial state of the molecule, traditionally referred to as V, but also on the rearrangement of charge in the resulting ion, R [14]. This gives:

$$\Delta I = \Delta V - \Delta R$$

where V represents the energy required to remove a core electron from a molecule in which the remainder of the electron structure remains unchanged from that of the neutral molecule. In the work of Børve and Thomas [14], it is shown that to calculate ΔV, an extended Koopmans' theorem can be used. A simple approximation to this theorem is eq. (4.5). Then ΔR can be found from ΔI and ΔV, by $\Delta R = \Delta V - \Delta I$. The results of the calculations are found

in Table 5.10. $\Delta\varepsilon_{HF}$ is the shift in orbital energies computed at the Hartree-Fock level. ΔU^{VCI} and ΔU^{HF} are differences in electrostatic energies of holes of unit positive charge computed at the atom to be ionized, obtained at the valence-correlated and Hartree-Fock levels respectively. ΔU^{VCI} corresponds to the DFT calculations performed in this work. The charge and electrostatic potentials of the carbon atoms are given in Appendix F. The ipso and methyl positions are not included in Table 5.10, as they are much less reactive than the other ring carbons. In this case the atoms considered are all part of an aromatic ring, thus the differences between $-\Delta\varepsilon_{HF}$, ΔU^{VCI}, ΔU^{HF}, and ΔV are small.

Two features are striking when looking at the columns for ΔV and ΔR. Firstly, ΔV seems to contribute a lot more to ΔI than ΔR does, as the numbers for ΔV are generally larger in absolute value. This is most obvious for mesitylene, where a difference of 0.29 eV is found. Secondly, ΔR seems to be more constant for the different atoms within each molecule, the largest difference being 0.04 eV, while for ΔV the largest difference is 0.23 eV. Also, comparing all of the molecules, one can see that ΔR is more constant than ΔV. Going downwards in the table, the molecules have generally increasing reactivity as a result of a higher number of substituents (see Figure 5.21). This is reflected in a small increase in ΔR because of increasing polarizability with the higher number of substituents. The conclusion is that initial state effects, ΔV, are more important for shift in ionization energies of atoms in chemically different environments, than final state effects, ΔR. Because of the good correlation between reactivity and core-ionization energies, one may assume that the reactivity of methylated benzenes also is influenced by the same initial- and final-state effects. Thus, the ground state electrostatic potential is far more important than the final-state reorganization energy in explaining reactivity differences. The final state corresponds in this case to the carbocation formed in the transition state. Reactivity of different molecules and the correlation with ionization energies have been studied before, and conclusions similar to this work have been made [88].

Chapter 6

Conclusion

Core-photoelectron spectra of benzene, methyl-substituted benzenes and a series of small molecules have been acquired with high-resolution radiation from third generation synchrotron facilities. From the spectra C1s ionization energies of the molecules have been extracted. Theoretical calculations have been performed in order to interpret complex experimental spectra.

C1s ionization energies of several small molecules of general chemical interest have been calibrated with argon as internal standard. Most of these molecules have been calibrated earlier, but is now done at high resolution using synchrotron radiation. The acquisition of the spectra was performed within a short period of time and with the same experimental settings. This leads to more internally consistent ionization energies for the whole group of molecules. Both adiabatic and vertical ionization energies were found. These are generally in good agreement with earlier measurements, except for CF_4.

For benzene and d-benzene one has been able to deconvolute the vibrational progression of the spectra with a high degree of accuracy, by means of extensive theoretical calculations. The splitting of the main peak observed in the benzene spectrum was mainly explained as a result of a strongly excited C-H bending mode. The two dominating modes in the d-benzene spectrum were found to be a C-D bending mode and a ring-stretching mode.

The spectra of the methyl-substituted benzenes were deconvoluted and assigned with aid from theoretical calculations. Due to the high resolution available one is able to distinguish between inequivalent but similar carbon atoms in each molecule. Vertical ionization energies for all carbon atoms were determined. Electrophilic substitution reactions for the methylated benzenes were investigated with respect to substituent effects and reactivity. The chemical factors that influence core ionization and the formation of a charged intermediate in electrophilic addition are believed to be the same. Therefore, it is expected that the two processes are correlated.

A linear correlation between the logarithm of the rate factors and shifts in core-ionization energies have been found for two sets of electrophilic reactions. Generally, a large negative shift, relative to benzene, leads to a higher reactivity. The methyl group is traditionally expected to be activating and ortho-para directing. The data show extreme position sensitivity of the ring carbons. The ortho-and para-positions are significantly more negatively shifted than the meta-positions and the ipso-carbons of the respective molecules. This correlates with the predicted ortho- and para-directing abilities of the methyl group.

By means of theoretical calculations one is able to separate effects of the initial state and of the final state on shift in core-ionization energies, ΔI. This relationship is given by:

$$\Delta I = \Delta V - \Delta R$$

where ΔV is the ground state potential energy due to charge distribution in the initial state, and ΔR represents the relaxation of the final state. The results show that the variation in substituent effects is predominantly determined by the initial state, and that the final-state charge rearrangement is very little influenced by the nature of the substituent. This result challenges the traditional view since resonance stabilization of the transition state for electrophilic reactions is considered to be crucial to the understanding of both reactivity and orientation effects in aromatic rings.

References

1 L. J. Sæthre, T. D. Thomas, S. Svensson, J. Chem. Soc., Perkin Trans. 2, 749 (1997).
2 L. J. Sæthre, T. D. Thomas, J. Org. Chem. 56, 3935 (1991).
3 M. R. Siggel, T. D. Thomas, J. Am. Chem. Soc. 108, 4360 (1986).
4 G. B. Sergeev, V. V. Smirnov, T. N. Rostovshchikova, Russ. Chem. Rev. 52, 259 (1983).
5 T. H. Lowry, K. S. Richardson, *Mechanisms and Theory in Organic Chemistry*, Harper and Row, New York, third edition, pp. 567-584, 1987.
6 A. Streitwieser, C. H. Heathcock, E. M. Kosower, *Introduction to organic chemistry*, fourth edition, 1992, Macmillan Publishing Company, pp. 712-714.
7 C. Eaborn, R. C. Moore, J. Chem. Soc., p 3640 (1959).
8 T. D. Thomas, L. J. Sæthre, S. L. Sörensen, S. Svensson, J. Chem. Phys. 109, 1041 (1998).
9 S. J. Osborne, S. Sundin, A. Ausmees, S. Svensson, L. J. Sæthre, O. Sværen, S. L. Sörensen, J. Végh, J. Karvonen, S. Aksela, A. Kikas, J. Chem. Phys. 106, 1661 (1997).
10 S. Ege, *Organic chemistry; Structure and Reacitvity*, D. C. Heath and Company, third edition, 1994.
11 T. W. G. Solomons, *Organic Chemistry*, John Wiley & Sons, Inc., fourth edition, 1988.
12 P. W. Atkins, R. S. Friedman, *Molecular Quantum Mechanics*, Oxford University Press Inc., New York, third edition, 1997.
13 L. J. Sæthre, T. D. Thomas, O. Gropen, J. Am. Chem. Soc. 107, 2581 (1985).
14 K. J. Børve, T. D. Thomas, J. Electron Spectrosc. Relat. Phenom. 107, 155 (2000).
15 C. D. Wagner, J. Electron Spectrosc. Relat. Phenom. 47, 283 (1988).
16 H. Siegbahn, O. Goscinski, Phys. Scr. 13, 225 (1976).
17 C. D. Wagner, Faraday Discuss. Chem. Soc. 60, 291 (1975).
18 D. A. Shirley, Phys. Rev. A 7, 1520 (1973).
19 T. D. Thomas, J. Electron Spectrosc. Relat. Phenom. 20, 117 (1980).
20 G. Margaritondo, *Introduction to Synchrotron Radiation*, Oxford University Press, Inc., New York, 1988.
21 E. E. Koch, D. E. Eastman, Y. Farge, *Handbook of Synchrotron Radiation*, edited by E. E. Koch, North-Holland, Amsterdam, 1983.
22 A. L. Robinson, *Soft X-ray Spectromicroscopy*, Ernest Orlando Lawrence Berkeley National Laboratory, Advanced Light Source, University of California, Berkeley, 1997.
23 MAX-lab internet pages: http://www.maxlab.lu.se/.
24 S. J. Osborne, *Synchrotron Radiation Studies of Resonantly and Non-Resonantly Excited Electron Spectra of Free Atoms and Molecules*, Uppsala University, 1997.
25 M. Bässler, J.-O. Forsell, O. Bjorneholm, R. Feifel, M. Jurvansuu, S. Aksela, S. Sundin, S. L. Sörensen, R. Nyholm, A. Ausmees and S. Svensson, J. Electron Spectrosc. Relat. Phenom. 101-103, 953 (1999).
26 S. Svensson, J.-O. Forsell, H. Siegbahn, A. Ausmees, G. Bray, S. Södergren, S. Sundin, S. J. Osborne, S. Aksela, E. Nõmmiste, J. Jauhiainen, M. Jurvansuu, J. Karvonen, P. Barta, W. R. Salaneck, A. Evaldsson, M. Lögdlund, A. Fahlman, Rev. Sci. Instrum. 67, 2149 (1996).
27 N. Mårtensson, P. Baltzer, P. A. Bruhwiler, J.-O. Forsell, A. Nilsson, A. Stenborg, B. Wannberg, J. Electron Spectrosc. Relat. Phenom. 70, 117 (1994).
28 Igor pro 3.14, WaveMetrics, Inc., 10200 SW Nimbus Ave, Suite G-7, Portland, OR 97223.
29 Edwin Kukk, Western Michigan University, Kalamazoo, Michigan.

30 P. van der Straten, R. Morgenstern, A. Niehaus, Z. Phys. D 8, 35 (1988).
31 K. Siegbahn, C. Nordling, G. Johansson, J. Hedman, P. F. Heden, K. Hamrin, U. Gelius, T. Bergmark, L. O. Werme, R. Manne, Y. Baer, *ESCA Applied to Free Molecules*, North Holland, Amsterdam, p. 163, 1969.
32 R. Spohr, T. Bergmark, N. Magnusson, L. O. Werme, C. Nordling, K. Siegbahn, Phys. Scr. 2, 31 (1970).
33 M. Coville, T. D. Thomas, Phys. Rev. A 43, 6053 (1991).
J. Nordgren, H. Ågren, C. Nordling, K. Siegbahn, Phys. Scr. 19, 5 (1979).
L. S. Cederbaum, W. Domcke, J. Chem. Phys. 64, 603 (1976).
36 H. Rabus, D. Arvanitis, M. Domcke, K. Baberschke, J. Chem. Phys. 96, 1560 (1992).
37 L. J. Sæthre, O. Sværen, S. Svensson, S. Osborne, T. D. Thomas, J. Jauhiainen, S. Aksela, Phys. Rev. A 55, 2748 (1997).
38 S. Sundin, L. J. Sæthre, S. L. Sörensen, A. Ausmees, S. Svensson, J. Chem. Phys. 110, 5806 (1999).
39 W. J. Hehre, L. Radom, P. v.R. Schleyer, J. A. Pople, *Ab Initio Molecular Theory*, John Wiley & Sons, Inc., 1986.
40 J. N. Murrel, S. F. Kettle, J. M. Tedder, *The Chemical Bond*, John Wiley & Sons, Inc., second edition, 1985.
41 J. B. Foresman, Æ. Frisch, *Exploring Chemistry with Electronic Stucture Methods*, Gaussian, Inc., Pittsburgh PA, second edition, 1996.
42 M. J. Frisch, Æ. Frisch, J. B. Foresman, *Gaussian* 94 *User's Reference*, Gaussian, Inc., Pittsburgh PA, 1995.
43a A. D. Becke, J. Chem. Phys. 98, 5648 (1993).
43b J. A. Pople, M. Head-Gordon, D. J. Fox, K. Raghavachari, L. A. Curtiss, J. Chem. Phys. 90, 5622 (1989).
43c L. A. Curtiss, C. Jones, G. W. Trucks, K. Raghavachari, J. A. Pople, J. Chem. Phys. 93, 2537 (1990).
44 P. Hohenberg, W. Kohn, Phys. Rev. 136, B864 (1964).
45 W. Kohn, L. J. Sham, Phys. Rev. 140, A1133 (1965).
46 J. C. Slater, *Quantum theory of Molecular and Solids,* Vol. 4, McGraw-Hill, New York, 1974.
47 A. D. Becke, Phys. Rev. A 38, 3098 (1988).
48 S. H. Vosko, L. Wilk, M. Nusair, Canadian J. Phys. 58, 1200 (1980).
49 C. Lee, W. Yang, R. G. Parr, Phys. Rev. B 37, 785 (1988).
50 B. Miehlich, A. Savin, H. Stoll, H. Preuss, Chem. Phys. Lett. 157, 200 (1989).
51 D. Nordfors, N. Mårtensson, H. Ågren, Phys. Rev. B 38, 12922 (1988).
52 D. Nordfors, *Ionization and protonation of free molecules*, Uppsala University, 1990.
53 E. B. Wilson, Jr., J. C. Decius, P. C. Cross, *Molecular vibrations*, Dover Publications, New York, 1955.
54 J. Bozek, T. X. Carrol, J. Hahne, L. J. Sæthre, J. True, T. D. Thomas, Phys. Rev. A 57, 158 (1998).
55 M. J. Frisch, G. W. Trucks, H. B. Schlegel, P. M. W. Gill, B. G. Johnson, M. A. Robb, J. R. Cheeseman, T. Keith, G. A. Petersson, J. A. Montgomery, K. Raghavachari, M. A. Al-Laham, V. G. Zakrzewski, J. V. Ortiz, J. B. Foresman, J. Cioslowski, B. B. Stefanov, A. Nanayakkara, M. Challacombe, C. Y. Peng, P. Y. Ayala, W. Chen, M. W. Wong, J. L. Andres, E. S. Replogle, R. Gomperts, R. L. Martin, D. J. Fox, J. S. Binkley, D. J. Defrees, J. Baker, J. P. Stewart, M. Head-Gordon, C. Gonzalez, J. A. Pople, GAUSSIAN 94, Revision D. 4, Gaussian, Inc., Pittsburgh PA, 1995.
56 T. Shimanouchi, *Tables of Molecular Vibrational Frequencies*, Consolidated Vol. I, NSRDS-NBS 39, US GPO, Washington, DC, p. 50, 1972.

57 K. J. Børve, *G2FC*, University of Bergen, 1999.
58 T. H. Dunning, P. J. Hay, *Modern Theoretical Chemistry*, Plenum, New York, 1976.
59 S. Huzinaga, J. Chem. Phys. 42, 1293 (1965).
60 W. J. Stevens, H. Basch, M. Krauss, J. Chem. Phys. 81, 6026 (1984).
61 T. Karlsen, K. J. Børve, J. Chem. Phys. 112, 7979 (2000).
62 L. J. Sæthre, T. D. Thomas, L. Ungier, J. Electron Spectrosc. Relat. Phenom. 33, 381 (1984).
63 T. D. Thomas, R. W. Shaw Jr., J. Electron Spectrosc. Relat. Phenom. 5, 1081 (1974).
64 G. Johansson, J. Hedman, A. Berndtsson, M. Klasson, R. Nilsson, J. Electron Spectrosc. Relat. Phenom. 2, 295 (1973).
65 T. D. Thomas, Oregon State University, Corvallis, unpublished results.
66 T. X. Carrol, N. Berrah, J. Bozek, J. Hahne, E. Kukk, L. J. Sæthre, T. D. Thomas, Phys. Rev. A 59, 3386 (1999).
67 L. Asplund, U. Gelius, S. Hedman, K. Helenelund, K. Siegbahn, P. E. M. Siegbahn, J. Phys. B: At. Mol. Phys. 18, 1569 (1985).
68 T. D. Thomas, N. Berrah, J. Bozek, T. X. Carroll, J. Hahne, T. Karlsen, E. Kukk, L. J. Sæthre, Phys. Rev. Lett. 82, 1120 (1999).
69 T. X. Carroll, J. Hahne, T. D. Thomas, L. J. Sæthre, N. Berrah, J. Bozek, E. Kukk, Phys. Rev. A 61, (042503) (2000).
70 L. J. Sæthre, unpublished results.
71 M. Tronc, G. C. King, F. H. Read, J. Phys. B: At. Mol. Phys. 12, 137 (1979).
72 J. Nordgren, L. Selander, L. Petterson, C. Nordling, K. Siegbahn, H. Ågren, J. Chem. Phys. 76, 3928 (1982).
73 J. J. Pireaux, S. Svensson, E. Basilier, P.-Å. Malmquist, U. Gelius, R. Caudano, K. Siegbahn, Phys. Rev. A 14, 2133 (1976).
74 L. J. Sæthre, M. R. F. Siggel, T. D. Thomas, J. Electron Spectrosc. Relat. Phenom. 49, 119 (1989).
75 R. G. Cavell, J. Electron Spectrosc. Relat. Phenom. 6, 281 (1975).
76 S. R. Smith, T. D. Thomas, J. Electron Spectrosc. Relat. Phenom. 8, 45 (1976).
77 W. J. Griffiths, S. Svensson, A. N. deBrito, N. Correia, C. J. Reid, M. L. Langford, F. M. Harris, C. M. Liegener, H. Ågren, Chem. Phys. 173, 109 (1993).
78 E. E. Rennie, B. Kempgens, H. M. Koppe, U. Hergenhahn, J. Feldhaus, B. S. Itchkawitz, A. L. D. Kilcoyne, A. Kivimaki, K. Maier, M. N. Piancastelli, M. Polcik, A. Rudel, A. M. Bradshaw, J. Chem. Phys. (2000) (in press).
79 B. Kempgens, H. M. Koppe, A. Kivimaki, M. Neeb, K. Maier, U. Hergenhahn, A. M. Bradshaw, Surf. Sci. Lett. 425, L376 (1999).
80 E. E. Rennie, C. A. F. Johnson, J. E. Parker, D. M. P. Holland, D. A. Shaw, M. A. Hayes, Chem. Phys. 229, 107 (1998).
81 M. N. Piancastelli, T. A. Ferret, D. W. Lindle, L. J. Medhurst, P. A. Heimann, S. H. Liu, D. A. Shirley, J. Chem. Phys. 90, 3004 (1989).
82 Y. Ma, F. Sette, G. Meigs, S. Modesti, C. T. Chen, Phys. Rev. Lett. 63, 2044 (1989).
83 L. J. Medhurst, T. A. Ferret, P. A. Heidmann, D. W. Lindle, S. H. Liu, D. A. Shirley, J. Chem. Phys. 89, 6096 (1988).
84 D. Nordfors, S. Svensson, U. Gelius, J. Phys. Colloque 48, 789 (1987).
85 C. Eaborn, J. Chem. Soc., 4858 (1956).
86 R. A. Benkeser, H. R. Krysiak, J. Am. Chem. Soc. 76, 6353 (1954).
87 de la Mare, *Progress in Stereochemistry*, edited by Klyne and de la Mare, Vol. II, Butterworths Scientific Publications, London, pp. 73-75 (1958).
88 O. Sværen, *Electron Spectroscopy and Chemical Reactivity*, University of Bergen, June 1997.

Appendix A

Curve Fitting Macro Package for Igor

by Edwin Kukk [29].

1. Introduction

The purpose of this macro package is to perform a least-squares curve fitting to an experimental spectrum, using Voigt lineshapes or analytical PCI-shapes, with advanced peak parameter linking arithmetics. The package consists of the following macros:

1) MakeDataWave - selects a part of a spectrum displayed in a graph and creates a new graph from it for curve fitting.

3) Background - allows to define a linear background for the fit.

2) InitPeakTable - Generates a table to show and edit the parameters for the peaks.

3) GraphParEdit - allows to edit peak positions and intensities interactively in the graph.

4) InitFit - calculates and displays the peaks with the parameters as given in the table.

5) Simplex - performs the iterative least-squares fitting.

6) AutoRestart - automatically restarts Simplex until the fit converges.

7) RestoreInitial - restores the parameters to the values they had before running Simplex.

8) ResultTable - generates a table with fit results for final printout.

9) Tags - attaches tags to the individual peaks in the graph.

10) SaveFit - saves fit parameters to a file.

11) LoadFit - loads fit parameters from file.

2. Getting started

a) At first you need to create an Igor data wave from the spectrum you want to study. This is a standard Igor procedure.

b) Create a graph displaying your spectrum. Use the cursors to select the region of the spectrum you want to fit. Then run MakeDataWave macro. It creates a new graph showing the selected region and displays a panel which allows you to define the background. By default, the background is kept fixed during the fitting procedure, but it can also be optimized during the fit.

c) Run the InitPeakTable macro, which creates a table for defining the initial parameters of the peaks. For setting up the parameters, see section "Peak Parameters" below.

d) After you have entered your first guess for the peak parameters, run the Initfit macro. It calculates and displays the peaks in the graph, together with their sum (black curve) and the difference from the experimental spectrum (dashed curve). The goodness parameter, c2, is also displayed.

e) You can now modify your initial guess either by changing the parameters in the table or by interactive editing in the graph, using the GraphEdit macro. After changing the parameters in the table, run InitFit to bring the fit up to date.
f) Once you have arrived at a reasonably good initial guess, you can start the fitting process by running macro Simplex. The section "Simplex" describes how this routine works and how to use it.
g) Finally, when your fit result is satisfactory, you can create a results table using macro ResultTable. This macro resolves the linking arithmetics for the linked peaks and also calculates peak areas and widths.
h) You can now add tags to the peaks in the graph by activating the graph and running the macro Tags.
i) As the final step, it is a good idea to create a layout where the result table and the fit graph are together. It can then be printed, for example.
j) The fit results can also be saved on disk, using the macro SaveFit.

3. Peak Parameters

The table "PeakTable" contains the parameters that define the fit. There are two types of parameters - the ones that contain the actual values and the ones that contain the linking information. For a simplest fit one can ignore the linking parameters - just make sure they are all set to 0 - no linked or fixed parameters whatsoever. The meaning of the rest of them is the following:
Label - a short text describing the peak. Useful when there are many peaks and a complex structure.
Shape - defines the analytical shape of the peak. Currently two shapes are available - "p" is a "PCI-shape", an asymmetrically distorted Voigt profile, convoluted by a gaussian. One can use this type as a symmetric shape, by setting the asymmetry parameter to 0 and not allowing it to change. The second, "v", defines a pseudoVoigt shape, which is a linear combination of a Lorentzian and a Gaussian. It is less precise that the first type, obtained by convoluting shapes, and does not include asymmetry.
En - stands for the energy (in general, X-value) of the peak maximum.
Int - peak intensity
Fwhm(L) and Fwhm(G) - full width at half maximum of the lorentzian and gaussian components of the peak
Asym - asymmetry parameter of the PCI-shape. It can also be negative.

When you generate a 'virgin' table by InitPeakTable, the rows will be empty except the first one (No. 0), which has a special meaning. It does not define a peak, but the variations used to initiate the least-squares fitting, which reflect your guess of how much a given type if parameter is going to change. It has some preset initial values that you can freely change. More about them under "Simplex"

Each of the next rows defines one peak. You can delete, add or copy the rows, should the need be. Take a look at your spectrum in "FitGraph" and determine the number of peaks needed and their approximate parameters. Don't forget the shape and width parameters! You can set the energy and intensities rather arbitrarily and modify them later. Run Initfit. The peaks should now appear in the graph. If they do not, check the parameters! To reposition the peaks, you can either edit the table manually or run Graphedit.

GraphEdit displays little red squares at the top of each peak, connected with red lines. You can move mouse cursor on those squares, press the left mouse button and drag them to a new location. A little panels also appears on the screen, with buttons "Refresh" and "Done". Use "Refresh" to update your graph and "Done"...when you are done. Try to obtain a reasonably good-looking fit before starting Simplex - it'll make its life much easier.

The background you defined already at the beginning, after making the data wave. You can always redefine the background by running the Background macro again, after which you need to run Initfit. Background level can be defined in tow ways - from the graph or by typing in the numerical values. The two checkboxes in the background panel define, how it behaves during the fit. You can uncheck the Fixed box, "unfreezing" the background so that it will be optimized by Simplex during the fit. Leaving the Constant box checked keeps the background equal across the spectrum, while unchecking it allows the left and right ends to have different values. The background will always remain linear, however. If you want Simplex to do the work and find the best background, don't start by defining zero background, since the initial variations are set to 10% of the background level and would therefore be -- zero.

There is also a possibility to use peak parameters saved to disk by using the Savefit macro. It is convenient, if you just want to save the results or to use the to fit a similar spectrum. To use the parameters from a file, you should first run MakeDataWave, if you haven't already done so. After that you can retrieve the fitting parameters from a file by using the LoadFit macro. Of course, the file must have been created by the SaveFit macro only.

4. Simplex

Simplex is the name for a blob on the multidimensional surface of the fit 'goodness' parameter. During the iteration process, this blob starts to crawl around, shrink, expand, squeeze or wiggle towards the lowest point on the surface in its vicinity (NB! not globally). This behavior gave the algorithm it's name - amoeba. The whole purpose of the game is, of course, to find the lowest spot, that is, to minimize the c2 value. The algorithm is not the fastest or best on Earth, but works. In the future it might be replaced by a more effective one. Take a look at row 0 of the table before starting Simplex, It determines the initial size of the "blob". The variation is given directly for the energy and intensity parameters - e.g., 0.01 means that Simplex starts to vary the energy parameter with the initial step of 0.01 energy units, whatever they happen to be. The variation is given as percentage for the intensity and width parameters - e.g. 0.1 for intensity means that the initial step will be 10 for a peak of the intensity 100, but 1000 for a peak with 10000 intensity.

Simplex displays information in the command window during the iteration. It shows how well the iteration converges. If the first values of c2 are very large (much more that 100, let's say), but your initial settings were rather good, then it means that you have given too large variations for one or more parameters. Simplex might still converge, but might also give strange results. On the other hand, if c2 starts to converge very slowly, then maybe the initial step sizes are too small. It will get there, eventually, but it might take very long. So try to increase the variations in row 0.

It seems to be a good strategy to start with rather large variations and run Simplex once or twice. When it gets closer to convergence, decrease the variations. There are two conditions at which Simplex stops. 1) The c2 has converged. Ideally, it should be close to unity, if your data contain real counts with Poisson distribution. It is still a good idea to run Simplex once more with rather small variations. 2) Maximum number of iterations is performed. The maximum number depends on how many free parameters there is. The condition at which Simplex stopped is shown in the command window. If it didn't converge, you definitely have to restart it, maybe with smaller variations, until convergency is achieved.

The macro AutoRestart can be used to restart Simplex automatically until the c2 converges within the given limit. It is useful for routine fits that take long time to run.

5. Linking

Smart linking of parameters is absolutely essential for a good fit. With all parameters free, an excellent match to the data is usually achieved, but the results do not necessarily make any sense physically. One should use all available knowledge about the spectrum to be analyzed in order to reduce the number of free parameters to minimum.

There are a number of special columns in the "PeakTable". Different parameters can be linked in a different way, so that it makes sense physically. Firstly, and most commonly, the width and asymmetry parameters can be set equal to the corresponding value of another peak. To do this, insert the number of the peak you want to link to into the "L/F" column of this parameter. For example, to set the Lorentzian widths of all peaks equal, link all "Fwhm(L)" parameters starting from peak 2 to peak 1. The width and asymmetry parameters can be also kept fixed by inserting the number "99" in their "L/F" column. Note that multiple linking (linking to a parameter that has already been linked to another parameter etc.) is allowed, but only upwards in the peak definition table.

The linking of energies and intensities is much more complex. They have 4 columns each for linking/fixing information. Inserting "1" in the "F" column fixes the corresponding parameter and the next 3 columns will be just ignored. Therefore, to use linking, make sure that "F" contains "0". (Note that the width and asymmetry parameters did not have separate "F" column and therefore the odd "99" encoding of the fix was used. This was done in order to keep the number of columns as small as possible)

There are two types of linking you can use depending of what kind of information is available.
1) Let's say you have 2 peaks and you know that they are exactly 1.5 eV apart and that the intensity of peak 2 is 50% of peak 1. But you don't know the absolute energies and intensities. Then give the parameters for peak 1 as free. For peak 2, enter 1.5 in the "En" column and 1 in the "+P" column, telling the fitting routine that
En(peak 2)=1.5+ En(peak 1)
For the intensity of peak 2, type 0.5 in the "Int" column and 1 in the "*P" column, meaning that
Int(peak 2)= 0.5 * Int(peak 1)
One can as well link peak 1 to peak 2, which will be kept free. The coefficients would then be -1.5 for energy and 2.0 for the intensity.

2) Let's now assume that you have 4 peaks and you know that the spacing between peaks 3 and 4 must be the same as the spacing between peaks 1 and 2, but you don't know, how much this spacing is! Same for the intensity - you know that the ratio of peak 3/peak 4 equals peak 1/peak 2, but don't know beforehand, what is this ratio. An example would be a photoelectron spectrum of a molecule with two spin-orbit split components both with the same vibrational progressions. In this case, a more advanced linking arithmetics has to be used.
For the energies, keep peaks 1-3 free. For peak 4 it is then known that its energy must be
En(peak 4)=En(peak 3) + (En(peak 2) - En (peak 1)).
To do this, enter 0 in the "En" column of peak 4 and then enter 3, 2, and 1 in the first "+P", second "+P" and in the third "-P" column, correspondingly. You can also enter a value different from 0 in "En", in which case the peak is shifted from its calculated position by that value.
For the intensities, the same logic applies - keep peaks 1-3 free and the intensity of peak 4 must be
Int(peak 4)=Int(peak 3) * (Int(peak 2) / Int(peak 1)).
Enter 1 in the "Int" column and 3, 2, and 1 in the "*P", "*P" and "/P" columns, correspondingly.
By entering a number other than 1 in "Int", the calculated intensity is multiplied by this coefficient.

Appendix B

Table B-1. Fwhm and asymmetry parameters for several small molecules, obtained from the least squares fits described in Section 5.1.

Molecule	Peak	Fwhm(L)	Fwhm(G)	Fwhm	Asym
Methane	1	100.4	84.4	155.2	0.3660
	2				0.3692
	3				0.3723
	4				0.3753
Ethane	1	101.7	76.9	150.0	0.3625
	2				0.3637
	3				0.3657
	4				0.3670
	5				0.3687
	6				0.3702
Ethene	1	105.8	102.8	179.4	0.3624
	2				0.3636
	3				0.3653
	4				0.3670
	5				0.3691
	6				0.3706
Ethyne	1	105.0[a]	84.8	159.4	0.3701
	2				0.3693
	3				0.3714
	4				0.3722
	5				0.3728
	6				0.3744
	7				0.3735
	8				0.3749
	9				0.3756
CO	1	93.5	80.5	146.2	0.4107
	2				0.4137
	3				0.4168
	4				0.4197
CO_2	1	98.1	100.0	170.4	0.4153
	2				0.4169
	3				0.4186
	4				0.4203
CF_4	1	78.6	77.7	134.4	0.4770
CH_3F	1	119.9	75.2	163.9	0.3914
	2				0.3951
	3				0.3988
CHF_3	1	79.0	108.1	160.9	0.4495
	2				0.4539

[a] Gerade peak.

Appendix C

Table C-1. Resulting fitting parameters of the benzene spectrum (Section 5.2). Ionization energies, intensities, vertical ionization energies, I (vert), Fwhm, and asymmetry parameter. Ionization energies in eV, Fwhm in meV.

Peak	I	Intensity	I (vert)	Fwhm(L)	Fwhm(G)	Fwhm	Asym
Adiabat	290.280	15807	290,394	126.5	55.0	156.1	0.3547
ν_{18}	290.356	1851					
ν_{2}	290.407	673					
ν_{6}	290.408	958					
ν_{14}	290.412	8202					
ν_{17}	290.430	574					
$\nu_{18} + \nu_{14}$	290.489	961					
$\nu_{6} + \nu_{14}$	290.541	495					
$2\nu_{14}$	290.545	2248					
$3\nu_{14}$	290.677	432					
ν_{1}	290.713	1908					
$\nu_{14} + \nu_{1}$	290.846	990					

Table C-2. Resulting fitting parameters of the d-benzene spectrum (Section 5.2). Ionization energies, intensities, vertical ionization energies, I (vert), Fwhm, and asymmetry parameter. Ionization energies in eV, Fwhm in meV.

Peak	I	Intensities	I (vert)	Fwhm(L)	Fwhm(G)	Fwhm	Asym
Adiabat	290.274	6152	290.376	137.6	55.0	165.6	0.3547
ν_{18}	290.347	880					
ν_{14}	290.377	2116					
ν_{17}	290.384	462					
ν_{2}	290.394	1877					
ν_{6}	290.399	230					
ν_{9}	290.437	344					
$\nu_{18} + \nu_{14}$	290.450	302					
$\nu_{18} + \nu_{2}$	290.467	268					
$2\nu_{14}$	290.480	386					
$\nu_{14} + \nu_{2}$	290.497	647					
$2\nu_{2}$	290.514	310					
ν_{1}	290.597	856					
$\nu_{14} + \nu_{1}$	290.701	295					
$\nu_{2} + \nu_{1}$	290.717	260					

Appendix D

Table D-1. C1s orbital eigenvalues of the inequivalent carbons in the methyl-substituted benzenes according to Hartree-Fock calculations. The numbering of the carbon atoms is shown in the text in Section 5.3. All energies in a.u.

Molecule	Atom	ε_{HF}	Molecule	Atom	ε_{HF}
Benzene	All	-11.24728	m-Xylene	C1, C3	-11.24834
		-11.24674			-11.24831
		-11.24674		C5	-11.24109
		-11.24557		C4, C6	-11.23307
		-11.24557			-11.23298
		-11.24501		C2	-11.23069
				CH_3	-11.22771
					-11.22771
Toluene	C1	-11.25071	p-Xylene	C1, C4	-11.24467
	C3, C5	-11.24398			-11.24466
		-11.24398		C2, C3,	-11.23711
				C5, C6	
	C4	-11.24014			-11.23700
	C2, C6	-11.23858			-11.23594
		-11.23851			-11.23587
	CH_3	-11.22953		CH_3	-11.22711
					-11.22711
o-Xylene	C1, C2	-11.24557	Mesitylene	C1, C3, C5	-11.24565
		-11.24449			-11.24562
	C4, C5	-11.23861			-11.24562
		-11.23758		CH_3	-11.22617
	C3, C6	-11.23620			-11.22617
		-11.23608			-11.22617
	CH_3	-11.22824		C2, C4, C6	-11.22563
		-11.22824			-11.22563
					-11.22566

Appendix E

Resulting fitting parameters of the spectra of the methyl-substituted benzenes: Energies (eV) of the individual peaks, vertical energies (eV), intensities, and Fwhm (meV). The asymmetry parameters are 0.62 for all peaks, according to the fit for benzene (Section 5.3). The numbering of the carbon atoms is shown in the text in Section 5.3.

Table E-1. Toluene

Peak	I	Intensity	I (vert)	Fwhm (L)	Fwhm (G)	Fwhm
C2,C6	290.088	1	290,138	73.2	221.7	277.2
	290.431	0.1704				
C4	290.082	0.5	290,132			
	290.425	0.0852				
C3,C5	290.226	1	290,276			
	290.569	0.1704				
C1	290.375	0.5	290,375			
CH_3	290.562	0.5609	290,679	73.2	221.7	277.2
	290.959	0.1742				
	291.356	0.0269				

Table E-2. o-Xylene

Peak	I	Intensity	I (vert)	Fwhm (L)	Fwhm (G)	Fwhm
C3,C6	289.937	1	289.99	73.2	221.7	277.2
	290.299	0.1704				
C5,C4	289.936	1	289.989			
	290.298	0.1704				
C1,C2	290.135	1.1704	290.135			
CH_3	290.444	1.2907	290.613	185.3	161.3	284.2
	290.881	0.4006				
	291.278	0.0621				

Table E-3. m-Xylene

Peak	I	Intensity	I (vert)	Fwhm (L)	Fwhm (G)	Fwhm
C2	289.854	1	289.904	73.2	221.7	277.2
	290.197	0.1704				
C4,C6	289.843	2	289.893			
	290.186	0.3408				
C5	289.971	1	290.021			
	290.314	0.1704				
C1,C3	290.179	2.3408	290.179			
CH3	290.463	2.929	290.582	38.0	256.2	282.4
	290.860	0.9094				
	291.257	0.1406				

Table E-4. p-Xylene

Peak	I	Intensity	I (vert)	Fwhm (L)	Fwhm (G)	Fwhm
C2,C3,C5,C6	289.931	1	289.981	73.2	221.7	277.2
	290.274	0.1704				
C1,C4	290.122	0.5852	290.122			
CH_3	290.464	0.6980	290.583	66.9	235.1	277.9
	290.861	0.2168				
	291.258	0.0337				

Table E-5. Mesitylene

Peak	I	Intensity	I (vert)	Fwhm (L)	Fwhm (G)	Fwhm
C2,C4,C6	289.646	1	289.696	73.2	221.7	277.2
	289.989	0.1704				
C1,C3,C5	290.097	1.0582	290.097			
CH_3	290.398	1.2063	290.517	73.2	228.8	277.8
	290.795	0.3743				
	291.192	0.0582				

Appendix F

Table F-1. Charge distribution of the carbons in benzene and the methyl-substituted benzenes, calculated by B3LYP. The numbering of the carbon atoms is shown in the text in Section 5.3.

Molecule	C1	C2	C3	C4	C5	C6	CH_3
Benzene				-0.153			
Toluene	0.432	-0.316	-0.142	-0.177	-0.142	-0.316	-0.603
o-Xylene	0.302	0.302	-0.332	-0.165	-0.165	-0.332	-0.600
m-Xylene	0.446	-0.434	0.446	-0.365	-0.123	-0.365	-0.608
p-Xylene	0.423	-0.309	-0.309	0.423	-0.309	-0.309	-0.607
Mesitylene	0.470	-0.512	0.470	-0.512	0.470	-0.512	-0.612

Table F-2. Electrostatic potentials of the carbons in benzene and the methyl-substituted benzenes, calculated by B3LYP and RHF. The numbering of the carbon atoms is shown in the text in Section 5.3. All potentials in a.u.

Molecule	C1	C2	C3	C4	C5	C6	CH_3
B3LYP theory							
Benzene				-14.745422			
Toluene	-14.740399	-14.752835	-14.749199	-14.750754	-14.749199	-14.752835	-14.753556
o-Xylene	-14.745667	-14.745667	-14.756438	-14.754297	-14.754297	-14.756438	-14.754862
m-Xylene	-14.743850	-14.760022	-14.743850	-14.757756	-14.752997	-14.757756	-14.755724
p-Xylene	-14.745516	-14.756190	-14.756190	-14.745516	-14.756190	-14.756190	-14.756043
Mesitylene	-14.747270	-14.764589	-14.747270	-14.764589	-14.747270	-14.764589	-14.757832
RHF theory							
Benzene				-14.717041			
Toluene	-14.711941	-14.724663	-14.719898	-14.723242	-14.719898	-14.72466	-14.72696
o-Xylene	-14.717447	-14.717447	-14.727263	-14.725778	-14.725778	-14.727263	-14.728383
m-Xylene	-14.714451	-14.732179	-14.714451	-14.730454	-14.722942	-14.730454	-14.728883
p-Xylene	-14.717838	-14.727199	-14.727199	-14.717838	-14.727199	-14.727199	-14.729560
Mesitylene	-14.716800	-14.737777	-14.716800	-14.737777	-14.716800	-14.737777	-14.730849